2018

Palmitoylation And Polarity: Regulation Of Asymmetric Partitioning Of Notch And Wnt Signaling By Reversible Lipid Modification In Dividing Cells

Ewa Stypulkowski
University of Pennsylvania, estypulkowski@gmail.com

Palmitoylation And Polarity: Regulation Of Asymmetric Partitioning Of Notch And Wnt Signaling By Reversible Lipid Modification In Dividing Cells

Abstract
Protein palmitoylation is a reversible lipid modification that regulates protein-membrane interaction, activity, trafficking, and stability in a spatio-temporal manner similar to phosphorylation and ubiquitination. Asymmetric cell division results in two distinctly fated daughter cells, by unequally partitioning proteins known as cell fate determinants. I have characterized a mechanism for protein palmitoylation to asymmetrically partition cell fate determinants, e.g. Numb and β-catenin, through the activity of the depalmitoylating enzyme APT1. Using point mutations, I have found specific palmitoylated residues on Numb are required for its asymmetric localization in dividing cells. By live-cell imaging, I have also identified a reciprocal interaction between APT1 and the Rho family GTPase, CDC42, which promotes asymmetric localization of Numb and β-catenin to the plasma membrane. In turn, this mechanism restricts Notch- or Wnt-responsive transcriptional activity to one daughter cell. Moreover, I show that altering APT1 expression levels alters the transcriptional signatures of MDA-MB-231 triple receptor-negative breast cancer cells, resembling altered Notch and β-catenin-mediated Wnt signaling. Furthermore, loss of APT1 depletes a specific subpopulation of tumorigenic cells. Together, this dissertation presents palmitoylation as a major mechanism of asymmetric cell division that maintains Notch- and Wnt-associated protein dynamics, gene expression, and cellular functions.

Degree Type
Dissertation

Degree Name
Doctor of Philosophy (PhD)

Graduate Group
Cell & Molecular Biology

First Advisor
Eric S. Witze

Keywords
Asymmetric cell division, Cell fate, Notch, Palmitoylation, Tumor heterogeneity, Wnt

Subject Categories
Cell Biology

PALMITOYLATION AND POLARITY:

REGULATION OF ASYMMETRIC PARTITIONING OF NOTCH AND WNT SIGNALING BY REVERSIBLE LIPID MODIFICATION IN DIVIDING CELLS

Ewa Stypulkowski

A DISSERTATION

in

Cell and Molecular Biology

Presented to the Faculties of the University of Pennsylvania

in

Partial Fulfillment of the Requirements for the

Degree of Doctor of Philosophy

2018

Supervisor of Dissertation:

_____

Eric S. Witze, Ph.D., Professor of Cancer Biology

Graduate Group Chairperson:

_____

Daniel Kessler, Ph.D., Associate Professor of Cell and Developmental Biology

Dissertation Committee:

Christopher J. Lengner, Ph.D., Associate Professor, Department of Biomedical Sciences

Peter S. Klein, MD, Ph.D., Professor of Medicine

M. Celeste Simon, Ph.D., Arthur H. Rubenstein, MBBCh Professor

Warren S. Pear, Ph.D., Gaylord P. and Mary Louise Harnwell Professor

PALMITOYLATION AND POLARITY:

REGULATION OF ASYMMETRIC PARTITIONING OF NOTCH AND WNT SIGNALING

BY REVERSIBLE LIPID MODIFICATION IN DIVIDING CELLS

Ewa Stypulkowski

DEDICATION

I dedicate this dissertation in the memory of my mother whose strength, courage, and grace during difficulty drives my passion for pursuing research focused on improving human health.

ACKNOWLEDGMENT

I am thankful to so many people for their support and help during my graduate career. I would like to thank the Developmental, Stem Cell, and Regenerative Biology program and the Department of Cancer Biology for the immense care put into creating a thriving research environment for trainees. Thank you to my collaborators who have contributed critical experiments that directly supported this work. I have so much gratitude for my thesis committee, for challenging me to think beyond my comfort zone and for shaping me to approach hypotheses with a critical eye. I extend a huge thank you to past and present members of the Witze lab for their combined experience and thoughtful guidance over the past years.

Above all, I thank my mentor, Eric Witze. Through his thoughtful supervision and encouragement, I have learned how to carry out big ideas into a completed work and have developed confidence in myself as a scientist. I am deeply grateful for his support.

I would also like to thank my friends and family for their unfailing support and reassurance, and especially, I extend my thanks to Colin K. Choi who has been a huge source of strength and motivation during this period.

ABSTRACT

PALMITOYLATION AND POLARITY: ASYMMETRIC PARTITIONING OF NOTCH AND WNT SIGNALING BY REVERSIBLE LIPID MODIFICATION IN DIVIDING CELLS

Ewa Stypulkowski

Eric S. Witze

Protein palmitoylation is a reversible lipid modification that regulates protein-membrane interaction, activity, trafficking, and stability in a spatio-temporal manner similar to phosphorylation and ubiquitination. Asymmetric cell division results in two distinctly fated daughter cells, by unequally partitioning proteins known as cell fate determinants. I have characterized a mechanism for protein palmitoylation to asymmetrically partition cell fate determinants, e.g. Numb and β-catenin, through the activity of the depalmitoylating enzyme APT1. Using point mutations, I have found specific palmitoylated residues on Numb are required for its asymmetric localization in dividing cells. By live-cell imaging, I have also identified a reciprocal interaction between APT1 and the Rho family GTPase, CDC42, which promotes asymmetric localization of Numb and β-catenin to the plasma membrane. In turn, this mechanism restricts Notch- or Wnt-responsive transcriptional activity to one daughter cell. Moreover, I show that altering APT1 expression levels alters the transcriptional signatures of MDA-MB-231 triple receptor-negative breast cancer cells, resembling altered Notch and β-catenin-mediated Wnt signaling. Furthermore, loss of APT1 depletes a specific subpopulation of tumorigenic cells. Together, this dissertation presents palmitoylation as a major mechanism of asymmetric cell division that maintains Notch- and Wnt-associated protein dynamics, gene expression, and cellular functions.

TABLE OF CONTENTS

LIST OF ILLUSTRATIONS

CHAPTER 1: INTRODUCTION

1.1 Summary

Significant effort has gone into elucidating the molecular mechanisms regulating the polarized protein localization of proteins in cells and tissues during development, homeostasis, and disease. Lipid modification is a class of post-translational modifications that facilitates and stabilizes protein targeting to intracellular membrane domains. This enables the formation of polarized signaling domains at the membrane to propagate downstream signal transduction. Protein palmitoylation is a reversible lipid modification that regulates protein-protein and protein-membrane interaction, activity, trafficking, and stability in a spatio-temporal manner similar to phosphorylation and ubiquitination. Despite an evolutionarily conserved requirement for palmitoylation on many key cellular processes, numerous technical challenges have made it difficult to study palmitoylation in real-time and *in situ*. These obstacles include a lack of antibodies to palmitoylated domains and live-cell imaging probes to measure palmitoylation at the single cell level. In this chapter, I will discuss the evidence, technological advances, and emerging roles for palmitoylation on protein function and cellular processes.

1.2 Overview

Cellular responses to intrinsic (genetic) cues or extrinsic (environmental) signaling cues are essential to drive polarized behaviors essential for embryonic development and tissue homeostasis such as axial patterning, convergent extension, wound healing, and tissue morphogenesis (*1*, *2*). Within the cell, molecular mechanisms drive the polarized segregation of

signaling effectors to specialized plasma and endomembrane domains in response to extrinsic and intrinsic cues to facilitate protein-protein interactions (*3*, *4*). Formation of these polarized domains, e.g. apical/basolateral, allows various parts of the cell to carry out specialized functions such as cell migration, invasion, and asymmetric cell division (*1*). Processes such as germ layer specification, differentiation, and proliferation require precise spatio-temporal regulation of various signaling pathways at distinct subcellular domains. In addition to spatial localization, the protein-protein interactions must be temporally regulated for proper development and tissue function. Loss of polarized protein localization may promote the excessive or insufficient duration signaling activity, resulting in developmental disorders (including embryonic lethality), neurodegenerative disorders, and cancer (*3*, *5*, *6*).

Soluble, cytosolic proteins can localize to the membrane through random diffusion; however, these transient interactions are insufficient to propagate a signal over time (*4*, *7–9*). Polarized protein localization is widely regulated by post-translational modifications that alter the structure and biophysical properties of proteins to modulate activity, stability, protein-protein interaction, and subcellular localization, and include phosphorylation, acetylation, ubiquitination, methylation, and lipid modification (*4*, *10–12*). Post-translational lipid modification increases the hydrophobicity of cytosolic proteins, which enables recruitment and stable association with lipid rafts and other membrane domains. This stable association can bring signaling effectors into close proximity of each other to propagate signaling cascades that, in turn, influence cell identity and function (*6*, *13–16*).

Myristoylation, prenylation, and palmitoylation are three of the most common lipid modifications; palmitoylation is unique in that the modification can be enzymatically reversed. Because of its dynamic properties, palmitoylation spatio-temporally modulates protein activity, stability, and transport between intracellular compartments, a key requirement of establishing cell

polarity (*4*, *6*, *12*). In this manner, palmitoylation is regarded as a regulatory switch similar to phosphorylation or ubiquitination (*6*, *16–18*).

First studied in viruses in the late 1970s, palmitoylation has since been examined in bacteria and eukaryotes from yeast to humans (*11*, *18–23*). It plays a role in diverse cellular and developmental processes including, but not limited to, receptor kinase activity (*24–33*), ion channel function (*32*, *34–41*), apoptosis (*29*, *42–44*), immunomodulation (*45–50*), cell junction assembly (*51–55*), cellular senescence (*56–58*), genomic stability (*24*, *59–62*), neural cells development (*63*, *64*), and progenitor cell maintenance (*25*, *55*, *65–67*). Palmitoylation also maintains the activity of signaling pathway such as Wnt (*68–71*), G-protein coupled receptor (*9*, *11*, *72*, *73*), epithelial growth factor receptor (*26*, *27*, *74*), and Ras (*9*, *11*, *75*, *76*). Disruption of palmitoylation has been linked to the pathogenesis of diseases from Huntington's disease (*77–80*), Alzheimer's disease (*44*, *81–83*), neuropsychiatric disorders (*84–87*), cancer (*26*, *60*, *70*, *71*, *88–94*), and exploratory studies may implicate aberrant palmitoylation on metabolic disorders (*35*, *95–97*), and musculoskeletal defects (*39*, *40*, *98–101*). These examples highlight the diverse biological functions regulated by palmitoylation, although may substrates and the regulation of palmitoylation during these processes still remain to be determined.

Uncovering how palmitoylation regulates protein interactions and localization within a cell may open new opportunities for understanding how signaling pathways are coordinated within an organism to ensure proper development and homeostasis, and how these pathways are dysregulated in disease which may advance the development of targeted therapeutic strategies.

1.3 Introduction to protein palmitoylation

Palmitoylation is the covalent linkage of a 16-carbon palmitate group to a cysteine residue via a labile thioester bond (*16*, *18*, *22*). Unlike myristoylated or prenylated proteins, where the lipid group generally remains attached for the protein's lifetime, palmitate is dynamically turned over. The rate of palmitate turnover varies between substrate as some proteins (TEAD, SNAP25 and synaptotagmin I) remain palmitoylated for hours, while others (Ras, CDC42, Lck, and PSD-95) are rapidly depalmitoylated within minutes (*11*, *15*, *102*). This turnover allows regulation of protein trafficking and sorting between membrane compartments like the Golgi, endoplasmic reticulum, and plasma membrane (*4*, *12*, *14*) (Fig. 1.1 A). Palmitoylation can also modulate the conformation and activity of transmembrane receptors and other integral membrane proteins to facilitate downstream activity by regulating the association between the cytosolic tail and the membrane to restrict or promote access to binding partners (*4*, *6*, *12*, *17*) (Fig. 1.1 B). Hydrophobic protein pockets can be palmitoylated to restrict accessibility to catalytic clefts, and palmitoylation can sterically hinder amino acid residues from ubiquitinating enzymes to inhibit protein degradation (*6*, *10*) (Fig. 1.1 C). These examples demonstrate how palmitoylation can modulate cellular responses (*12–14*).

A single lipid group is generally not sufficient to maintain a stable protein-membrane interaction, and therefore, proteins are dual-lipid modified with palmitate and another lipid group (*4*, *9*). Proteins containing a single prenyl or myristate group, such as Ras, Fyn kinase, or Gα subunits, briefly associate with membranes (*4*, *9*). Adding a second lipid group increases the amount of time a protein resides at a membrane, thus promoting a sustained downstream signal cascade (*4*, *9*, *10*, *14*). For example, prenylated Ras preferentially localizes to the Golgi, but the addition of palmitate drives its localization to plasma membrane. Regulated cycling between the Golgi and plasma membrane maintains appropriate Ras distribution within the cell to keep Ras

signaling in check (*4*, *9*). Inhibiting depalmitoylation with small molecule agents results in nonspecific intracellular localization and downregulated Ras signaling (*9*, *75*, *103*). A member of the Src family of kinases, Lyn, is dually myristoylated and palmitoylated; this is thought to prevent chromosome missegregation by restricting Lyn at the plasma membrane and preventing nuclear translocation (*24*). Dual lipid modification also facilitates the cycling of neuronal synaptic proteins PSD-95 and GAP43 cycle between the cytosol and synaptic membranes or axonal outgrowths (*9*, *11*, *14*). These examples demonstrate how palmitoylation serves as a critical mechanism to spatio-temporally regulate protein localization to maintain signaling activity and protein interactions, such as ligand-receptor interactions (*17*).

While the majority of palmitoylated proteins undergo enzymatically regulated cycles of palmitoylation and depalmitoylation, a smaller number of palmitoylated proteins are irreversibly modified (*10*). Ligands and hormones like Spitz (an EGFR-activating ligand), Hedgehog, Wnt, and preghrelin are irreversibly palmitoylated, which facilitates proper post-translational processing and secretion out of the cell (*9*, *10*, *16*). Although a recent study identified Wnt ligands are depalmitoylated by Notum (*104*), irreversibly palmitoylated proteins are not known to cycle between palmitoylated and unpalmitoylated states as reversibly modified proteins do. While irreversible palmitoylation is critical for cell signaling, this chapter will discuss the biological function of the more ubiquitously studied reversible palmitoylation.

1.4 Enzymatic regulation of palmitoylation-depalmitoylation cycles

Palmitoylation is catalyzed by two classes of evolutionarily conserved enzymes: palmitoyltransferases and depalmitoylating enzymes (*9*, *10*) (Fig. 1.2). The multi-pass DHHC transmembrane proteins make up the largest class of palmitoyltransferases. This family was first

isolated in yeast and is characterized by a cysteine-rich domain containing a highly conserved DHHC (Aspartate-Histidine-Histidine-Cysteine) zinc-finger motif (*105–107*). The number of DHHC enzymes varies with species, e.g. 7 in yeast, 23 in mammals, 24 in plants and invertebrates (*D. melanogaster)* (*16*, *18*, *23*). As a large group, DHHCs share many functional redundancies and substrates. Unlike myristoylation or prenylation, which have defined substrate recognition sequences, palmitate can be added to any cysteine (*10*, *22*). Because of this, a defined palmitoylation-recognition sequence has not yet been identified making it difficult to predict palmitoylated proteins based on amino acid sequence. Ankyrin-repeat domains have been suggested as a potential DHHC recognition sequence (*15*, *108*, *109*). Specific substrate-DHHC pairs have also been observed depending on tissue context, cellular compartment, or even amino acid sequence (*15*, *23*, *110*). Due to the abundance of palmitoylated proteins, the size of the DHHC famil, and ambiguity in substrate-DHHC specificity have made it challenging to characterize bona-fide substrate-enzyme pairs *in vivo* (*14*, *17*).

Palmitate transfer from enzyme to substrate is a two-step process, which involves forming a palmitate-DHHC intermediate through autopalmitoylation. Upon substrate binding, palmitate is transferred from the DHHC to cysteine residues on the substrate though a thioester bond (*111*). While free palmitate is abundantly found in the cell, palmitoyl-CoA is the source of palmitate for DHHC enzymes (*17*, *112*). DHHC enzymes are localized on various intracellular membrane domains including the Golgi, endoplasmic reticulum, vesicles, and plasma membrane (*6*, *15*). Palmitoylation occurs both at the Golgi, where all palmitoylated proteins are trafficked out to cellular domains, and at local membrane domains, raising the possibility that palmitoylation may be spatially restricted to occur in proximity of palmitoyltransferases (*113*, *114*). DHHC expression and localization may also be cell-cycle and tissue dependent (*6*, *15*, *24*, *62*, *102*, *115*, *116*). Segregating DHHCs to distinct compartments may serve as nucleating factors

to enrich for palmitoylated proteins at distinct membrane domains as in synaptic membranes, focal adhesions, and in asymmetrically dividing cells. This may ensure palmitoylation occurs at correct cellular compartments to regulate signaling activity (*15, 46, 52, 71, 113*).

Depalmitoylating enzymes make up a much smaller group and the mechanism of depalmitoylation remains unclear; however, structural analysis suggests members may belong to the larger α/β hydrolase family (*6, 9*). Acyl-protein thioesterases 1 and 2 (APT1 and APT2) and protein palmitoyl-thioesterases 1 and 2 (PPT1 and PPT2) are among the best-studied depalmitoylating enzymes (*6, 9, 15, 23*). APTs are primarily cytosolic proteins and transiently localize to membranes to catalyze depalmitoylation (*6, 117*). While the lack of a defined palmitoylation sequence has made identifying specific APT substrates challenging, most reversibly-palmitoylated proteins including Ras, MCAM, and Gα subunits, appear to be targets (*15, 23, 70–72, 75*). In contrast, PPTs are thought to be restricted to lysosomes to depalmitoylate substrates targeted for degradation (*14, 118*). The ABHD17 family and orthologs, a subset of the α/β hydrolase family, are newly identified depalmitoylating enzymes in mammalian cells and in parasites. Whether the substrate pool for ABHD17 enzymes is as diverse as for APTs remains to be determined (*12, 18, 119*).

Palmitoylation may also be regulated at the transcriptional level adding another layer of spatio-temporal regulation of protein localization and signaling activity. Micro-RNAs and SNAIL have been shown to regulate the expression of palmitoyltransferases and depalmitoylating enzymes, and may contribute to dysregulated palmitoylation-mediated protein signaling in disease (*17, 73, 120, 121*).

1.5 Function of palmitoylation in protein trafficking, activity, and stability

Similar to phosphorylation or ubiquitination, palmitoylation modulates intracellular trafficking, activity, and stability, and is regarded as a regulatory switch for proteins (*17*). The role of palmitoylation on polarized protein trafficking has been best characterized in neural cells, especially at the synapses (*6*, *11*, *12*, *14*). Synapses are polarized structures that relay electrochemical signals from dendrites to axons between adjacent neurons, and the polarized trafficking of synaptic proteins is essential for transmitting these signals between neurons (*11*, *122*). During neurotransmission, synaptic proteins including PSD-95, AMPA receptors, GABA receptors, NMDA receptors, δ-catenin, GRIP1, SynDIG1, SNAP-25, and synaptotagmin-1, shuttle between the cytosol, Golgi, vesicles, and synaptic membrane by palmitoylation (*11*, *14*, *34*, *55*, *77*, *78*, *108*, *123–127*). The immune synapse is similarly polarized when lymphocytes come in contact with target cells, which is required to activate lymphocyte function. Like in the neural synapse, palmitoylation regulates the shuttling of CD4, CD8, LAT, Lck/Fyn kinases between organelles and the synaptic membrane (*48*, *50*, *128–130*).

As mentioned earlier, Ras is palmitoylated at the Golgi to localize to the plasma membrane where it interacts with binding partners. Similarly, depalmitoylation keeps Ras signaling activity in check by localizing it back to the Golgi where it is inactive (*9*, *14*). As a small GTPase, Ras interacts with effectors PI3K, PLCξ, and RAF at the plasma membrane in its active, GTP-bound form. In its inactive GDP-bound form, Ras is localized to the Golgi for reactivation (*131*). Expression of palmitoylation-deficient mutant Ras or small molecule inhibition of APTs disrupts Ras activation and intracellular localization (*76*, *103*). Thus, the spatiotemporal regulation and distribution of Ras signaling activity requires palmitoylation (*103*, *132*). Fyn and GPCR activation cycles and intracellular shuttling between the Golgi to the plasma membrane are also dependent on palmitoylation in a manner similar to Ras (*15*, *133*).

Additional examples of palmitoylation-mediated intracellular trafficking are vast and diverse. Protein folding and assembly requires Calnexin, which localizes to endoplasmic reticulum-mitochondrial interaction domains and the nucleus through palmitoylation (*43*, *134*). Neurochondrin, a negative regulator of Ca++/calmodulin activity in neurons, is targeted and trafficked from endosomes to dendrites via palmitoylation (*32*). Palmitoylation of Bax, FAS death receptor, and Lck kinase mediates translocation from the cytosol to the mitochondria to induce apoptosis (*29*, *42*). Insulin-stimulated GLUT4 translocation to the plasma membrane from the cytosol is regulated by palmitoylation of the AKT substrate, CLIP-59 (*96*). Palmitoylation also ensures wing disc development by regulating the trafficking of the EGFR ligand Spitz to the basolateral membrane of cells (*74*). Furthermore, inhibition of GAD65 palmitoylation has been shown to downregulate the synthesis of GABA, a critical neurotransmitter (*77*). Sortilin, c-Met, and SRC kinases are additional examples of proteins requiring palmitoylation for their intracellular trafficking and activity (*24*, *92*, *135*, *136*).

Palmitoylation regulates protein activity by bringing interacting partners into close proximity, and can modulate kinase activity through conformational changes (*6*, *18*, *118*). EGFR is phosphorylated and interacts with signaling effectors on its cytosolic tail, which has been shown to be palmitoylated. This is thought to sterically hinder phosphorylation, Grb2 binding, and modulate its association with the plasma membrane in the absence of ligand binding (*26*, *27*). During glucose uptake in adipocytes, Caveolin2 is phosphorylated by Insulin receptor. Caveolin2 is also palmitoylated under these conditions, and it is thought the crosstalk between palmitoylation and phosphorylation induces a PI3K/Akt- and ERK- signaling cascade that promotes adipocyte proliferation and survival (*137*). FcLR4 is expressed in a subset of B lymphocytes and must be palmitoylated to be activated by phosphorylation; this in turn may enhance the activation of its substrate, NF-κβ (*45*). Palmitoylation inactivates Fat by inhibiting its

phosphorylation to regulate imaginal wing disc size by Hippo signaling (*138*, *139*). The methyltransferase activity and Golgi localization of the transcriptional repressor EZH2 is dependent on palmitoylation (*60*). Palmitoylation induces a conformational shift in the C-terminal tail of the ion channel STREX BK to sequester it at the plasma membrane, which activates the channel by sterically inhibiting phosphorylation from its negative regulator, Protein Kinase A (PKA) (*35*, *37*).

Correct protein folding and stability is regulated by crosstalk between ubiquitination and palmitoylation (*4*, *6*, *14*). Palmitoylated inhibitory SMADs are localized to the plasma membrane to target BMP type I receptors for ubiquitination, and modulate TGF-β/BMP signaling (*140*). Palmitoylation of the yeast SNARE protein, TLG1, induces a conformational shift that inhibits ubiquitination by facilitating endosomal and Golgi retention (*141*). Palmitoylation is also necessary for the stability of the Hippo pathway transcription factor, TEAD (*142*). Degradation of the anthrax receptor TEM8 is inhibited by palmitoylation, which prevents its targeting to lipid rafts where it would otherwise be ubiquitinated (*143*). In the endoplasmic reticulum, palmitoylation of the Wnt co-receptor LRP6 induces a conformational shift in the receptor which ensures correct folding of the protein and stability by blocking ubiquitination recognition sites (*68*).

These examples highlight an essential role for palmitoylation on maintaining signaling activity through protein conformation, stability, and binding partner interactions. Extracellular stimuli may also vary the intracellular distribution of DHHC enzymes and rate of palmitoylation, which may alter protein activity dynamics (*15*). Furthermore, localizing various DHHCs enzymes to distinct cellular compartments may also function as another layer of regulation to modulate protein trafficking and activity. Examining these protein distributions within tissues may shed insights on how signaling is disrupted in disease.

1.6 Palmitoylation function during development

Numerous studies, including the works mentioned thus far, have implicated palmitoylation as a key spatio-temporal regulator of signaling activity and demonstrate how altered palmitoylation is a factor in disease progression. Palmitoylation has been implicated as a critical factor in cell fate determination and differentiation in diverse species from plants to mammals. Across 31 plant species, DHHC-containing palmitoyl transferases were differentially expressed during cell growth and proliferation in different tissues at various developmental stages, even within the same plant (*144*). DHHC13 is thought to modulate Smad6 activity to specify ectoderm and mesoderm in zebrafish embryos (*65*). Palmitoylation has also been implicated in reproductive development where DHHC7 drives follicle stimulated hormone signaling in Sertoli cells in the testes, to ensure proper spermatogenesis and fertility (*145*). Ovaries expressing a palmitoylation-deficient Dad mutant showed a severe loss in the germline stem cell compartment and aberrant TGF-β/BMP signaling in *D. melanogaster* oocytes (*140*).

DHHC21-mediated palmitoylation of Fyn kinase is required for keratinocyte differentiation from epidermal stem cells and hair follicle development in mice, and inhibition of DHHC21 resulted in hair follicles with decreased Wnt signaling suggesting palmitoylation functions in epithelial homeostasis (*25*). Additionally, DHHC16 and DHHC5 have been suggested as critical factors of stem cell homeostasis *in vivo* and *in vitro,* where independent studies found these palmitoyltransferases to modulate the switch between multipotency and differentiation in neural stem and progenitor cells (*63*, *86*). Palmitoylation of the stem cell determinant, Poltergeist, is similarly essential to maintain the stem cell compartment in *Arabidopsis* roots (*66*).

Signaling pathways such as Wnt, Notch, Hippo, and EGFR are tightly coordinated during

embryogenesis to promote cell proliferation and differentiation. Modulating the activity of signaling pathways promotes organ specification, tissue remodeling, and inhibits aberrant proliferation in the adult. These examples identify a critical role for palmitoylation in understanding how signaling events are spatio-temporally regulated in response to ligand stimulation during embryogenesis and cell fate decisions.

1.7 Palmitoylation during cellular homeostasis and tissue maintenance

Because palmitoylated proteins are expressed in most tissues and play a role in maintaining homeostasis, any disruptions would be expected to result in developmental defects and disease. In addition to DHHC21, epithelial and skeletal tissue function is dependent on DHHC13. Loss of function mutations in DHHC13 are associated with various skin disorders including alopecia and hypotrichosis in patients. Furthermore, inhibiting DHHC13 activity in mice results in gross skeletal defects, decreased bone mass, multiple organ failure, osteoporosis, and amyloidosis (*25, 146–148*). Studies have shown DHHC7 and DHHC17 maintain glucose homeostasis in adipocytes in response to insulin signaling, and have identified additional palmitoylated substrates adipocytes with proteomic screens (*95, 96, 149*). Regulation of palmitoylation has also been shown to maintain lipid metabolism in liver and muscle, suggesting dysregulated palmitoylation may contribute to the development of metabolic disorders such as insulin resistance, hyperglycemia, and diabetes (*95–97, 150, 151*).

Gene expression and genomic stability may require palmitoylation, and over a quarter of palmitoylated mammalian substrates were identified as nuclear proteins (*18, 152*) . The transcription factor SNAIL, a known driver of epithelial-to-mesenchymal transition in tumors, regulates the expression of palmitoyltransferases and depalmitoylating enzymes. As many

palmitoylated substrates are also involved in cell polarity and tumor development, SNAIL may also affect the function these proteins at both the transcriptional and post-translational level (*121*, *153*). Palmitoylation of TEAD, a transcription factor of the Hippo pathway, promotes its interaction with transcriptional co-activators YAP and TAZ to mediate Hippo pathway signaling during tissue growth and muscle differentiation (*101*, *142*). Lyn kinase, as mentioned earlier, is palmitoylated in a cell-cycle dependent manner to inhibit its nuclear localization and prevent chromosomal segregation errors (*24*). Both loss of DHHC16 and pharmacologic inhibition of palmitoylation impair DNA damage response in cells by blocking G2/M progression and inhibiting ATM-p53 signaling (*59*). In yeast, palmitoylation of the telomere-binding protein Rif1 modulates transcriptional silencing and heterochromatin formation (*61*). Furthermore, silencing DHHC8 in radiation-treated mesothelioma cells impairs G2/M progression, and increases chromosomal instability and apoptosis (*62*).

In recent years, palmitoylation has been found to play a large part in immune cell fate and function in adult tissues. A key step in immune cell function is antigen stimulated protein recruitment to the immune synapse. Similar to neuronal synapses, the polarized recruitment of many synaptic proteins requires palmitoylation (*46*). The development of memory B lymphocytes and T cells is dependent on palmitoylation of the immunomodulatory receptors FcLR4 and LAT, respectively (*45*, *48*). Interestingly, palmitoylation itself is regulated during periods of anergy (inactivity) and activation. This is observed with LAT, where its palmitoylation is downregulated in anergic T cells (*47*).

Ion-mediated second messenger signaling (calcium- or sodium-mediated) affects the function of many enzymes, mediates electric impulses, and is essential for cellular homeostasis. Acute regulation of ion channels and pumps is critical to maintain ion homeostasis and flux to prevent cellular stress and death (*41*, *154*). Several pumps and channels have been reported to be

palmitoylated in various tissues including cardiac and skeletal myocytes, fibroblasts, pancreatic β-cells, and embryonic kidney cells. Additionally, both pharmacologic and genetic perturbation of palmitoylation may induce mitochondrial dysfunction and cellular stress (*35*, *36*, *39*, *40*, *100*, *155*). Senescence and apoptosis prevent the accumulation of damaged cells in healthy tissues, and studies show evidence of these cellular responses requiring palmitoylation (*26*, *29*, *33*, *56*, *156*) [26,29,33,56,160].

Extensive studies mentioned in this chapter demonstrate palmitoylation is critical for neural development and function. Communication between neurons requires the precise coordination of neurite formation and synaptic communication, two processes that both require palmitoylation for polarized protein transport as mentioned earlier (*157*). Dysregulated palmitoylation is closely associated with the onset of disorders such as Huntington's disease, Alzheimer's, anxiety, learning disorders, and schizophrenia (*6*, *11*). Decreased or complete loss of DHHC13 and DHHC17 is a major driver of Huntington's onset and progression (*78–80*, *158*, *159*). In addition to maintenance of synapse function, DHHC7, DHC12, and DHHC21 may be misexpressed in Alzheimer's patients and have been implicated in preventing amyloid plaques widely thought to contribute to Alzheimer's pathogenesis (*82*, *83*, *160*). Suppression of DHHC5, DHHC8, and DHHC13 activity and expression has also been linked to learning/memory defects, schizophrenia, and anxiety disorders (*84*, *85*, *87*, *161*).

Surprisingly, the role of depalmitoylating enzymes on homeostasis and disease remains poorly understood. APT1-knockout male mice display significantly decreased body fat according to the International Mouse Phenotype Consortium, suggesting APT1 is critical for adipose tissue development, homeostasis, and endocrine regulation by adipose tissue (IMPC). Both APT1 male and female knockout mice have also been characterized with behavioral defects (IMPC). However, the mechanisms by which APT1 maintains behavior and adipose homeostasis remain

unknown. Mutations in PPT1 have also been identified and associated with infantile Batten disease, a debilitating and fatal neurodegenerative disorder (*162*). Examining palmitoylation with other posttranslational modifications during cellular processes in normal tissues may uncover novel regulatory networks for spatiotemporal signaling pathway regulation.

1.8 Palmitoylation function in cancer development

Several DHHC enzymes may demonstrate tumor promoting or tumor suppressor function, or both, in various cancers. Downregulated expression of DHHC2 has been correlated with increased liver metastasis and poor prognosis for gastric and colorectal cancers (*90*, *163*). Silencing DHHC3 expression results in suppressed tumor cell migration and invasion through decreased Integrin α6β4 palmitoylation, suggesting potential oncogenic function. Conversely, DHHC3 may also function as a tumor suppressor as its decreased expression was observed in squamous cell cervical cancer and hepatocellular carcinoma (*23*, *164*, *165*). Overexpressed zHHC5 was reported as a driver of tumor initiation in non-small cell lung cancer cell models, and has also been linked to increased tumorigenic and self-renewal potential of p53-mutant glioma cells (*60*, *166*).

The hormone receptors ERα, ERβ, PR, and AR have been identified as substrates of DHHC7, suggesting DHHC7 activity may contribute to the development of hormone-positive tumors. Palmitoylation of these receptors facilitates their membrane localization, which has been associated with enhanced metastasis and tumorigenic potential through nuclear-independent activity (*23*, *118*, *167*). Scribble, a regulator of cell polarity and neuronal synaptic function, is a membrane-localized tumor suppressor. Its membrane localization is regulated by DHHC7, and is inhibited by the EMT driver SNAIL, which has been shown to transcriptionally repress

palmitoylation (*53*, *153*). Future examination of SNAIL on palmitoyltransferase expression may reveal greater insights on the localization and expression of tumor suppressors and polarity regulators in the developing embryo, adult tissue, and within tumors. Increased DHHC11 expression has also been associated with aggressive bladder tumors (*91*). Additionally, DHHC13 may exhibit tumor suppressor function in melanoma and other skin carcinomas (*57*, *146*). High DHHC14 expression is correlated with poor disease outcomes in gastric cancer patients, and was found to increase tumor cell invasion and migration (*89*). Numerous studies have demonstrated that palmitoylation of CD9, CD44, CD151, Claudin7, and c-Met, require palmitoylation for metastatic potential (*88*, *92*, *93*, *164*, *168*). Palmitoyltransferases may also be differentially expressed or serve different functions within the same type of tumor. In breast, ovarian, colorectal and blood tumors, DHHC9 expression was downregulated while DHHC20 and DHHC21 are overexpressed (*23*, *94*, *167*). DHHC14 and DHHC17 may also function differentially as tumor suppressors or oncogenic drivers depending on the cancer type (*23*).

Depalmitoylating enzymes, while less studied, also exhibit differing functions in tumor development and progression. APT1 is frequently amplified in various human cancers including prostate, uterine, and breast, and this amplification may correlate with poorer survival outcomes according to The Cancer Genome Atlas (TCGA). PPT1 is also generally amplified in tumors, while APT2 and PPT2 is often deleted or mutated (TCGA). Wnt5a stimulates APT1 phosphorylation driving its depalmitoylating activity, and expression of APT1 phosphomimetic or inactivating mutants implicates APT1 as a regulator of melanoma cell invasion and metastasis, thus uncovering a role for depalmitoylation in Wnt5a-overexpressing tumors (*70*, *169*).

Protein palmitoylation may also be exploited for therapeutic purposes. For example, silencing DHHC20 and EGFR palmitoylation deficient mutants increase the sensitivity to EGFR kinase inhibitors in human triple receptor negative breast cancer cells and in Kras mutant cells

(*26*, *170*). As mentioned in previous sections, small molecule inhibition of APT1 can disrupt Ras membrane localization and downregulate signaling. These molecules have been explored as a therapeutic strategy in suppressing Hras and Nras mutant function, although with variable results (*75*, *103*, *119*, *171*). With such a large pool of palmitoylated substrates, identifying bona-fide substrate-enzyme pairs may uncover greater therapeutic efficacy and specificity to palmitoylated proteins when designing inhibitors or drug combination treatments (*23*). This strategy has been employed to target Ras depalmitoylation is induced upon FKBP12 binding. Pharmacologic inhibition of FKBP12 was shown to increase amounts of palmitoylated Ras at the plasma membrane, potentially increasing exposure of the active Ras form to inhibitors (*172*). Understanding these enzyme-substrate interactions may also increase our understanding of drug resistance in recurrent tumors to uncover areas for therapeutic development.

1.9 Palmitoylation establishes and maintains polarity

As mentioned in earlier sections, palmitoylation directs protein polarity within cells and across multicellular structures to facilitate and maintain responses to signaling pathways. Pharmacologic inhibition and genetic screens identified palmitoyltransferases necessary for the formation and growth of polarized root hairs, which are sensory structures in *Arabidopsis that* transmit external stimuli (*173*). The division and growth of fission yeast occurs along a polarized axis, which promotes membrane growth as the yeast increase in size. Establishment this polarized axis is dependent on the membrane localization of yeast casein kinase 1γ ortholog, Cki3, which is driven by palmitoylation, and yeast expressing palmitoylation-deficient Cki3 show a growth delay (*31*).

In *D. melanogaster* wing discs, Approximated palmitoylates Fat, a negative regulator of growth that restricts Dachs accumulation at apical junctions to inhibit Hippo signaling(*138*). Palmitoylation of Fat negatively regulates its activity, allowing for Dachs accumulation at apical junction to drive wing growth (*138, 139*). The association of the discs large homolog, MPP3, and nectins at apical cell junctions is also dependent on palmitoylation of MPP3; this has also been shown necessary to set up the polarity of the developing *D. melanogaster* embryo (*174*). The formation and stability of polarized cell junctions is crucial in the maintenance of epithelial barrier integrity and cell-cell communication (*175*). Proteins required for cell junction assembly and maintenance, including PMP22, Plakophilin, JAM3, SNAIL, and Claudin7, maintain their polarized localization and function through direct palmitoylation (*51, 52, 54, 88, 99, 121*).

Cytoskeletal regulators and components have also been reported as palmitoylated substrates. Palmitoylation of tubulin has been shown to be essential for membrane association during cell division and spindle stability during meiosis in yeast. Whether palmitoylation is also required for membrane association in non-dividing cells, polarized trafficking, or if its palmitoylation is regulated in a cell-cycle dependent manner remains to be determined (*176–178*). Other small GTPases involved in actin reorganization and vesicular trafficking, such as RhoB, RAC1, and RAB10, require palmitoylation to localize at membrane compartments (*179–181*). Additionally, palmitoylation of the master polarity regulator CDC42 is necessary for proper dendrite formation and synaptic function in hippocampal neurons (*181–183*).

As polarity is essential to properly localize signaling components in the developing embryo and in adults to maintain tissue integrity, it is thought to function as a tumor suppressor mechanism (*184*). How palmitoylation establishes these interactions may uncover greater insights into developmental disease and tumor initiation and progression.

1.10 Limitations to studying palmitoylated proteins

Palmitoylation was first discovered in 1979, the same year as phosphorylation and four years after ubiquitination (*185–187*). Although it is as common as phosphorylation and ubiquitination, very little is known about the biological impact and function of palmitoylation in an organism. Detection methods also lag far behind those of phosphorylation and ubiquitination (*188*).

Libraries of hundreds of putative palmitoylated substrates have been assembled from genomic and proteomic screens from diverse species including *Drosophila melanogaster*, *Caenorhabditis elegans*, yeast *(Schizosaccharomyces pombe, Cryptococcus neoformans, Saccharomyces cerevisiae)*, parasites (*Toxoplasma gondii*, *Plasmodium falciparum)*, *Danio rerio*, *Arabidopsis thaliana* and mammals (human: prostate cancer cells, B lymphoid cells, endothelial cells, Jurkat T cells, platelets, rat neurons, and mouse T cell hybridoma cells) (*16*, *18*, *22*, *58*, *63*, *65*, *66*, *189–192*). Although palmitoylated proteins can be detected with high-throughput means such as mass spectrometry, the hydrophobicity, poor solubility, and poor fragmentation of palmitoylated proteins has made this approach extremely challenging and prone to false negatives (*188*, *193*). Furthermore, validating bona-fide palmitoylated substrates from libraries is predominantly based off generating point mutants and can be an unwieldy endeavor if the number of palmitoylated cysteines is unknown or if data sets are large (*15*, *18*). *In silico* approaches, such as Swiss-palm, CSS-palm, and GPS-lipid, predict putative substrates and palmitoylated residues based on databases of known palmitoylated sequences (*18*, *152*). Again, the lack of a consensus sequence can result in false omission or identification, and thus, *in silico* approaches should be combined with protein structure analysis and biochemical validation.

Limitations in protein-based and fluorescence-based have also increased the difficulty of identifying and validating palmitoylated substrates. Immunoblotting based approaches in cell and tissue lysates can be used identify changes in global palmitoylation or validate specific substrates from libraries or *in silico* methods. When combined with metabolic labeling using azido- or alkyne-palmitate analogs, this approach can provide insights into relative palmitate turnover. However, metabolic labeling may not be sensitive enough to detection of proteins with a low turnover rate, resulting in false reporting as non-palmitoylated (*18*). Acyl-biotin exchange (ABE) and variations have also emerged as a reliable and relatively sensitive detection immunoprecipitation-based assay where the reactive thiol on palmitoylated cysteines is replaced with a biotin analog (*194*, *195*). Because metabolic labeling is not required in this assay, substrates can theoretically be detected regardless of palmitate turnover rates. A variation of the ABE assay, known as the acyl-PEG exchange (APE), can also be used to detect the number of palmitoylated cysteines on a protein (*196*). These assays must be rigorously controlled to prevent reporting of false-positives, as any reactive cysteine can be detected (*11*, *16*, *177*).

Another significant setback is the challenge of visualizing the spatio-temporal regulation of palmitoylated protein localization and turnover *in situ*. The lack of a defined consensus sequence has made it difficult to design antibodies to palmitoylated domains (*15*). Live-imaging probes have also not yet been designed to examine temporal dynamics of palmitoylation within cells (*18*). Early imaging approaches have involved fluorescently tagging palmitoyltransferases, depalmitoylating enzymes, putative substrates, and corresponding mutants, and imaging subcellular localization. TIRF and FRAP microscopy techniques may also assess the localization dynamics of palmitoylated substrates by live-cell microscopy (*15*). Caveats of these imaging approaches include an inability to assess is palmitate incorporation in real time, and substrates may not have been rigorously validated as palmitoylated (*15*, *102*).

The first successful imaging protocol incorporated metabolic labeling to visualize palmitoylated protein localize at plasma membrane, at membrane domains near the mitotic spindle, and at the cytokinetic furrow (*115*). Advancing this protocol, Gao *et. al*, utilized this metabolic labeling approach and combined it with *in-situ* proximity ligation to detect the subcellular localization of palmitoylated Wnts, Hedgehog, and tubulin in fixed cells (*177*). Although prone to false-positives and requiring rigorous validation, these methods have expanded our understanding of the spatial organization of palmitoylated effectors.

Development of small molecule inhibitors can interrogate the role of palmitoylation on protein localization, activity, and protein-protein interactions. 2-bromopalmitate (2-BP) is utilized as a pan-palmitoyltransferase inhibitor. However, results are inconclusive unless validated with genetic knockdown or protein mutants as 2-BP exhibits many off-target effects, and may disrupt lipid homeostasis and metabolism at high concentrations (*6*). Depalmitoylating enzyme inhibitors have been more successful in terms of specificity and toxicity. Palmostatin B and Palmostatin M are common inhibitors to APT1 and APT2, and to a lesser degree, PPT1 and PPT2 (*67*, *75*, *103*, *132*) [67,75,103,131]. Newly identified piperazine amide compounds ML-348 and ML-349 display high sensitivity and specificity for APT1 and APT2, respectively (*171*). These compounds have been employed successfully to examine palmitoylation dynamics *in vitro*, but not yet used *in vivo*. Although there is still a great deal of information missing including structure analysis, crystal structures for APT1, DHHC15, DHHC17, and DHHC20 have been solved (*197–199*). This structural analysis of DHHCs may uncover new functional insights into the regulation of palmitoylation, and may contribute to the development of specific inhibitors with minimal off-target effects. Additionally, specific inhibitors may be used better understand the biologic function, protein interaction, and the dynamic regulation of palmitoylation during development or

in disease settings (*15*, *18*). These studies open up future work into developing specific small molecule inhibitors for therapeutic strategies in patients.

1.11 Discussion

While the function and regulation of palmitoylation on normal cellular functions, development, and disease is still rather unclear, palmitoylation is emerging as an essential regulatory component of cell signaling. The last few years have seen substantial advances in new detection protocols and assay sensitivity, and new studies are identifying novel palmitoylated substrates uncovering greater networks of pathway crosstalk. For example, many signaling pathways are activated during hair follicle development including Wnt and ERK, and palmitoylation is known to play a major role in hair follicle formation (*25*, *148*). In addition to Wnt ligands, the signaling pathway components LRP6 and casein kinase have been shown to be palmitoylated in the last 15 years (*28*, *69*, *200*). How palmitoylation facilitates crosstalk for these pathways during hair follicle formation has not been explored. Furthermore, whether palmitoylation coordinates the assembly of the Wnt signaling complex and downstream activity upon ligand binding in a tissue-dependent context, or even within the same cell, remains an unanswered but important question. Additionally, palmitoylation remains poorly defined within many critical developmental signaling pathways, as in the case of Notch, where Numb is the only component known to be palmitoylated to date (*71*).

Numerous examples in this chapter discuss how palmitoylation facilitates polarized protein trafficking between cellular components. Polarity itself is regulated by a complex signaling network, yet only a few polarity regulators (e.g. CDC42, Scribble, Rac) have been shown to be palmitoylated (*53*, *179*, *181–183*). Palmitoylation of additional polarity components

such as PAR proteins and atypical PKC is currently unknown. How palmitoylation coordinates these protein interactions to establish polarity in both development and disease will be vital to address. The numerous examples in these sections also demonstrate how palmitoylation plays a prominent, but relatively unexplored role, in disease onset and highlight areas where palmitoylation can be exploited for therapeutic strategies.

In this dissertation, I identify a function for APT1 and DHHC20 in establishing polarized protein localization during cell division. I also present a role for APT1 in maintaining gene signatures and in restricting transcription activity of cell-fate signaling pathways to one daughter cell. Furthermore, I interrogate how loss of APT1 decreases the self-renewal potential of breast cancer cells and alters the distribution of tumorigenic cells. With these findings, I present a molecular mechanism for palmitoylation-mediated of asymmetric cell division and develop a conceptual framework for the maintenance of tumor cell heterogeneity.

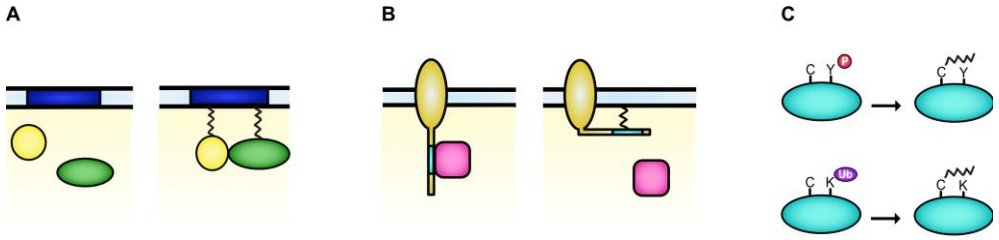

Figure 1.1 Palmitoylation regulates protein-protein interaction, activity, and stability. (**A** to **C**) Palmitoylation promotes the membrane localization of cytosolic proteins (yellow and green) to specialized domains (dark blue) to facilitate protein-protein interaction at the membrane (A), can sequester cytosolic facing domains or receptors and integral membrane proteins (dark yellow) to inhibit effector (pink) binding (B), and may sterically hinder other posttranslational modifications such as phosphorylation (red) or ubiquitination (purple) to regulate protein activity and stability (C).

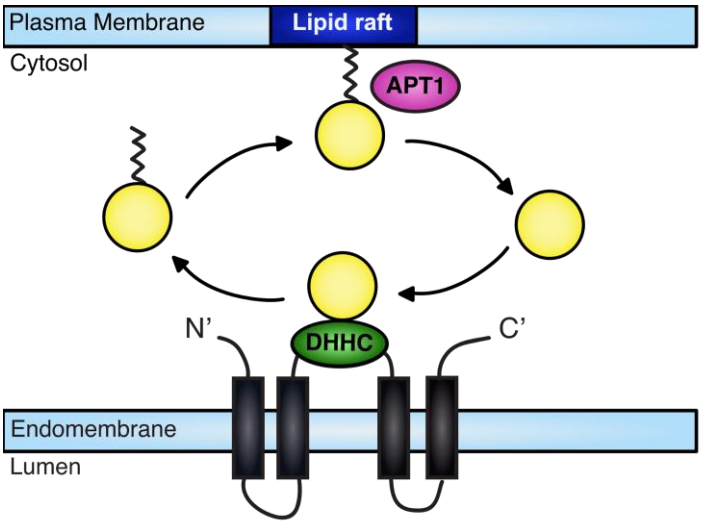

Figure 1.2 Schematic of palmitoylation. Addition of palmitate to a protein is catalyzed by the DHHC class of enzymes localized on endomembrane (e.g. Golgi, endoplasmic reticulum, vesicles) or on the plasma membrane, which facilitates membrane association. Depalmitoylating enzymes, such as APT1, localize to the membrane to cleave palmitate from substrates via its catalytic cleft. This process allows both APT1 and the non-palmitoylated substrate to relocalize to the cytosol for recycling or degradation. Adapted from Conibear *et. al.* (*9*).

CHAPTER 2: IDENTIFICATION OF PALMITOYLATION ON ASYMMETRIC PROTEIN SEGREGATION AND TRANSCRIPTIONAL ACTIVITY

From Stypulkowski, *et. al*. The depalmitoylase APT1 directs the asymmetric partitioning of Notch and Wnt signaling during cell division. *Sci. Signal.* **11,** (2018). Reprinted with permission from AAAS.

2.1 Summary:

Asymmetric cell division is a key mechanism of generating and maintaining diverse cell populations, such as stem cells and differentiated cells. Understanding the mechanisms regulating the asymmetric localization of cell fate determinants in dividing cells is critical as loss of asymmetric division has been associated with the improper expansion of cell populations and altered cell fate, resulting in abnormal tissue function. As discussed in Chapter I, palmitoylation is a mechanism of localizing proteins to subcellular membrane domains and can regulate signal transduction activity in the cell. However, the function of palmitoylation has not been examined in asymmetrically dividing cells. In this Chapter, I show that asymmetric protein localization in dividing cells is dependent on palmitoylation. Furthermore, I demonstrate how the depalmitoylating enzyme, APT1, and palmitoyltransferase, DHHC20, affect the asymmetric expression of transcriptionally regulated GFP reporters between daughter cells. These findings introduce lipid modification as a regulator of asymmetric cell division.

2.2 Introduction:

The development of multicellular organisms relies on the ability to generate functionally diverse tissues and organs from an unspecialized stem cell (*201*). One mechanism of generating this cellular heterogeneity is through asymmetric cell division where proteins driving cell identity, also known as cell-fate determinants, are unequally distributed between two dividing daughter cells. Stem cells are the best-characterized population that undergoes an asymmetric cell divisions, producing a self-renewing stem cell and a differentiating daughter cell (*5*).

To initiate an asymmetric division, cell fate determinants must be localized to the plasma membrane domains in an orientation perpendicular to the mitotic spindle. This ensures that one daughter will inherit more cell-fate determinants upon cytokinesis, which activates a downstream transcriptional program that will establish a distinct identity from the other daughter cell (*202–205*) (Fig. 2.1). For example, *D. melanogaster* neuroblasts divide asymmetrically to produce a self-renewing neuroblast and a differentiating daughter cell (*206, 207*). This polarity of cell-fate determinants may be induced through extrinsic signals from the extracellular environment or through intrinsic polarity (*208*). Like developing embryos and normal tissues, cells within tumors also vary in functions such as proliferation, survival, self-renewal, quiescence, genomic instability, and therapeutic resistance (*209–211*). However, the contributors of tumor cell heterogeneity are not fully understood. Genomic instability, epigenetic alterations, and microenvironment interactions are major contributors but are not the only factors (*212–214*). While asymmetric cell division has been commonly thought to function as a tumor suppressive mechanism to prevent aberrant stem cell outgrowth (*184*, *201*), its contribution to cellular heterogeneity later in tumor development is not fully understood.

The Notch and Wnt signaling pathways have been shown to be key drivers of cell

identity. Numb, an antagonist of Notch, is asymmetrically partitioned to the plasma membrane of dividing *D. melanogaster* neuroblasts, and is inherited by the cell fate to differentiate into a neuron (*206*, *207*, *215–217*). In mammalian cells, Numb is asymmetrically partitioned in dividing mammary epithelial precursors, hematopoietic stem cells, and T-lymphocyte precursors (*202*, *218*, *219*). Likewise, β-catenin, a regulator of canonical Wnt and progenitor cell fate, is asymmetrically localized at the plasma membrane of dividing mouse embryonic stem cells and *C.elegans* seam cells, and is excluded from the differentiating daughter cell (*204*, *220*).

How Numb and β-catenin are unequally partitioned and retained at the membrane has been a major challenge in the field, although several mechanisms have been proposed. Mouse embryonic stem cells grown *in vitro* and *C. elegans* seam cells divide asymmetrically in response to a localized extracellular Wnt stimulus. This reorients the mitotic spindle so that the daughter cell closest in proximity to the Wnt signal inherits β-catenin and retains a progenitor fate (*220*, *221*). Likewise, Numb is segregated asymmetrically along an apical-basolateral axis in dividing *D. melanogaster* neuroblasts, where the apical cell in contact with the neuroepithelium retains a progenitor fate, while the basal cell inherits Numb and differentiates (*206*, *215*, *217*) (Fig. 2.2 A). This would suggest that an extracellular cellular signaling gradient could induce the localization in a concentration-dependent manner to induce an asymmetric division, such as in the stem cell niche (*5*, *222*, *223*). Phosphorylation-induced signal cascade have also been proposed as a mechanism of asymmetrically segregating proteins in dividing cells. Studies from several groups have shown that aPKC phosphorylates Numb directly to displace it from the apical membrane. Additionally, apical aPKC localization is maintained through a negative feedback loop with Lgl, a target that is phosphorylated by aPKC to restrict Numb to the basolateral domain (*215*, *224*, *225*) (Fig. 2.2 B). Partitioning protein degradation machinery between daughter cells has also been proposed as a mechanism of asymmetrically segregating proteins (*203*). In the mouse

embryonic stem cells and in *C. elegans* seam cells mentioned above, β-catenin asymmetry is reinforced by the asymmetric segregation of the APC destruction complex (which phosphorylates β-catenin) in the daughter cell farthest away from the Wnt signal (*204*, *220*)(Fig. 2.2 C). It is important to note is these mechanisms function together to establish and maintain polarized protein localization. What remains unclear is how these asymmetric domains of cell fate determinants are maintained at the plasma membrane over the course of cell division long enough to result in altered cell fate (Fig. 2.2 D).

Although lipid modifications have been shown in Chapter I to regulate protein polarity and intracellular localization, the role of lipid modifications on protein localization during asymmetric cell division has not been studied. Being a reversible lipid modification, palmitoylation could promote asymmetric membrane association and also allow for interaction with cytosolic proteins through depalmitoylation (Fig. 2.2 D). Additionally, the role of asymmetric cell division on tumor cell heterogeneity remains unclear, although palmitoylation has been shown to be a key regulator of protein localization and activity in cancer as discussed in Chapter I. Here, I use triple receptor negative breast cancer and osteosarcoma cell lines, derived from tumors reported to exhibit a high degree of cellular heterogeneity (*226–230*), as a biochemically tractable model to interrogate the cell-intrinsic factors that regulate asymmetric protein localization in dividing cells. I show that not only are Numb and β-catenin asymmetrically localized in dividing cancer cells, but also this localization is dependent on APT1 and DHHC20. Furthermore, pharmacologic inhibition of APT1 recapitulates this observation. I also show that Numb and β-catenin are palmitoylated in cancer cells, and mutation of specific cysteine residues on Numb decreases both its palmitoylation and asymmetric localization. Finally, I show that Notch- and Wnt- transcriptional GFP reporters are asymmetrically expressed in daughter cells, and this asymmetric activation is dependent on APT1 and DHHC20. Together, these results

provide evidence for a role for palmitoylation-mediated asymmetric cell division, which may contribute to tumor cell heterogeneity.

2.3 Activity of the depalmitoylating enzyme APT1 is required for asymmetric localization of proteins

The depalmitoylating enzyme APT1 has been previously shown to promote the transient and asymmetric localization of cell adhesion molecules during interphase in response to extracellular signals (*70*). To test the hypothesis that APT1 directs the asymmetric localization of Notch and Wnt signaling-associated cell fate determinants, during cell division, I first set up parameters to score a dividing cell as asymmetric. I examined the spatial organization of Numb, β-catenin, and the palmitoylated proteins CD44 and RhoB (*93*, *180*, *231*, *232*) in fixed cells to determine if asymmetric protein localization was a common trait in dividing cells. Using the human MDA-MB-231 triple receptor–negative breast cancer cell line, dividing cells were identified by immunostaining for acetylated tubulin, a marker of stabilized tubulin structures such as the mitotic spindle and cytokinetic midbody (*233*), and counterstained for Numb, β-catenin, CD44, or RhoB. To rule out the possibility of any observed asymmetric protein localization being the result of intracellular diffusion, I expressed a control GFP plasmid and assessed GFP localization by immunofluorescence. To assess whether a cell divided asymmetrically or not, I measured and plotted the percentage difference in the mean fluorescence pixel intensity of the protein signal across dividing cells with the following equation (Fig. 2.3 A, B):

$$\Delta\ \%\ \text{difference} = \frac{(\text{ROI 1} - \text{ROI 2})}{((\text{ROI 1} + \text{ROI 2})/2)}\ \text{X } 100$$

Generally, most dividing cells displayed symmetric protein localization in the absence of exogenous stimuli (Fig. 2.3 B). Individual cells with a percentage difference of 20 or greater were scored as asymmetric, and the total percentage of asymmetrically dividing cells was plotted according to the equation below:

$$\% \text{ asymmetric in total population} = \frac{\#\text{ cells with \% difference} > 20}{\text{total \# cells}} \text{ X } 100$$

β-catenin was asymmetrically localized in 26.1% of cells, Numb in 29.4% of cells, RhoB in 8.3% of cells, CD44 in 12.2% of cells, and GFP in 8.5% of cells (Fig. 2.3 C-G). Treating cells with Palmostatin B (PalmB), a pharmacological inhibitor of APT enzymes (*234*), reduced the asymmetric localization of Numb by 3.0-fold (29.4% vs. 9.9%) and β-catenin by 3.3-fold (26.1% vs. 8.0%) (Fig. 2.3 C, D). The percentage of cells with asymmetrically localized GFP, CD44, or RhoB were not higher than the background percentages observed for β-catenin and Numb (approximately 8%), and were unaffected by PalmB treatment (fig. 2.3 E-G). These findings suggest that APT enzymes are required for establishing asymmetric localizations of Numb and β-catenin in dividing cells.

2.4 APT1 and DHHC20 are required for asymmetric Numb and β-catenin localization in dividing cells

Having shown the asymmetric localization of Numb and β-catenin (Fig. 2.3 A, B) can be perturbed by inhibiting the activity of depalmitoylating enzymes, I asked whether APT1 was specifically required. To address this question, I knocked down APT1 with a short hairpin RNA (shRNA) (Fig. 2.4 c). In APT1 knockdown cells, asymmetric localization of Numb was reduced by 6-fold (29.4% vs. 4.9%), and asymmetric localization of β-catenin was reduced by 4.1-fold

(26.1% vs. 6.4%). Ectopic expression of wild-type human APT1 ($APT1^{WT}$) from a plasmid restored asymmetric localization of Numb and β-catenin to baseline control conditions (Fig. 2.4 E-H). However, ectopic expression of a catalytically inactive mutant form of APT1, in Ser^{119} in the catalytic domain is mutated to Ala ($APT1^{S119A}$) (*132*, *235*), failed to rescue asymmetric Numb and β-catenin localization (Fig. 2.4 E-H). This indicates that the catalytic activity of APT1 is critical for asymmetric Numb and β-catenin localization.

Of the 23 DHHC palmitoyltransferases found in mammalian cells, DHHC20 is one of three localized to the plasma membrane and is also known to be expressed in MDA-MB-231 cells, where it palmitoylates EGFR and attenuates EGFR signaling (*26*, *236*). Therefore, I would expect it to be available to palmitoylate targets like Numb and β-catenin. To determine whether loss of DHHC20 affected protein localization, I knocked down DHHC20 and observed reduced asymmetric localization of Numb and β-catenin in a manner similar to APT1 knockdown (Fig. 2.4 D-F, I, J).

The dependence of Numb and β-catenin asymmetric localization on APT1 suggests that Numb and β-catenin may be palmitoylated. To evaluate protein palmitoylation in native cell conditions, I used acyl-biotin exchange (ABE) assays (*194*). In the ABE assay, proteins are treated with N-ethylmaleimide to block free thiol groups, then the Cys-palmitoyl thioester linkages are cleaved with hydroxylamine (HAM), and the newly exposed thiol groups are coupled to biotin. The modified proteins are then purified with streptavidin (Fig. 2.5 A). Results of ABE assays were consistent with Numb and β-catenin being palmitoylated under normal growth conditions (Fig. 2.5 B, C). Treating cells with PalmB increased the total amounts of palmitoylated Numb and β-catenin (Fig. 2.5 B, C), indicating that palmitoylation of these proteins was inhibited in part by APT enzymes. As a negative control, I did not detect palmitoylation of the extracellular signal–regulated kinase (ERK), which is not known to bepalmitoylated (Fig. 2.5 D).

Together, these findings uncover a role for APT1, and palmitoylation in general, in the spatial distribution of the palmitoylated cell fate determinants Numb and β-catenin.

2.5 Asymmetric localization of Numb requires palmitoylation of the phosphotyrosine binding domain

Although I found β-catenin to be palmitoylated, β-catenin cortical localization is mediated through association with cadherins at tight junctions (*237*, *238*). However, the necessity of palmitoylation for the membrane localization of β-catenin is unclear and will be discussed in later chapter. The conserved phosphotyrosine binding (PTB) domain of Numb is required for association of Numb with the plasma membrane and for asymmetric localization of Numb in *D. melanogaster* through mechanisms that are still unknown (*239*). I sought to directly test whether palmitoylation of Numb is required for its asymmetric localization. Using the palmitoylation prediction algorithm CSS-Palm (*240*) and through identification of solvent-exposed cysteine residues within the PTB domain crystal structure (*241*), three conserved and potentially palmitoylated cysteine residues (Cys^{37}, Cys^{160}, and Cys^{165}) were identified and mutated to Ala (Fig. 2.6 A, B). The Numb triple Cys-to-Ala mutant ($Numb^{AAA}$) showed reduced palmitoylation as measured by metabolic labeling of cells with palmitic acid azide, which allowed for the study of palmitate turnover on Numb (Fig. 2.6 C). Endogenous β-catenin was also metabolically labeled with palmitic acid azide, confirming the efficiency of labeling in all reactions (Fig. 2.6 C). These results demonstrate that Numb and β-catenin are continuously palmitoylated in MDA-MB-231 cells.

Next, I visualized the dynamic localization and segregation of fluorescently labeled Numb and APT1 during cell division by live-cell imaging. Because MDA-MB-231 cells shifted from a

flat, spread morphology to a raised, rounded morphology out of the imaging plane during cell division, I instead utilized U2 OS human osteosarcoma cells, which maintained a consistent rounded morphology within the imaging plane during division. U2 OS cells were transduced to stably express a mCherry-Histone B (H2B) plasmid, allowing for the unambiguous identification of cells undergoing division in real time. Over the course of cell division, cyan fluorescent protein (CFP)-tagged APT1^{WT} (APT1^{WT}-CFP) and yellow fluorescent protein (YFP)-tagged Numb^{WT} (Numb^{WT}- YFP) exhibited highly dynamic asymmetric localization (Fig. 2.6 D). At the beginning of the cell division cycle, Numb^{WT} was concentrated at one end of the cell at the plasma membrane, but as daughter cells formed, the localization of Numb shifted to membrane regions at and near the cleavage furrow. Finally, as daughter cells separated, Numb was partitioned to the plasma membrane of the cell that emerged from the same side of the mother cell to which Numb was initially concentrated. APT1^{WT} co-segregated with Numb to membrane regions and retained in daughter cells with high Numb signal as indicated by line-scan analysis of YFP and CFP pixel intensity along the division axis (Fig. 2.6 D, Movie S1-3, red arrows). This suggests that APT1 either responds to the same spatial cues as Numb. Alternatively, APT1 may direct Numb localization or vice versa. YFP-tagged Numb^{AAA} (Numb^{AAA}-YFP) was live-imaged to determine the contribution of Numb palmitoylation on its localization. Numb^{AAA} showed a 1.5-fold reduced asymmetric localization in dividing cells as compared to Numb^{WT} (Fig. 2.6 E). Finally, knocking down APT1 reduced asymmetric Numb^{WT} localization but did not further reduce the asymmetry of Numb^{AAA} (Fig. 2.6 E). These results collectively show that the asymmetric partitioning of Numb is actively maintained by a mechanism that requires both APT1-mediated depalmitoylation and palmitoylation of Cys^{37}, Cys^{160}, and/or Cys^{165} within the PTB domain.

2.6 APT1 restricts Wnt and Notch transcriptional activity to one daughter cell

One downstream effect of asymmetrically partitioning cell fate determinants during cell division is the activation of different transcriptional networks in the two daughter cells, resulting in cells with unique transcriptional profiles (*203*, *204*, *206*). I hypothesized that APT1 could also mediate the partitioning of asymmetric transcriptional activity of the Notch and Wnt-β-catenin signaling pathways to one daughter cell. I expressed GFP reporter transgenes containing Notch-activated RBPJ (recombination signal binding protein for immunoglobulin kappa J region) binding sites (pGF1-Notch) (*242*, *243*) or Wnt-activated TCF and Lef1 binding sites (pGF1-TCF/Lef1) in MDA-MB-231 cells, which were then immunostained for GFP and acetylated tubulin in daughter cells (Fig. 2.7 A, B). After plotting the distribution of asymmetric divisions as described in fig. S1, I observed asymmetric Notch and TCF/Lef1 reporter signal in 22.7% and 31.7% of daughter cells, respectively. A control GFP reporter containing a minimal CMV promoter (mCMV) lacking pathway-specific promoter elements showed symmetric signal in most cells and confirmed that the observed asymmetries were dependent on the TCF/Lef1 and Notch enhancer elements (Fig. 2.7 C, D). Pharmacologically inhibiting APT1 with PalmB treatment reduced asymmetric Notch reporter signal by 3.1-fold (31.7% vs. 10.2%), and Wnt reporter signal by 2.6-fold (22.7% vs. 8.7%), respectively (Fig. 2.7 E, F). Knocking down APT1 or DHHC20 also reduced asymmetric Notch and Wnt reporter signal, indicating that palmitoylation can restrict Notch- and Wnt-dependent transcription to one daughter cell (Fig. 2.7 G, H).

Together these findings suggest palmitoylation may direct the localization of a Wnt activating factor and a Notch inhibitory factor to restrict transcription to one daughter cell.

2.7 Discussion

Maintaining a balance between asymmetric and symmetric divisions is essential for sustaining cell diversity during development and in adult tissues. Asymmetric divisions maintain the size of cell populations, such as proliferative stem cells and non-dividing differentiated cells, to generate cellular heterogeneity and carry out minor tissue repairs. Symmetric divisions are expansive and can generate identical cells when rapid growth is necessary, such as during early embryogenesis, tissue formation, and large-scale tissue repair after injury. Disruption of asymmetric cell division can lead to tissue failure, resulting in disease, due to the aberrant overgrowth of the progenitor population as in the case of acute myeloid leukemia and neuroblastoma, or may contribute to aging as stem cells lose the ability to self-renew and tissue repair cannot be carried out. As fate-determinant proteins direct cell identity, regulating the intracellular distribution of these proteins during cell division is necessary to prevent the improper expansion of cell populations.

As mentioned in the introduction, several mechanisms have been proposed to regulate asymmetric cell division including protein-protein interaction, asymmetric partitioning of degradation machinery, and an extracellular signaling gradient. APT1 was previously shown to promote the polarized localization of a palmitoylated substrate in response to extracellular stimuli in melanoma cells (*70*). However, whether lipid modifications were required for asymmetric protein localization has not been examined in great detail. Numb has been found by other groups to be myristoylated, although inhibition of myristoylation did not disrupt asymmetric Numb localization in neuroblasts (*239*, *244*). Palmitoylated β-catenin was identified in several palmitoylomes; however, β-catenin palmitoylation remained unconfirmed until recently (*60*, *71*, *121*, *245*, *246*). The results presented here uncover a cell-intrinsic mechanism through which APT1 and DHHC20 restrict the localization of the cell fate determinants β-catenin and Numb and

the downstream transcriptional responses to Wnt and Notch signaling to one daughter cell during cell division. Importantly, by manipulating APT1 activity, I have demonstrated that the asymmetric activation of Notch and Wnt transcriptional reporters can be altered without potentially directly affecting the expression of transcription factors or upstream signaling factors. Furthermore, palmitoylation directly promotes asymmetric Numb localization as point mutations in conserved cysteine residues in Numb inhibit not only its palmitoylation but also its asymmetric localization. Because inhibition of palmitoylation reduces the percentage of cells with asymmetrically localized cell fate determinants, these results suggest it facilitates a controlled, rather than a stochastic, process.

I found APT1 inhibition did not completely block the asymmetric localization of β-catenin and Numb, as 8% of dividing cells still were asymmetric. This is similar to the percentage of cells with asymmetrically localized GFP that does not respond to APT1 inhibition, suggesting palmitoylation is a key contributing factor, but not the sole mechanism, responsible for asymmetric protein localization. This palmitoylation-independent asymmetric localization could be the effect of previously reported asymmetric partitioning of machinery that maintains protein abundance such as the proteasome (*203*, *247*) or protein translation machinery (*248*, *249*), which could result in localized differences in protein degradation or synthesis during cell division. Wnt5a has been reported to stimulate APT1 depalmitoylating activity, resulting in polarized protein localization (*70*). While the Numb and β-catenin asymmetries shown have occur without exogenous ligand stimulation, it is possible that palmitoylated proteins may localize asymmetrically in response to extracellular stimulation in a different cancer setting or in a non-transformed setting. Future studies will address whether palmitoylation-mediated plasma membrane recruitment is initiated by ligand binding, as well as interplay with other proposed mechanisms.

The observation that both decreased palmitoylation of the Numb^{AAA} mutant, or increased palmitoylation of Numb upon APT1 knockdown, can inhibit asymmetric localization suggests it is the dynamic, plasma membrane association that promotes asymmetry. Similar to an early study characterizing palmitoylated protein localization at the cytokinetic midbody (*115*), I also find APT1 and Numb localize at the midbody, which implies a factor may serve as a recruitment platform for palmitoylated proteins. Having shown β-catenin is palmitoylated and asymmetrically localized, it is possible that its asymmetric localization may require palmitoylation in a mannaer similar to Numb. Additionally, future studies will uncover whether palmitoylation is necessary for the stability or activity of Numb or β-catenin, which may affect their intracellular localization and asymmetric Notch- or Wnt- transcription. Finally, another area of study would be to determine how these palmitoylation-deficient Numb and β-catenin mutants affect Notch and Wnt signaling and transcriptional activation.

Palmitoylation is a dynamic process that regulates cell polarity through cycles of membrane association and dissociation. In addition to gradients, asymmetric degradation machinery, and phosphorylation cascades, palmitoylation may be another component in that stabilizes or establishes asymmetric protein localization during division. The data presented here show a previously unstudied role for palmitoylation on asymmetric cell division and potentially on cell identity.

MATERIALS AND METHODS

Cell Culture

MDA-MB-231 and U2OS cells were cultured in DMEM + glutamax (Thermo Fisher; Cat. No. 10566-016) and 10% fetal bovine serum. For drug treatment, cells were treated with DMSO (Sigma; Cat. No. D2650), 10μM Palmostatin B (EMD Millipore; Cat. No. 178501) prepared in DMSO, or 5 μM 2-bromopalmitate (Sigma; Cat. No. 21604-1G) prepared in DMSO for 16 hours before staining or harvesting for cell lysates. Cells were treated with 0.5ug/mL puromycin for selection.

Stable cell lines

HEK cells were transfected with 0.69 μg/μL of a GAG, Rev, and Vsvg mix and 1.42 μg/μL of the following plasmids: Scramble control, GFP-PRRL, $APT1^{WT}$ -CFP-Flag-PRRL, APT1 (S119)-CFP-Flag-PRRL, pGF-Notch-mCMV-GFP-puro (System Biosciences; Cat. No. TR020PA-P), pGF-TCF/Lef-mCMV-GFP-puro (System Biosciences; Cat. No.TR013PA-P), or pGF-mCMV-GFP (System Biosciences; Cat. No. TR011PA-1), for 24 hours with LT-1 transfection reagent (Mirus Bio. Cat. MIR2300). The aforementioned APT1 plasmids were designed with short hairpin resistant sequences for rescue studies. Virus was collected 72 hours after infection with 0.5-1mL virus used for stable cell line generation. U2OS cells were infected with $APT1^{WT}$ -CFP-FLAG or APT1(S119)-CFP-FLAG lentivirus for 24 hours, then recovered in complete DMEM for 48 hours prior to cell cultureMDA-MB-231 were infected with the aforementioned lentivirus for 24 hours and recovered in complete DMEM for 48 hours prior to cell culture.

Short hairpin design

shRNA for APT1

F 5'-
CCGGTAGGCCTGTTACATTAAATATCTCGAGATATTTAATGTAACAGGCCTATTTTTG
-3'
R 5'-
AATTCAAAAATAGGCCTGTTACATTAAATATCTCGAGATATTTAATGTAACAGGCCT
A-3'

Alignment of Numb

Numb sequences from *D. melanogaster* **(**P16554), *M. musculus* (Q9QZS3), *D. rerio* (Q5FBC1), and *H. sapiens* (P49757) were chosen from UniProt canonical sequences. Alignment was performed with Clustal Omega. Conserved domains were identified by the Conserved Domain Database (NCBI).

Mutagenesis

Site-directed mutagenesis of Numb C37, C160, and C165 to alanine, and APT1 S119 to alanine were performed using QuikChange multisite-directed mutagenesis kit (Agilent; Cat. No. 210515). Potential palmitoylated cysteines on Numb were identified using CSS-Palm 3.0 developed by Zhou. *et. al.* (*240*) and analysis of the PTB domain crystal structure. Mutants were sequence verified by the DNA Sequencing Facility at the Perelman School of Medicine, University of Pennsylvania.

Live-cell imaging

MDA-MB-231 cells were not conducive to studying the dynamics of asymmetric localization at the plasma membrane by live-imaging, as these cells frequently divided out of the focal imaging plane. Thus, U2 OS cells stably expressing mCherry-Histone H2B facilitated protein tracking over time and allowed for the study of the dynamics of asymmetric localization at the plasma membrane over the course of cell division. U2 OS cells stably expressing $APT1^{WT}$ -CFP-FLAG-PRRL or $APT1^{S119A}$-CFP-FLAG-PRRL were transfected with 2 μg of $NUMB^{WT}$-YFP-FLAG-

PRRL or NUMB^{AAA}-YFP-FLAG- PRRL for 24 hours using LT-1 (Mirus Bio; Cat. No. MIR2300) according to manufacturer's protocol. Cells were imaged 48 hours after transfection in HBSS (Life Technologies; Cat. No. 14175079) containing 2% fetal bovine serum, 1 mg/mL glutamine, and 20mM HEPES pH 7.4 at 37^{o}C. Cells were imaged using the Leica DMI6000 B inverted microscope.

Immunofluorescence

MDA-MB-231 cells were plated on glass coverslips and treated as described. Cells were fixed in 10% formalin, blocked in 5% BSA in TBS containing 0.1% Triton-X (Roche), incubated in primary antibody (β-catenin (9581S; 1:500), CD44 (3570S; 1:500) Cell Signaling Technologies), (Numb (ab14140; 1:500)/ APT1 (ab91606; 1:500)/ GFP (ab290; 1:500)/ Caveolin (ab17052; 1:500), Abcam), (DHHC20, Sigma; Cat. No. HPA014483; 1:500), (Acetylated tubulin (sc23950), RhoB (sc-8048), Santa Cruz), 1:1000), for 1-2 hours at room temperature, incubated in secondary antibody (Alexafluor 488 goat anti-mouse (A11001)/ Alexafluor 594 goat anti-rabbit (A11012), Life Technologies; 1:1000) for 1 hour at room temperature, and mounted in DAPI-mount (Southern Biotech; Cat. No. 0100-20). Cells were imaged using the Leica DMI6000 B inverted microscope on 40X magnification and colonies were imaged on 20X magnification.

Western Blotting

200,000 MDA-MB-231 cells were plated on 60mm tissue culture dishes and were lysed in Tris lysis buffer (50mM Tris pH 7.4 buffer, 150mM NaCl, 2% Triton-X, 1μg/ml leupeptin, 1μg/ml aprotinin, 2μg/ml pepstatin A). Proteins were run out on 10% acrylamide gel and probed with Flag 1:500 (Sigma; Cat. No. F3165), APT1 1:500, Numb 1:1000; β-catenin 1:1000; and DHHC20 1:1000, at 4ºC, overnight, then incubated in secondary anti-rabbit HRP (Jackson Immunoresearch; Cat. No. 211-032-171) or anti-mouse HRP (Jackson Immunoresearch; Cat. No.

115-035-003) for 1 hour at room temperature. Blots were developed in Pierce ECL Chemilluminescence solution (Thermo Fisher; Cat. No. 32106).

Acyl-Biotin Exchange (ABE) Assay

The protocol is adapted from Wan et al., 2007 (*194*) **:** 200,000 MDA-MB-231 cells were plated on 60mm tissue culture dishes and were harvested by scraping in ABE lysis buffer (50mM HEPES pH 7.4, 1% Triton X-100, 150mM NaCl, 5mM EDTA, 50mM N-ethyl-maleimide (NEM), 1µg/ml leupeptin, 1µg/ml aprotinin, 2µg/ml pepstatin A). Lysates were clarified by centrifugation at 15,000 RPM for 10 minutes, and incubated with NEM overnight at 4ºC. The samples were m/c precipitated twice then resuspended in 80µL 4%SDS buffer. The samples were split in half and 160µL of hydroxylamine buffer (0.7M hydroxylamine pH 7.4, 50mM HEPES pH 7.4, 0.2% Triton X-100, 150mM NaCl, 5M EDTA) was added to one half of the sample and control 0.2% Triton X-100 buffer (50mM HEPES pH 7.4, 0.2% Triton X-100, 150mM NaCl, 5mM EDTA) was added to the remaining sample and incubated at room temperature for 1hour. The samples were m/c precipitated and resuspended in 40µL4%SDS buffer containing 10µM Biotin-HPDP (Thermo Fisher; Cat. No. 21341). 160µLof 0.2% Triton X-100 buffer +10µM Biotin-HPDP was added and incubated at RT for 1hour. The samples were m/c precipitated and resuspended in 20µL of 4%SDS buffer followed by addition of 800µL of 1% Triton X-100 buffer (50µL removed for analysis as "input"). 30µL of streptavidin agarose buffer (50mM HEPES pH 7.4, 0.2% Triton X-100, 150mM NaCl, 5mM EDTA) was added to the remaining sample and incubated at room temperature for 1hour. The samples were m/c precipitated and resuspended in 40µL 4%SDS buffer containing 10µM Biotin-HPDP (Pierce). 160µL of 0.2% Triton X-100 buffer +10µM Biotin-HPDP was added and incubated at RT for 1hour. The samples were m/c precipitated and resuspended in 20µLof 4% SDS buffer followed by addition of 800µL of 1% Triton X-100 buffer (50µLremoved for analysis as "input"). 30µLof streptavidin agarose beads

(Thermo Scientific; Cat. No. 20349) were added to the samples and incubated 20 overnight at 4ºC rotating. The samples were washed in 1% Triton-X100 buffer and analyzed by SDS PAGE.

Click Chemistry Assay for Palmitoylation

200,000 U2 OS cells were plated on 60mm tissue culture dishes and were transfected with 2µg Numb ^{WT} or Numb^{AAA} YFP-FLAG for 24 hours, labeled with 100µM palmitic acid azide (Life Technologies; Cat. No. C10265). Cells were prepared using the Click-IT protein reaction buffer (Life Technologies; Cat. No. C10276) according to manufacturer's protocol and analyzed with Western blot as described above.

Quantification and linescan analysis

Cells were quantified by drawing around the mitotic spindle poles, or around each daughter cell in cytokinesis using the Leica LAS AF software as shown in Fig. S1A. Percent difference was calculated from the Mean Gray Values generated in Leica LAS AF and calculated as described in Fig. S1A. The distribution of acquired percentage differences for each experimental condition were plotted as dot plots. Cells with a percentage difference of 20 or greater were counted as asymmetric and plotted in a bar graph. All graphs were generated with Prism software. Linescan analysis of pixel intensity was performed on still frames from live-cell movies using ImageJ software.

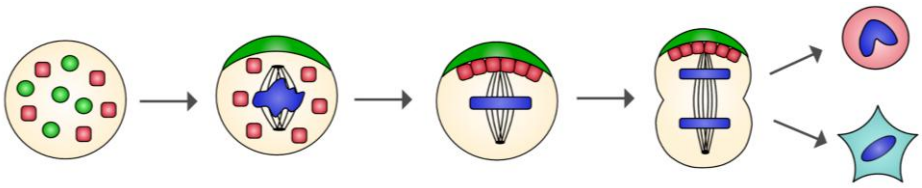

Figure 2.1 Schematic of asymmetric cell division. Establishment of intrinsic polarity (green) is one of the first steps that must occur for an asymmetric division. Cell fate determinants (red) are segregated and aligned perpendicular to the mitotic spindle. Upon cytokinesis, fate determinants are unequally inherited by one daughter cell. This unequal partitioning differentially activates transcriptional programs, resulting in non-identically fated daughter cells. Adapted from Congdon et. al. (*250*).

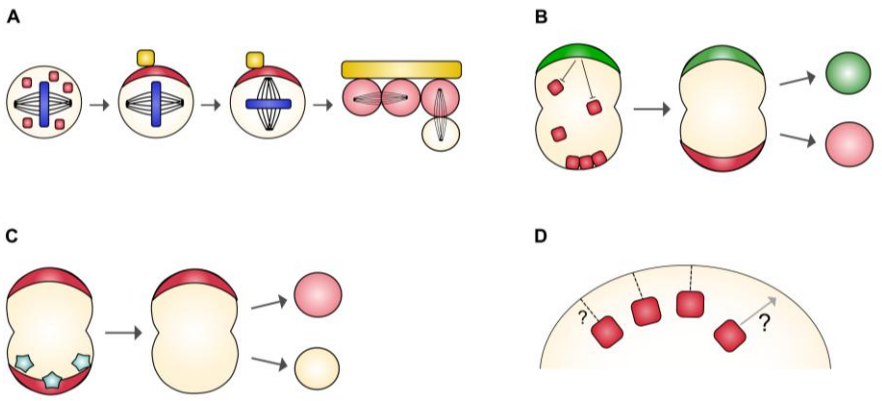

Figure 2.2 Reported mechanisms of asymmetric cell division to generate non-identical daughter cells. (A) Within a stem cell niche**,** binding of extracellular ligands (yellow) may induce mitotic spindle rearrangement and asymmetric recruitment of cell fate determinants (red) along the division axis. (**B**) Phosphorylation-induced inhibitory signaling (green) may restrict the asymmetric localization of cell fate determinants (red) to the opposite membrane through intrinsic mechanisms or extracellular stimuli. (**C**) Asymmetric inheritance of proteosome components (blue) may also induce the degradation of cell fate determinants upon cytokinesis. (**D**) In spite of this evidence, the mechanisms driving the asymmetric targeting and localization of cell fate determinants to the plasma membrane during cell division remain unclear. Adapted from Knoblich *et. al.* (*201*).

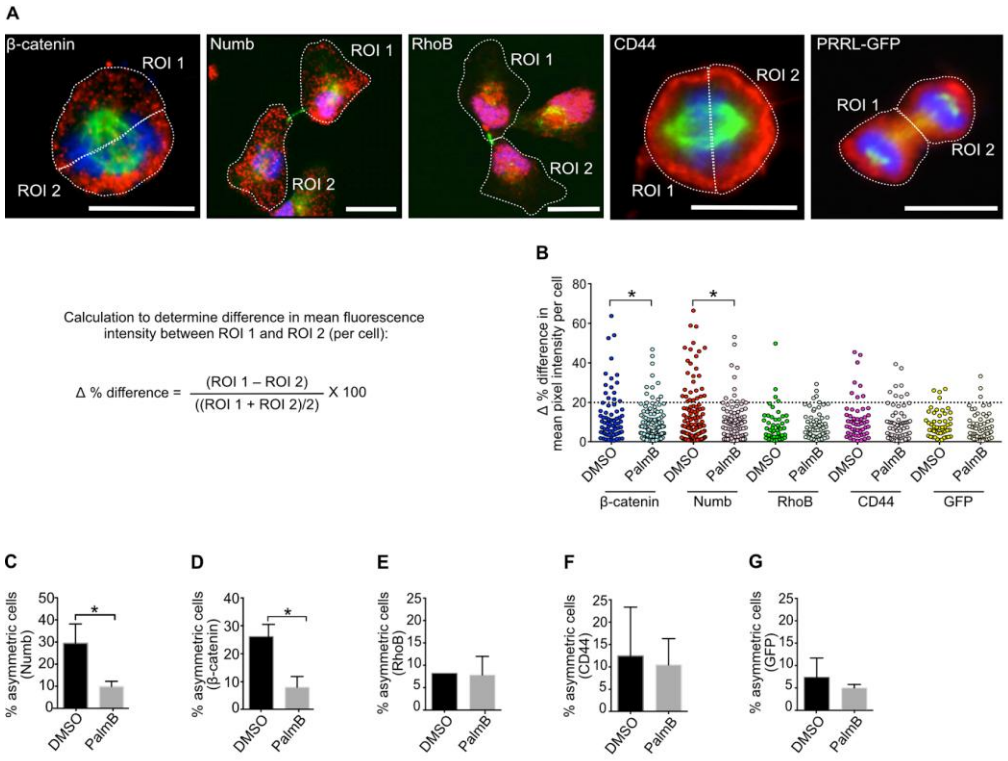

Figure 2.3 Scoring method for determining asymmetric divisions. (**A**) Images of dividing MDA-MB-231 cells stained for β-catenin, Numb, RhoB, CD44, or GFP (red), acetylated tubulin (green), and nuclei (blue). Regions of interests (ROI), outlined in white dotted line, were obtained by drawing around each spindle pole or daughter cell in the image. The mean grey values generated from each ROI were used to calculate the percentage difference, which was obtained by dividing the difference in ROI values by the average of the ROI values and multiplying by 100. Scale bars, 15μm. (**B**) Distribution dot plots showing the difference in mean fluorescence pixel intensity of β-catenin (blue), Numb (red), RhoB (green), CD44 (magenta), or GFP (in cells expressing an empty GFP vector; yellow) across dividing MDA-MB-231 cells treated with PalmB (lighter color) or DMSO (saturated color). The distribution of the percentage differences of all quantified cells was plotted, and cells with a difference of >20% (dotted line) were scored as asymmetric. n = 106-123 cells scored for each experimental group. Each dot represents a single cell. (**C to G**) Quantification of dividing MDA-MB-231 cells showing asymmetric β-

catenin (C), Numb (D), RhoB (E), CD44 (F), or GFP (G) localization after treatment with PalmB or DMSO control. *$P < 0.05$, t test. Error bars indicate standard deviation (SD).

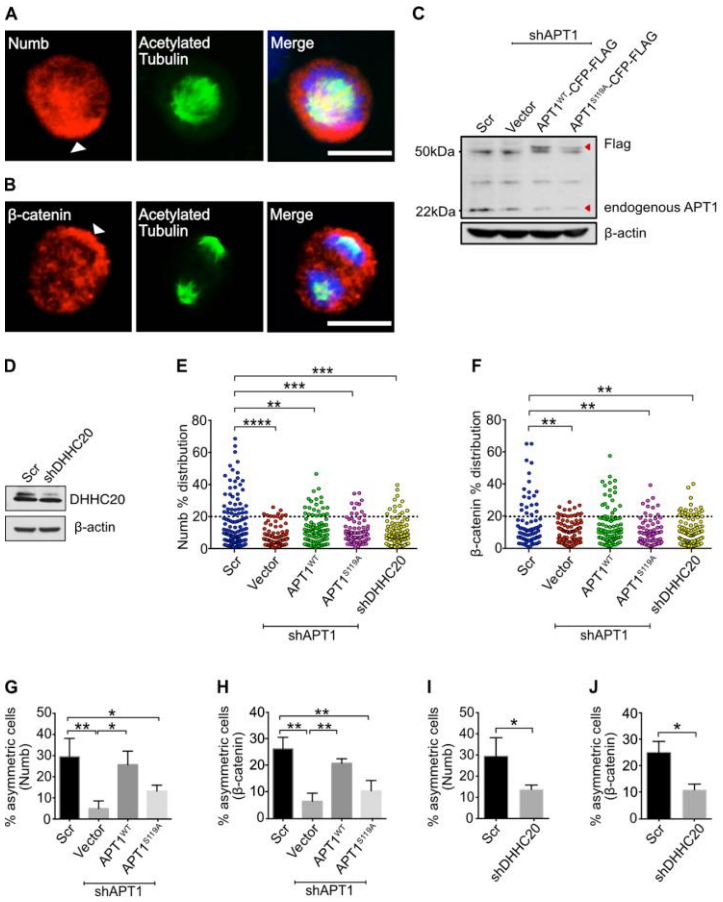

Figure 2.4 Asymmetric Numb and β-catenin localization is dependent on APT1 and DHHC20. (**A and B**) Images of dividing MDA-MB-231 cells stained to show endogenous Numb (A) and β-catenin (B) in red, acetylated tubulin in green, and nuclei in blue. Arrowheads indicate asymmetric localization of Numb and β-catenin. Scale bars, 15 μm. (**C**) Immunoblot of MDA-MB-231 cell lysates showing knockdown of endogenous APT1 by shAPT1. Wild-type APT1 ($APT1^{WT}$-CFP-FLAG) or a catalytically inactive APT1 mutant ($APT1^{S119A}$-CFP-FLAG) were co-expressed with the shRNA for APT1 rescue experiments. Cells expressing a scrambled (Scr) shRNA sequence were used as a negative control for APT1 knockdown, and cells expressing the empty vector were used as the negative control for the APT1 rescue experiments. (**D**) Immunoblot of MDA-MB-231 cell lysates when DHHC20 was knocked down with shDHHC20. Cells expressing a scrambled (Scr) shRNA sequence were used as a negative control for

DHHC20 knockdown. (**E and F**) Distribution dot plots showing the difference in mean fluorescence pixel intensity of endogenous Numb (**E**) and β-catenin (**F**) across dividing MDA-MB-231 cells. The distribution of the percentage differences of all quantified cells was plotted, and cells with a difference of >20% (black dotted line) were scored as asymmetric. n = 508–to 582 cells scored for each experimental group. Each dot represents a single cell. Asterisks indicate statistically significant differences between the indicated groups. (**G and H**) Quantification of the number of dividing MDA-MB-231cells showing asymmetric Numb (G) and β-catenin (H) localization when APT1 was knocked down with shAPT1, and when wild-type APT1 ($APT1^{WT}$) or the catalytically inactive $APT1^{S119A}$ mutant was coexpressed with shAPT1. Cells expressing a scrambled (Scr) short hairpin RNA (shRNA) sequence were used as a negative control for APT1 knockdown, and cells expressing the empty vector were used as a negative control for the APT1 rescue experiments. (**I and J**) Quantification of the number of dividing MDA-MB-231 cells showing asymmetric Numb (I) and β-catenin (J) localization when DHHC20 was knocked down with shDHHC20. $*P < 0.05$, $**P < 0.01$, $***P < 0.001$ analysis of variance (ANOVA) (E to H) or t test (I and J). Error bars indicate SD.

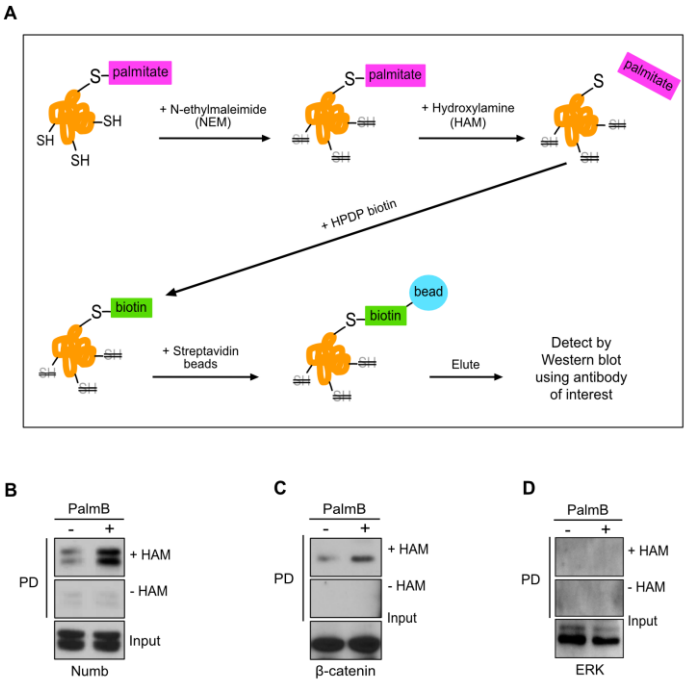

Figure 2.5 Numb and β -catenin are palmitoylated in MDA-MB-231 cells.

(**A**) Schematic representation of the ABE assay. Cell lysates are treated with N-ethylmaleimide to block free thiol groups. Then, the Cysteine-palmitoyl thioester linkages are cleaved with hydroxylamine (HAM), and the newly exposed thiol groups are coupled to biotin. The modified proteins are then purified with streptavidin and analyzed by Western blotting. (**B to D**) Immunoblots showing biotin-labeled Numb (B), β -catenin (C), and ERK (D) in MDA-MB-231 cell lysates after acyl-biotin exchange (ABE) assays and pulldown on streptavidin beads (PD). Cells were grown in the presence of either PalmB or vehicle control (DMSO). Input lanes show cell lysates before pulldown. Samples without hydroxylamine (−HAM) were negative controls for the ABE reactions.

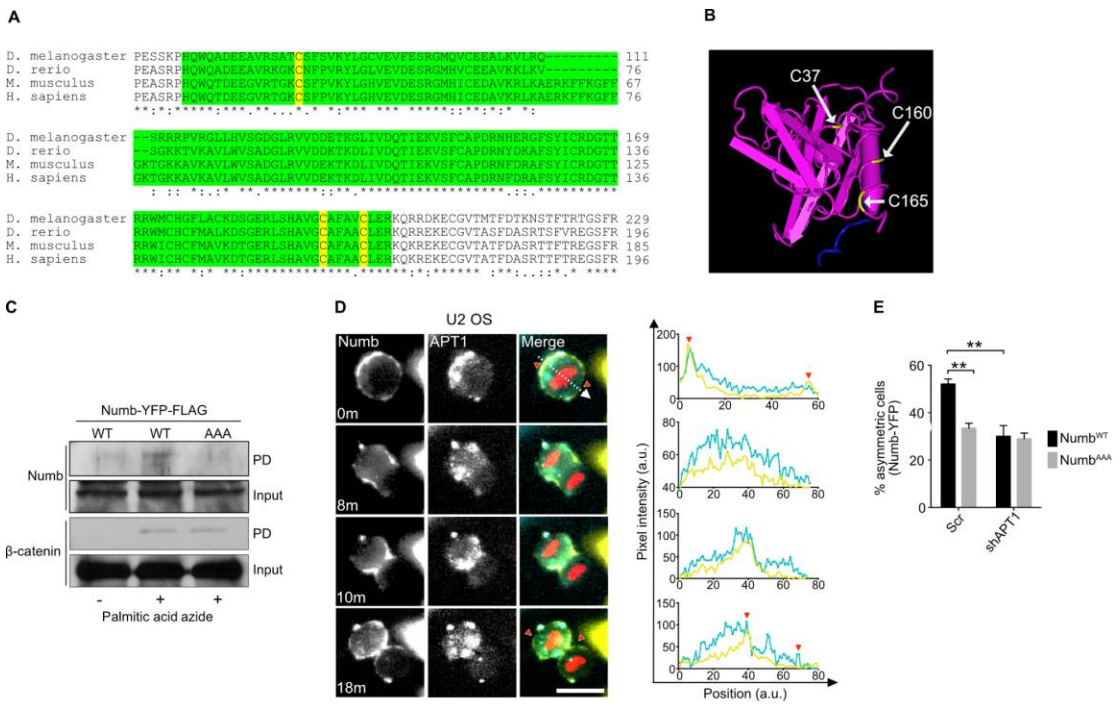

Figure 2.6 Palmitoylation and APT1 activity drive Numb localization. (**A**) Sequence comparison of the N terminus of Numb from fruit fly (*Drosophila melanogaster*), zebrafish (*Danio rerio*), mouse (*Mus musculus*), and human (*Homo sapiens*). The phosphotyrosine domain (PTB) is highlighted in green, and the putative palmitoylated cysteines are highlighted in yellow. Conserved residues are indicated by an asterisk (*). (**B**) Crystal structure of the *D. melanogaster* Numb PTB domain indicating putative palmitoylated residues C37, C160, and C165 in yellow. (**C**) Immunoblot showing transgenically expressed wild-type Numb ($Numb^{WT}$) or the $Numb^{AAA}$ mutant and endogenous β-catenin in U2 OS cell lysates after purification of palmitoylated proteins. Cells were metabolically labeled with palmitic acid azide or treated with DMSO (vehicle control), and then lysates were subjected to click chemistry to convert the palmitic acid moiety to biotin, pulled down on streptavidin beads, and used for immunoblotting. Input was taken from cell lysates before pulldown. (**D**) Time-lapse images of dividing U2 OS cells coexpressing $Numb^{WT}$-YFP (yellow), $APT1^{WT}$-CFP (blue), and mCherry–Histone H2B (red). Fluorescence pixel intensity was measured along the division axis (dashed line), and the

corresponding pixel values of Numb (yellow line) and APT1 (blue line) along the division axis were plotted on graphs. Red arrowheads on images and graphs indicate the peak Numb and APT1 pixel intensity at the membrane or cytokinetic midbody. Time is shown in minutes (min). a.u., arbitrary units. Scale bars, 15 µm. (**E**) Quantification of the number of dividing U2 OS cells showing asymmetric localization of $Numb^{WT}$-YFP (black bar) and $Numb^{AAA}$-YFP (gray bar) when each was coexpressed with shAPT1. Cells expressing a scrambled (Scr) shRNA sequence were used as a negative control for APT1 knockdown. $^{**}P < 0.01$, t test and ANOVA. Error bars indicate SD.

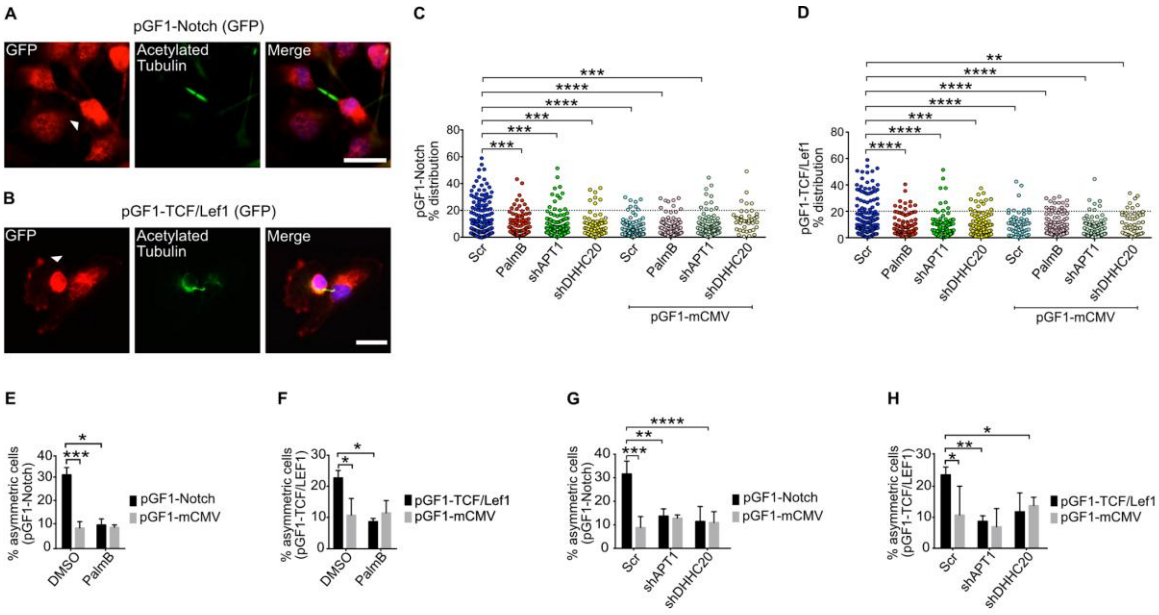

Figure 2.7 APT1 restricts Wnt and Notch transcriptional activity to one daughter cell. (**A and B**) Images of cytokinetic MDA-MB-231 cells stained to show the expression of the pGF1-Notch GFP reporter (A) or pGF-1 TCF/Lef1 GFP reporter (B) (red), acetylated tubulin (green), and nuclei (blue). Arrowheads indicate asymmetric localization. Scale bars, 15 µm. (**C and D**) Distribution dot plots showing the difference in mean fluorescence pixel intensity of pGF1-Notch reporter (C) or pGF1-TCF/Lef1 reporter (D) across dividing cells. Cells expressing an empty pGF1-mCMV GFP reporter were used as a negative control for the reporters. The distribution of the percentage differences of all quantified cells was plotted, and cells with a difference of >20% (dotted line) were scored as asymmetric. n = 784 to 822 cells scored for each experimental group. Each dot represents a single cell. Asterisks indicate statistically significant differences between the indicated groups. (**E and F**) Quantification of dividing MDA-MB 231 cells showing asymmetric localization of pGF1-Notch GFP reporter (E) or pGF1-TCF/Lef1 GFP reporter (F) (black bars) after treatment with PalmB or DMSO vehicle control. Cells expressing an empty pGF1-mCMV reporter (gray bars) were used as a negative control for reporter expression. (**G and H**) Quantification of the number of dividing MDA-MB-231 cells showing asymmetric

localization of the pGF1-Notch GFP reporter (G) or pGF1-TCF/Lef1 GFP reporter (H) (black bars) when coexpressed with shAPT1, and shDHHC20. Cells expressing an empty pGF1-mCMV GFP reporter (gray bars) were used as a negative control for reporter expression, and cells expressing a scrambled (Scr) shRNA sequence were used as a negative control for knockdown. *$P < 0.05$, **$P < 0.01$, ***$P < 0.001$, and ****$P < 0.0001$, t test (between reporters and pGF1-mCMV) or ANOVA (C to H). Error bars indicate SD.

CHAPTER 3: HOW DOES PALMITOYLATION ESTABLISH PROTEIN POLARITY ?

From Stypulkowski, *et. al*. The depalmitoylase APT1 directs the asymmetric partitioning of Notch and Wnt signaling during cell division. *Sci. Signal.* **11,** (2018). Reprinted with permission from AAAS.

3.1 Summary

In Chapter II, I have shown that polarized protein localization is dependent on palmitoylation. Several outstanding questions that arise are: 1) what are the factors, if any, that may be asymmetrically recruiting Numb and β-catenin to the plasma membrane, and 2) are palmitoylation components, e.g. substrates and enzymes, interacting with known polarity-establishing machinery in cell to maintain these polarized domains? To address the first question, I show palmitoylated proteins are localized within close proximity of APT1 and DHHC20. I also demonstrate that total palmitoylated proteins are asymmetrically localized and inhibition of APT1 alters the spatial distribution of palmitoylated proteins within a dividing cell. To determine how this palmitoylation-induced polarity is established, I examine how the polarity complex, namely CDC42, affects the localization of APT1, Numb, and β-catenin as well as transcription outputs between daughter cells. Together, these data provide mechanistic insight into how palmitoylation interacts with known cellular machinery to regulate cell polarity.

3.2 Introduction

Polarity is the unequal distribution of cellular components within a cell, e.g. proteins, mRNA transcripts, vesicles, and organelles (*251*). This allows the cell to form specialized

domains, often at the plasma membrane, which can drive processes such as apical-basolateral domain specification, directed cell migration, synapse formation, vesicular trafficking, and asymmetric cell division (*252, 253*). Mechanisms, such as positive feedback loops and directed protein trafficking, nucleate molecularly distinct domains at the plasma membrane and regulate the rate of protein-membrane association and dissociation to maintain these domains over time (*7, 8, 254*) (Fig. 3.1). What remain unclear are the mechanisms that target and maintain protein localization to the plasma membrane. As reviewed in Chapter I, substrates can be palmitoylated at and trafficked from the Golgi to intracellular domains, but can also be palmitoylated locally at molecularly distinct membrane domains (*113, 114, 236*). Thus, palmitoylation may a potential mechanism to nucleate protein polarity at the plasma membrane. However, whether additional mechanisms interact with palmitoylation to maintain these polarized domains is not fully explored.

CDC42 is a central regulator of several signaling pathways necessary to establish and maintain polarity, including spatially reorganizing actin and microtubules to direct the trafficking and fusion of vesicles with the plasma membrane (*255–259*). Together with Par3, Par6, and aPKC, CDC42 has also been implicated in driving asymmetric divisions of the *C. elegans* zygote, *D. melanogaster* neuroblasts, and budding yeast (*1*, *260–263*). A member of the Ras superfamily of small GTPases, CDC42 activity and function is spatially and temporally regulated by cycles of GTP hydrolysis and GDP exchange (*255*, *264*, *265*). When active, CDC42 is able to bind and traffic substrates from the Golgi to the membrane, which are released when GTP is hydrolyzed to GDP (*264*, *266*, *267*). Extensive studies have shown that disrupting this GTP/GDP exchange results in lost of cell polarity (*264–266*). Thus, cycling between and active and inactive state is critical for CDC42 to nucleate and maintain spatially discrete protein domains at the membrane.

CDC42 localization and function is also regulated by lipid modifications (*181*). CDC42 has two alternatively spliced exons that result in a prenylated or palmitoylated isoform (*182, 183*). Although, prenylated CDC42 has been conventionally accepted as the widely expressed isoform, recent studies are discovering expression of palmitoylated CDC42 in various cell types from platelets, T-lymphocytes, and transformed cell lines (*121, 190, 191, 246, 268*). Like the prenylated isoform, palmitoylated CDC42 regulates substrate trafficking between intracellular compartments and the plasma membrane; however, the function of palmitoylated CDC42 has only been studied during dendrite formation in neurons (*183*). It is currently unclear if palmitoylated CDC42 targets are different from prenylated CDC42, and if the two isoforms function redundantly. Additionally, while DHHC8 was shown to palmitoylate CDC42 (*85, 269*), interactions with depalmitoylating enzymes have not been fully explored.

The localization of palmitoylation cycle components, e.g. DHHCs, APT1, lipid rafts, and palmitoylated proteins, may offer insights into how cell-fate determinants are asymmetrically localized in dividing cells. Several studies have shown DHHC enzymes are differentially expressed and localized within the cell; these differentially localized palmitoyltransferases are thought to establish spatially distinct membrane domains by maintaining local palmitoylation cycles (*15, 113, 114*). APT1 is a primarily cytosolic protein that is recruited to the membrane to depalmitoylate substrates in an unclear mechanism (*19, 132*). In this study, I find APT1 activity is required for its own asymmetric localization and the asymmetric localization of total palmitoylated proteins in dividing cells. Furthermore, APT1 is observed to localize at membrane domains enriched in DHHC20 and palmitoylated proteins. Whether palmitoylation-rich domains are established by CDC42 is also poorly defined. Here, I examine the role of CDC42 activity and palmitoylation on asymmetric APT1, Numb, and β-catenin localization. With this chapter, I

present a mechanism where CDC42 and APT1 function together to nucleate and maintain asymmetric protein localization in dividing cells.

3.3 Asymmetric localization of APT1 during cell division requires APT1 catalytic activity

Having determined that APT1 activity is essential for asymmetric localization of Numb and β-catenin, I next examined whether the catalytic activity of APT1 is required for its own asymmetric localization. Immunostaining fixed cells showed that endogenous APT1 was asymmetrically localized in 22.3% of control cells. Expressing the catalytically inactive form $APT1^{S119A}$ reduced this asymmetric localization by 2.4-fold to 9.4%, whereas expressing $APT1^{WT}$ had no significant effect (Fig. 3.2 A-C). Knocking down DHHC20 also reduced asymmetric APT1 partitioning, suggesting that DHHC20 promotes asymmetric localization of APT1 (Fig. 3.2 B, D).

To gain detailed insights into how APT1 activity promotes and maintains the dynamics of its own asymmetric localization, I compared the spatiotemporal distribution of ectopically expressed $APT1^{WT}$-CFP versus $APT1^{S119A}$-CFP by live-cell imaging in wild-type U2 OS cells. In 52.6% of dividing cells, $APT1^{WT}$-CFP asymmetry was maintained at the plasma membrane through cytokinesis (Fig. 3.2 E, G; Movies S4-5). The asymmetric localization of $APT1^{S119A}$-CFP was significantly reduced to 20.6% of cells, similar to the asymmetric localization of GFP-vector (16.9%) (Fig. 3.2 F, G; Movies S6-7). Additionally, the catalytically inactive mutant $APT1^{S119A}$-CFP was not discretely localized to the plasma membrane at the start of division and appeared to be stuck at the cytokinetic midbody during cytokinesis (Fig. 3.2 F, Movie S6-7). The data up to this point demonstrate that asymmetric localization of APT1 requires its catalytic activity and suggest a role for protein depalmitoylation activity at the site of asymmetric protein localization.

3.4 Palmitoylating and depalmitoylating enzymes localize asymmetrically with palmitoylated proteins during cell division

To clarify the purpose of APT1 accumulation at sites of asymmetrically localized proteins, I hypothesized that APT1 localizes to regions of high protein palmitoylation. Fixed MDA-MB-231 cells were immunostained for Numb and β-catenin, which were asymmetrically partitioned to the same region of a dividing cell as APT1. DHHC20 also displayed asymmetric localization to the same membrane region as APT1 (Fig. 3.3 A). Additionally, the distribution of APT1 and DHHC20 overlapped with that of caveolin, a palmitoylated protein (*270*) and lipid raft component, at the plasma membrane (Fig. 3.3 B). The results up to this point suggest DHHC20-mediated palmitoylation of substrates could recruit APT1 to the membrane.

The presence of both the depalmitoylating enzyme APT1 and palmitoylating enzyme DHHC20 in plasma membrane–associated domains led me to test whether these regions were also enriched for palmitoylated proteins. Because there are currently no palmitoylation-specific antibodies to visualize the localization of palmitoylated proteins, I modified the ABE assay for immunofluorescence and detected asymmetric localization of total palmitoylated proteins, which were labeled with biotin, at the cortex of dividing cells (Fig. 3.4 A). This asymmetric localization depended on the activity of APT1, as PalmB treatment decreased the enrichment of palmitoylated proteins at the cortex and reduced the percentage of cells showing asymmetric localization of palmitoylated proteins by 4.1-fold (31.4% vs. 7.6%). The immunofluorescence signal generated by the modified ABE assay was confirmed to be specific to palmitoylated proteins; negative control staining of samples in which HAM was omitted from the ABE reaction showed greatly reduced signal and symmetric localization (Fig. 3.5 B, C). To determine the localization of palmitoylated proteins relative to APT1 and DHHC20 and whether this asymmetric localization was only observed during mitosis, I performed the modified ABE immunofluorescence assay on

non-dividing cells. Both APT1 and DHHC20 puncta were localized to regions enriched in palmitoylated proteins at membrane ruffles as assessed by confocal microscopy (Fig. 3.5 A, B). The data thus far indicate that both APT1 and DHHC20 localize to regions enriched in palmitoylated proteins, potentially to establish a local palmitoylation cycle.

3.5 A constitutively active CDC42 mutant promotes asymmetric localization of APT1, Numb, and β-catenin during cell division

I next examined whether APT1-mediated asymmetric protein partitioning functions independently of known polarity-establishing mechanisms. The Par-aPKC-CDC42 polarity complex promotes the asymmetric cell division in budding yeast, the *C. elegans* embryo, and in *D. melanogaster* neuroblasts (*215*, *260*, *271*). CDC42 and PARD3 (the mammalian homolog of Par3) were knocked down to assess the requirement of these factors for APT1, Numb, and β-catenin localization (Fig. 3.6 A, B). Asymmetric localization of endogenous APT1 was reduced by 2.6-fold (22.3% vs. 8.5%) in CDC42 knockdown cells, and by 4.3-fold (22.3% vs. 5.2%) in PARD3 knockdown cells (Fig. 3.6 C, D). PARD3 knockdown reduced the asymmetric localization of β-catenin, but not that of Numb (Fig. 3.6 E-H). I next asked if CDC42 and APT1 double knockdown would completely abolish asymmetric Numb and β-catenin partitioning. The percentage of cells showing asymmetric partitioning of Numb and β-catenin in the double knockdown condition did not further decrease as compared to APT1 or CDC42 single knockdown (Fig. 3.6 E-H). This suggests there might be a basal level of asymmetric distribution for both of these proteins that is independent of both APT1 and CDC42.

I next investigated whether APT1 asymmetric localization depended on CDC42 by altering CDC42 activity. In its active GTP-bound state, CDC42 is able to bind substrates and

traffic them to the membrane. Once inactivated through GTP hydrolysis, CDC42 is disengaged from substrates and released into the cytosol (*255, 264, 265*). Work from other groups has shown that expression of either GTP-locked or GDP-locked mutant forms of CDC42 can interfere with CDC42-dependent cellular processes (*1, 255, 258, 264–266*). I employed live-cell imaging of $APT1^{WT}$-CFP and YFP-tagged CDC42 mutants to test the function of CDC42 activity on APT1 localization. Cells expressing a GTP-locked, constitutively active CDC42 mutant ($CDC42^{V12}$) or a GDP-locked, inactive CDC42 mutant ($CDC42^{N17}$) showed reduced asymmetry of $APT1^{WT}$ during cell division as compared to cells expressing a control GFP vector (Fig. 3.7 A, B). In fixed cells, knocking down CDC42 and expressing shRNA-resistant $CDC42^{V12}$ or $CDC42^{N17}$ also significantly reduced asymmetric APT1 and β-catenin localization (Fig. 3.7 C, D, F, H). Compared to CDC42 knockdown, which had minimal effect, expressing $CDC42^{V12}$ or $CDC42^{N17}$ resulted in a strong reduction of asymmetric Numb localization (Fig. 3.7 E, G).

To demonstrate the requirement of CDC42 cycling activity on APT1 localization in cells, I expressed a YFP-tagged constitutively active CDC42 mutant that retains GTP-GDP cycling ($CDC42^{F28L}$). Previously shown by other groups to mimic CDC42-mediated effector binding and subcellular localization (*266*), $CDC42^{F28L}$ increase asymmetric $APT1^{WT}$ localization by 1.3-fold (52.6% vs. 67.0%) (Fig. 3.7 B). Expressing shRNA-resistant $CDC42^{F28L}$ in CDC42 knockdown cells was sufficient to rescue β-catenin and APT1 asymmetric localization, but only partially rescued asymmetric Numb localization in CDC42 knockdown cells (Fig 3.7 C-H). Additionally, expression of $CDC42^{V12}$, $CDC42^{N17}$, or $CDC42^{F28L}$ did not significantly alter the low percentage of asymmetrically localized catalytically inactive $APT1^{S119A}$ as compared to $APT1^{WT}$ by live-cell imaging (Fig. 3.7 B). These results demonstrate a requirement for the polarity complex and, specifically, CDC42 activity in promoting the asymmetric partitioning of APT1 and β-catenin to the membrane. However, although Numb asymmetric localization required CDC42 activity,

overall it appears to be less dependent than APT1 and β-catenin on the canonical Par-aPKC-CDC42 polarity complex.

3.6 The reciprocal interaction between APT1 and palmitoylated CDC42 is sufficient to promote asymmetric protein partitioning during cell division

In addition to cycling between GTP and GDP, CDC42 function is also maintained in part by membrane association though a polybasic region and lipid modification of the C-terminal tail (*255, 258*). There are two known naturally occurring exon splice variants of CDC42 with distinct lipid modifications– a solely prenylated splice variant and a dually palmitoylated and prenylated splice variant (*182*). I asked whether either CDC42 splice variant could rescue asymmetric protein localization in CDC42 knockdown cells during division by expressing shRNA-resistant constructs of the dually lipid modified isoform ($CDC42^{Palm}$) or the solely prenylated CDC42 ($CDC42^{Pren}$) splice variants (Fig. 3.8 A) and examining the localization of Numb, β-catenin, and APT1 in fixed cells. In CDC42 knockdown cells, expressing $CDC42^{Palm}$ was sufficient to fully rescue APT1 asymmetry, whereas expression of $CDC42^{Pren}$ appeared to inhibit asymmetric APT1 localization (Fig. 3.8 A, D). $CDC42^{Palm}$ and $CDC42^{Pren}$ had little effect on asymmetric Numb localization in CDC42 knockdown cells. $CDC42^{Palm}$ rescued asymmetric β-catenin localization to baseline control conditions, but $CDC42^{Pren}$ had no observable effect (Fig. 3.8 B, C, E, F). These results suggest that palmitoylated CDC42 promotes asymmetric localization of specific downstream proteins, and APT1 may reciprocally promote asymmetric localization of palmitoylated CDC42 during cell division.

To spatiotemporally visualize CDC42 and APT1 localization during cell division, I measured the distribution of $APT1^{WT}$-CFP and $CDC42^{Pren}$-YFP or $CDC42^{Palm}$-YFP by live-cell

imaging. CDC42^{Palm} expression increased the percentage of asymmetric APT1^{WT}-CFP in dividing cells by 1.5-fold (52.6% vs. 82.7%) whereas CDC42^{Pren} suppressed asymmetric partitioning of APT1^{WT}-CFP by 1.9-fold (52.6% vs. 27.2%). In contrast, neither isoform sufficiently altered asymmetric partitioning of catalytically inactive APT1^{S119A} (Fig. 3.9 A). This led me to ask whether APT1 was sufficient to promote asymmetric CDC42^{Palm} localization. Both APT1^{WT}-CFP and CDC42^{Palm}-YFP were asymmetric at the plasma membrane early during division, and asymmetrically redistributed to the membrane of one daughter cell upon cytokinesis (Fig. 3.9 B). As expected, expression of APT1^{S119A} inhibited asymmetric redistribution of CDC42^{Palm}-YFP and retained CDC42^{Palm}-YFP at the cytokinetic midbody (Fig. 3.9 c). I next asked whether CDC42^{Palm} was endogenously expressed in MDA-MB-231 cells using exon-spanning primers. I detected the endogenous transcript for this palmitoylated CDC42 splice variant by PCR (Fig. 3.10 A, B). Furthermore, I detected CDC42 palmitoylation in U2 OS cells by the ABE assay and demonstrated that treatment with PalmB increased the amount of palmitoylated CDC42, whereas treatment with the palmitoyltransferase inhibitor 2-bromopalmitate (2BP) decreased palmitoylation (Fig. 3.10 C). These results suggest that palmitoylated CDC42 could function with APT1 in these cells either at a basal level or in a subset of cells to promote asymmetric protein localization.

3.7 CDC42 and APT1 interact to maintain differential activation of Notch- and Wnt-mediated transcription between daughter cells

In Chapter II, APT1 was determined to be required for asymmetric activity of Notch and Wnt transcription GFP reporters (Fig. 3.11 A). I hypothesized this asymmetric reporter expression was regulated by palmitoylation and polarity. To address this hypothesis, CDC42 and

DHHC20 were knocked down in MDA-MB-231 cells expressing pGF1-Notch or pGF1-TCF/Lef1 and asymmetric reporter signal was assessed. Knocking down CDC42 significantly disrupted asymmetric Wnt reporter signal, whereas the Notch reporter signal was unchanged, as compared to the pGF1-mCMV negative control (Fig. 3.11 C-F). This was consistent with observations of asymmetric Numb localization upon CDC42 knockdown. Additionally, CDC42 and APT1 may function in the same pathway that stimulates signal-activated transcription because double knockdown of APT1 and CDC42 did not appreciably decrease asymmetric Wnt or Notch reporter signal over APT1 or CDC42 single knockdown (Fig. 3.11 C-F). Similar to APT1, knocking down DHHC20 decreased asymmetric Notch and Wnt reporter expression (Fig. 3.11 C-F). Together these findings suggest palmitoylation directs the localization of a Wnt activating factor and a Notch inhibitory factor to restrict transcription to one daughter cell.

3.8 Discussion

The data presented show an interdependence of APT1 and CDC42 activity for their own asymmetric localization. This interdependence could occur through association of two distinct compartments of the plasma membrane: the lipid bilayer and the membrane-associated, cortical actin cytoskeleton. CDC42 establishes polarity in cells by spatially reorganizing the cytoskeleton to direct vesicular traffic to and fusion with the plasma membrane (*255*, *257*, *259*). Because active GTP-bound CDC42 is membrane-associated, APT1 could promote the recruitment of palmitoylated proteins that also stimulate CDC42 function to the plasma membrane, e.g. the CDC42 activator Intersectin, which is also activated by Numb (*272*). This is consistent with current models of diffusible, membrane-bound molecules establishing distinct polarized domains at the plasma membrane in a feedforward manner (*8, 271*). It has also been hypothesized that the

formation of polarized domains can be inhibited if the protein association rate outpaces the dissociation rate at the plasma membrane, or vice versa (*7*, *8*). Constitutively GTP-bound $CDC42^{V12}$ is unable to release its substrate and has been shown to continuously accumulate at the plasma membrane. This results in protein mislocalization at neighboring domains and eventual loss of polarity (*264*, *265*). This could explain why polarized membrane domains are sensitive to changes in CDC42 protein abundance, activity, and lipid-modification, as demonstrated by the findings presented in this chapter.

An interesting, but unanswered question, is to understand how the activity of palmitoylated CDC42 is regulated. Palmitoylated CDC42 and prenylated CDC42 are 95% similar in sequence, but appear to be expressed and function differently(*181*, *182*). The palmitoylated isoform is stably associated with membrane fractions, while the prenylated isoform is found in both the cytosol and membrane. Additionally, palmitoylation inhibits RhoGDIα binding, another mechanism of removing Rho GTPases at the plasma membrane in a GTP-hydrolysis independent manner (*182*). Palmitoylated CDC42, but not prenylated CDC42, is required to initiate and maintain dendrite formation and branching in neurons (*183*, *273*). Apart from DHHC8 (*85*, *269*), little else is known about the DHHCs and depalmitoylating enzymes that regulate palmitoylated CDC42 localization and function. How palmitoylation coordinates the palmitoylated CDC42 membrane localization remains to be determined. Here, I have shown that palmitoylated CDC42 is asymmetrically localized in dividing cells and this required APT1 activity, suggesting that APT1 is one of the depalmitoylating enzymes. Additionally, palmitoylated CDC42 promotes the asymmetric localization of β-catenin (and Numb to a lesser degree) potentially in a feedforward manner with APT1. The data presented here also demonstrate that the palmitoylated isoform transcript is expressed in triple receptor negative breast cancer cells, albeit at a low level. Interestingly, expression of palmitoylated CDC42 has been detected in human breast cancer and

prostate cancer cell lines (*121*, *268*). Future studies may reveal whether palmitoylated CDC42 is expressed in all cells, but at a level undetectable by conventional means, or if it is re-expressed in disease settings which may contribute to aggressive phenotypes.

Whereas the asymmetric distributions of CDC42 and APT1 appear to be interdependent, the depletion of either protein individually has distinct effects on the Wnt and Notch pathways. Knocking down CDC42 significantly reduces both APT1 and β-catenin asymmetric localization, without significantly affecting the localization of Numb. This would suggest that although asymmetric β-catenin and Numb localization require APT1 activity, only the asymmetric localization of β-catenin requires asymmetric localization of APT1. CDC42 is known to promote canonical Wnt signaling activity by sequestering adenomatosis polyposis coli (APC), a component of the β-catenin destruction complex, to the plasma membrane in an actin-dependent manner (*274*, *275*). Thus, maintenance of the actin cytoskeleton by CDC42 may be required for asymmetric β-catenin localization, but not as much for Numb. As such, the requirement for CDC42 may be necessitated by unique mechanisms of Wnt signal activation distinct from a requirement for APT1 activity.

Little is known about the interaction between Notch signaling components and CDC42. Notch and CDC42 have been suggested to function in parallel pathways to regulate dendrite formation in neurons (*276–278*). The data presented in the chapter show Numb localization is sensitive to CDC42 activity, consistent with a reported interaction between Numb isoforms 5 and 6 and CDC42 (*279*). While the results here do not show a strong requirement for CDC42 on Notch signaling asymmetry, it is possible other polarity complexes are involved as Notch is regulated by the Crumbs polarity complex (*280*, *281*). How palmitoylation may regulate Notch localization and activity at the membrane also remains to be determined.

The connection between palmitoylation and polarity is not limited to CDC42. The Scribble polarity complex interacts directly with CDC42 and is required for asymmetric cell division in *D. melanogaster* (*282, 283*). Two of its members, Scribble and Discs large (also known as SAP97 and PSD-95 in mammalian cells), are palmitoylated (*53*, *107*, *153*, *284*). Membrane palmitoylated protein 5 (MPP5), a member of the Crumbs polarity complex and regulator of cell junction assembly, is also palmitoylated (*174*, *285*). Future study may reveal insights into the regulation of cell polarity by palmitoylation and potential conserved roles. Additionally, cell polarity is thought to be a mechanism of tumor suppression (*184*, *286*) and the data presented here suggest modulating the palmitoylation cycle is sufficient to disrupt polarity in cancer cell lines. It will be interesting to learn whether disrupting palmitoylation of polarity regulators, e.g. Scribble and CDC42, is an important step in oncogenic transformation.

MATERIALS AND METHODS

Cell Culture

MDA-MB-231 and U2OS cells were cultured in DMEM + glutamax (Thermo Fisher; Cat. No. 10566-016) and 10% fetal bovine serum. For drug treatment, cells were treated with DMSO (Sigma; Cat. No. D2650), 10μM Palmostatin B (EMD Millipore; Cat. No. 178501) prepared in DMSO, or 5 μM 2-bromopalmitate (Sigma; Cat. No. 21604-1G) prepared in DMSO for 16 hours before staining or harvesting for cell lysates. Cells were treated with 0.5ug/mL puromycin for selection.

Stable cell lines

HEK cells were transfected with 0.69 μg/μL of a GAG, Rev, and Vsvg mix and 1.42 μg/μL of the following plasmids: Scramble control, GFP-PRRL, $APT1^{WT}$ -CFP-Flag-PRRL, APT1 (S119)-CFP-Flag-PRRL, FLAG- CDC 42 Pren -PRRL, FLAG-CDC42-V12-PRRL, FLAG-CDC42-N17-PRRL, FLAG-CDC42-F28-PRRL, FLAG-CDC42 Palm-PRRL, pGF-Notch-mCMV-GFP-puro (System Biosciences; Cat. No. TR020PA-P), pGF-TCF/Lef-mCMV-GFP-puro (System Biosciences; Cat. No.TR013PA-P), or pGF-mCMV-GFP (System Biosciences; Cat. No. TR011PA-1), for 24 hours with LT-1 transfection reagent (Mirus Bio. Cat. MIR2300). The aforementioned APT1 and CDC42 plasmids were designed with short hairpin resistant sequences for rescue studies. Virus was collected 72 hours after infection with 0.5-1mL virus used for stable cell line generation. U2OS cells were infected with $APT1^{WT}$ -CFP-FLAG or $APT1^{S119A}$-CFP-FLAG lentivirus for 24 hours, then recovered in complete DMEM for 48 hours prior to cell culture

Short hairpin design

shRNA for PARD3
F: 5’-
CCGGGCCATCGACAAATCTTATGATCTCGAGATCATAAGATTTGTCGATGGCTTTTTG
-3'
R: 5'-
AATTCAAAAAGCCATCGACAAATCTTATGATCTCGAGATCATAAGATTTGTCGATGG
C-3'

F: 5'-
CCGGGCCATCGACAAATCTTATGATCTCGAGATCATAAGATTTGTCGATGGCTTTTTG
-3'
R: 5'-
AATTCAAAAAGCCATCGACAAATCTTATGATCTCGAGATCATAAGATTTGTCGATGG
C-3'

F: 5'-
CCGGAGTCAATTGGATTTCGTTAAACTCGAGTTTAACGAAATCCAATTGACTTTTTTG
-3'
R: 5'-
AATTCAAAAAAGTCAATTGGATTTCGTTAAACTCGAGTTTAACGAAATCCAATTGAC
T-3'

shRNA for CDC42
F: 5'-
CCGGCGGAATATGTACCGACTGTTTCTCGAGAAACAGTCGGTACATATTCCGTTTTTG
-3'
R: 5'-
AATTCAAAAACGGAATATGTACCGACTGTTTCTCGAGAAACAGTCGGTACATATTCC
G-3'

F: 5'-
CCGGTGCTTGTTGGGACTCAAATTGCTCGAGCAATTTGAGTCCCAACAAGCATTTTTG
-3'
R: 5'-
AATTCAAAAATGCTTGTTGGGACTCAAATTGCTCGAGCAATTTGAGTCCCAACAAGC
A-3'

F: 5'-
CCGGAGATTACGACCGCTGAGTTATCTCGAGATAACTCAGCGGTCGTAATCTTTTTTG
-3'
R:
5'AATTCAAAAAAGATTACGACCGCTGAGTTATCTCGAGATAACTCAGCGGTCGTAAT
CT-3'

shRNA for APT1

F 5'-
CCGGTAGGCCTGTTACATTAAATATCTCGAGATATTTAATGTAACAGGCCTATTTTTG
-3'
R 5'-
AATTCAAAAATAGGCCTGTTACATTAAATATCTCGAGATATTTAATGTAACAGGCCT
A-3'

Live-cell imaging

MDA-MB-231 cells were not conducive to studying the dynamics of asymmetric localization at the plasma membrane by live-imaging, as these cells frequently divided out of the focal imaging plane. Thus, U2 OS cells stably expressing mCherry-Histone H2B facilitated protein tracking over time and allowed me to study the dynamics of asymmetric localization at the plasma membrane over the course of cell division. U2 OS cells stably expressing $APT1^{WT}$ -CFP-FLAG-PRRL or APT1(S119)-CFP-FLAG-PRRL were transfected with 2 μg of YFP-CDC42 Pren-PCDNA3.1, YFP-CDC42 Palm-PCDNA3.1, YFP-CDC42 V12-PCDNA3.1, YFP-CDC42 N17-PCDNA3.1, YFP-CDC42 F28-PCDNA3.1, for 24 hours using LT-1 (Mirus Bio; Cat. No. MIR2300) according to manufacturer's protocol. Cells were imaged 48 hours after transfection in HBSS (Life Technologies; Cat. No. 14175079) containing 2% fetal bovine serum, 1 mg/mL glutamine, and 20mM HEPES pH 7.4 at 37^{o}C. Cells were imaged using the Leica DMI6000 B inverted microscope.

Immunofluorescence

MDA-MB-231 cells were plated on glass coverslips and treated as described. Cells were fixed in 10% formalin, blocked in 5% BSA in TBS containing 0.1% Triton-X (Roche), incubated in primary antibody (β-catenin, Cell Signaling Technologies; Cat. No. 9581S; 1:500), (PARD3 (ab64646; 1:500)/ APT1 (ab91606; 1:500)/ GFP (ab290; 1:500)/ Caveolin (ab17052; 1:500), Abcam), (DHHC20, Sigma; Cat. No. HPA014483; 1:500), (Acetylated tubulin, Santa Cruz; Cat. No. sc23950), 1:1000), for 1-2 hours at room temperature, incubated in secondary antibody

(Alexafluor 488 goat anti-mouse (A11001)/ Alexafluor 594 goat anti-rabbit (A11012), Life Technologies; 1:1000) for 1 hour at room temperature, and mounted in DAPI-mount (Southern Biotech; Cat. No. 0100-20). Cells were imaged using the Leica DMI6000 B inverted microscope on 40X magnification and colonies were imaged on 20X magnification.

Western Blotting

200,000 MDA-MB-231 cells were plated on 60mm tissue culture dishes and were lysed in Tris lysis buffer (50mM Tris pH 7.4 buffer, 150mM NaCl, 2% Triton-X, 1µg/ml leupeptin, 1µg/ml aprotinin, 2µg/ml pepstatin A). Proteins were run out on 10% acrylamide gel and probed with PARD3 1:1000, CDC42 1:500 (Cytoskeleton; Cat. No. ACD03), Flag 1:500 (Sigma; Cat. No. F3165), APT1 1:500, and DHHC20 1:1000, at 4ºC, overnight, then incubated in secondary anti-rabbit HRP (Jackson Immunoresearch; Cat. No. 211-032-171) or anti-mouse HRP (Jackson Immunoresearch; Cat. No. 115-035-003) for 1 hour at room temperature. Blots were developed in Piere ECL Chemilluminescence solution (Thermo Fisher; Cat. No. 32106).

Acyl-Biotin Exchange (ABE) Assay

The protocol is adapted from Wan et al., 2007 (*194*) **:** 200,000 MDA-MB-231 cells were plated on 60mm tissue culture dishes and were harvested by scraping in ABE lysis buffer (50mM HEPES pH 7.4, 1% Triton X-100, 150mM NaCl, 5mM EDTA, 50mM N-ethyl-maleimide (NEM), 1µg/ml leupeptin, 1µg/ml aprotinin, 2µg/ml pepstatin A). Lysates were clarified by centrifugation at 15,000 RPM for 10 minutes, and incubated with NEM overnight at 4ºC. The samples were m/c precipitated twice then resuspended in 80µL 4%SDS buffer. The samples were split in half and 160µL of hydroxylamine buffer (0.7M hydroxylamine pH 7.4, 50mM HEPES pH 7.4, 0.2% Triton X-100, 150mM NaCl, 5M EDTA) was added to one half of the sample and control 0.2% Triton X-100 buffer (50mM HEPES pH 7.4, 0.2% Triton X-100, 150mM NaCl,

5mM EDTA) was added to the remaining sample and incubated at room temperature for 1hour. The samples were m/c precipitated and resuspended in 40µL4%SDS buffer containing 10µM Biotin-HPDP (Thermo Fisher; Cat. No. 21341). 160µLof 0.2% Triton X-100 buffer +10µM Biotin-HPDP was added and incubated at RT for 1hour. The samples were m/c precipitated and resuspended in 20µL of 4%SDS buffer followed by addition of 800µL of 1% Triton X-100 buffer (50µL removed for analysis as "input"). 30µL of streptavidin agarose buffer (50mM HEPES pH 7.4, 0.2% Triton X-100, 150mM NaCl, 5mM EDTA) was added to the remaining sample and incubated at room temperature for 1hour. The samples were m/c precipitated and resuspended in 40µL4%SDS buffer containing 10µM Biotin-HPDP (Pierce). 160µLof 0.2% Triton X-100 buffer +10µM Biotin-HPDP was added and incubated at RT for 1hour. The samples were m/c precipitated and resuspended in 20µLof 4%SDS buffer followed by addition of 800µL of 1% Triton X-100 buffer (50µLremoved for analysis as "input"). 30µLof streptavidin agarose beads (Thermo Scientific; Cat. No. 20349) were added to the samples and incubated 20 overnight at 4ºC rotating. The samples were washed in 1% Triton-X100 buffer and analyzed by SDS PAGE.

ABE Assay for Immunofluorescence

Washes were performed in 1X ABE buffer + 0.2% Triton-X + 0.1% SDS. Cells were seeded onto coverslips. Cells were fixed in 10% formalin + 50mM NEM for 10 minutes at room temperature and washed once before being incubated overnight in 1X ABE buffer + 0.2% Triton-X + 0.1% SDS* + 50mM NEM at 4ºC. The following day, 3 x 15 minute washes were performed. Cells were incubated in HA+ or HA- buffer for 2 hours at room temperature, then washed 3 x 15minutes. Cells were incubated in Biotin-HPDP buffer for 1 hour at room temperature and washed for 3 x 20 minutes. Cells were Incubated in primary antibody (Biotin, 1:500; Abcam; Cat. No. ab53494), at 4ºC overnight, and immunofluorescence was performed as described above.

Quantification and linescan analysis

Cells were quantified by drawing around the mitotic spindle poles, or around each daughter cell in cytokinesis using the Leica LAS AF software as shown in Fig. S1A. Percent difference was calculated from the Mean Gray Values generated in Leica LAS AF and calculated as described in Fig. S1A. The distribution of acquired percentage differences for each experimental condition were plotted as dot plots. Cells with a percentage difference of 20 or greater were counted as asymmetric and plotted in a bar graph. All graphs were generated with Prism software. Linescan analysis of pixel intensity was performed on still frames from live-cell movies using ImageJ software.

PCR

To confirm the expression of FLAG-CDC42 plasmids in shCDC42 MDA-MB-231 cells, I isolated RNA and prepared cDNA from FLAG-prenylated CDC42, FLAG-CDC42-V12, FLAG-CDC42-N17, FLAG-CDC42-F28, FLAG-palmitoylated CDC42 cell lines. PCR reaction was performed using 2ug of cDNA, 10X PCR buffer (Sigma; Cat. No. P2192), 10mM dNTPs (Life Technologies; Cat. no. 18252015), Taq polymerase (Sigma; Cat. No D1806) and 10μM of hCDC42-palm and hCDC42-prenyl primers mentioned above, which are designed to span the alternatively spliced exon. The reaction was run out on a 1.4% agarose gel.

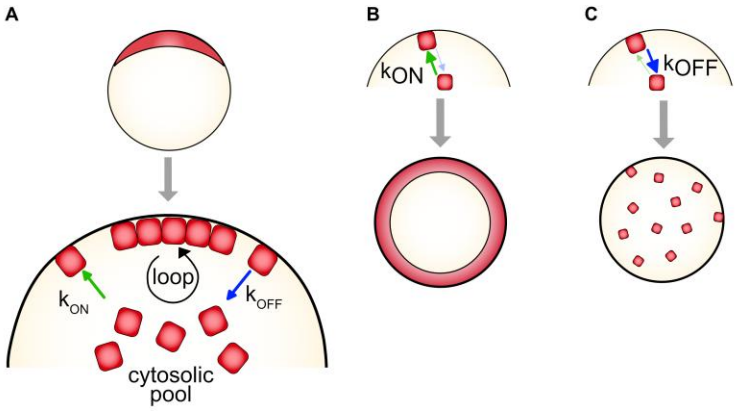

Figure 3.1 Schematic mechanism of establishing cell polarity. (**A** to **C**) The formation of polarized protein domains is largely determined by a feedback of membrane association (k_{ON}) and dissociation (k_{OFF}) rates between the cytosolic pool and the membrane (A). If the k_{ON} outpaces the k_{OFF}, protein recruitment to the membrane is sustained and molecules are not removed from the membrane quickly enough. This results in loss of distinct protein domains (B). If the k_{OFF} outpaces the k_{ON}, increased membrane dissociation interferes with the formation of stable membrane domains, resulting in an expanded cytoplasmic protein pool and loss of polarized domains at the membrane (C). Adapted from Thompson *et. al.* and Altschuler *et. al.* (*8*, *254*)

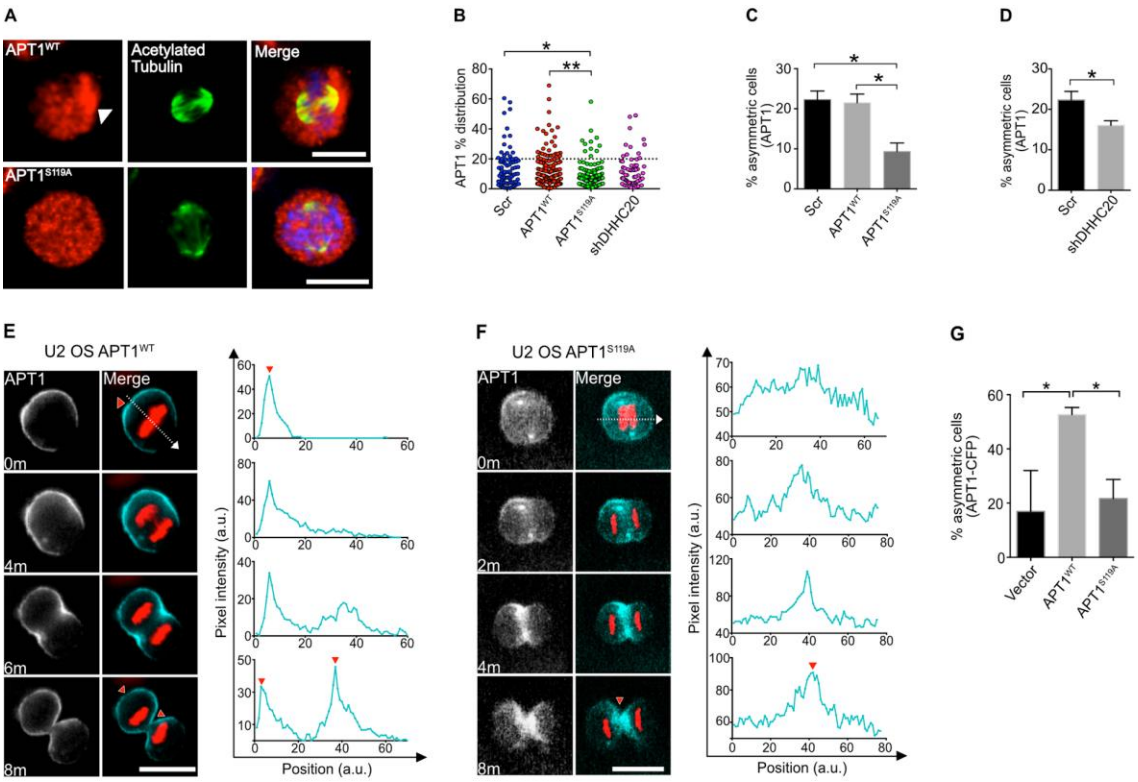

Figure 3.2 Asymmetric APT1 localization requires its catalytic activity in MDA-MB-231 and U2 OS cells. (**A**) Images of dividing MDA-MB-231 cells stained to show APT1 (red), acetylated tubulin (green), and nuclei (blue). Arrowheads indicate asymmetric localization of APT1. Scale bars, 15µm. (**B**) Distribution dot plots showing the difference in mean fluorescence pixel intensity of APT1 across dividing MDA-MB-231 cells. The distribution of the percentage differences of all quantified cells was plotted, and cells with a difference of >20% (dotted line) were scored as asymmetric. (**C** and **D**) Quantifications of dividing cells showing asymmetric APT1 when $APT1^{WT}$ or $APT1^{S119A}$ was overexpressed (C), or when DHHC20 as knocked down with shDHHC20 (D). Cells expressing a scrambled (Scr) shRNA sequence were used as a negative control for knockdown or overexpression. n = 302 cells scored for the experimental group. Each dot represents a single cell. Asterisks indicate statistically significant differences between the indicated groups. (**E and F**) Time-lapse images of dividing U2 OS cells

coexpressing either APT1^{WT}-CFP (E) or APT1^{S119A}-CFP (F) with mCherry–Histone H2B (red). Fluorescence pixel intensity was quantified as in (C). Scale bars, 15 µm. (**G**) Quantification of the number of dividing U2 OS cells showing asymmetric APT1^{WT}-CFP or APT1^{S119A}-CFP localization. Cells expressing an empty green fluorescent protein (GFP) plasmid (Vector) were used as a negative control. n = 102 to 143 cells scored for each group from three independent experiments. *P< 0.05 and **P < 0.01, t test and ANOVA. Error bars indicate SD.

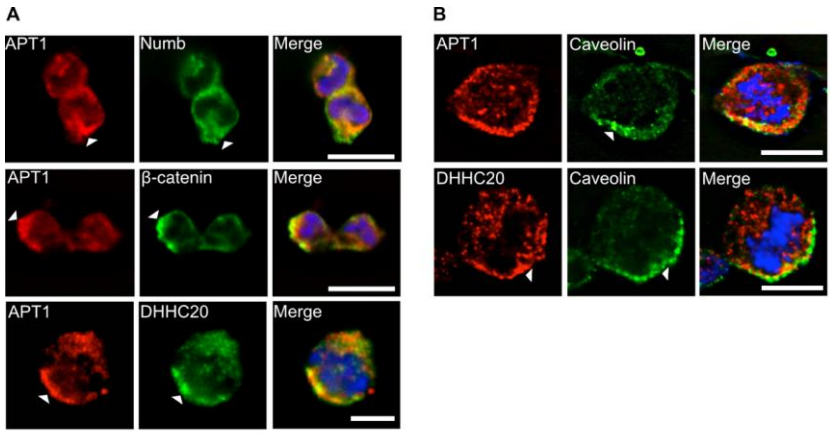

Figure 3.3 APT1 and DHHC20 asymmetrically partitioned with caveolin-rich membrane domains during cell division. (**A**) Images of dividing MDA-MB-231 cells stained to show endogenous APT1 (red), Numb, β-catenin, or DHHC20 (green), and nuclei (blue). (**B**) Images of dividing MDA-MB-231 cells stained to show endogenous APT1 (B) or DHHC20 (C), caveolin, and nuclei. Asymmetric localization is indicated by arrowheads (A to C). Scale bars, 15 μm.

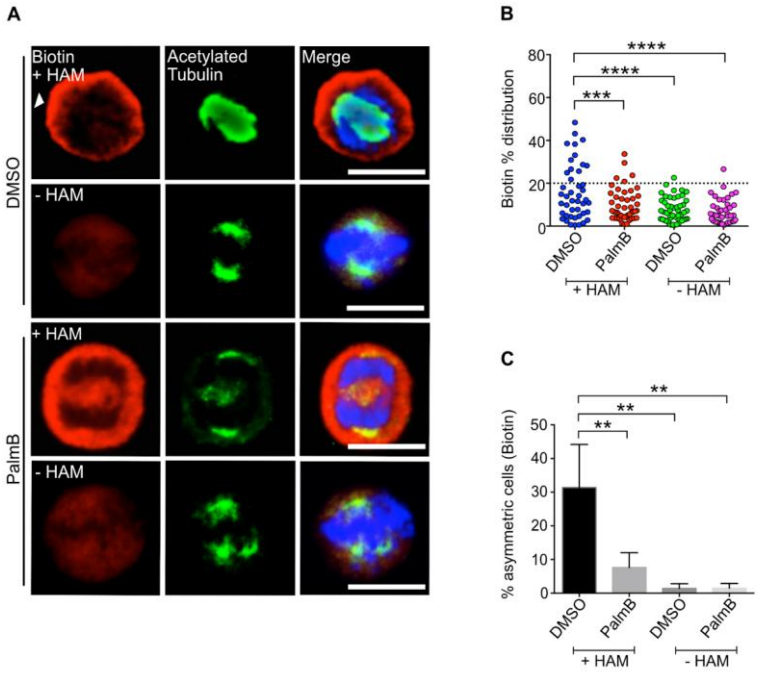

Figure 3.4 Asymmetric localization of bulk palmitoylated proteins in dividing cells is inhibited with Palmostatin B. (**A**) Images of dividing MDA-MB-231 cells treated with PalmB or DMSO and stained to show biotin-labeled palmitoylated proteins (red), acetylated tubulin (green), and nuclei (blue) by ABE immunofluorescence. Samples without HAM (−HAM) were negative controls for the ABE reaction. Scale bars, 15 µm. (**B**) Distribution dot plots showing the difference in mean fluorescence pixel intensity of biotin-labeled palmitoylated proteins. The distribution of the percentage differences of all quantified cells was plotted, and cells with a difference of >20% (dotted line) were scored as asymmetric. n = 91 to 101 cells scored for each experimental group. Each dot represents a single cell. Asterisks indicate statistically significant differences between the indicated groups. (**C**) Quantification of the number of dividing MDA-MB-231 cells showing asymmetric palmitoylated proteins after treatment with PalmB or DMSO control. $^{**}P < 0.01$ and $^{****}P < 0.0001$, t-test and ANOVA. Error bars indicate SD.

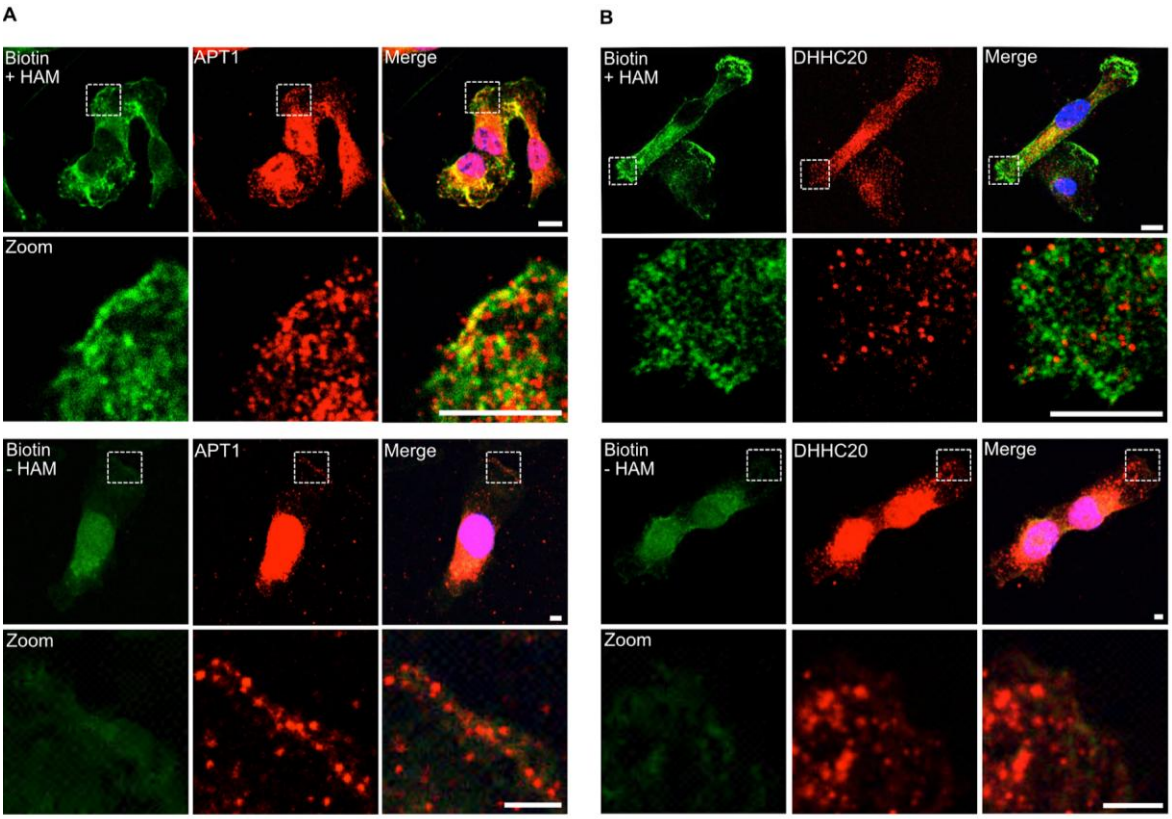

Figure 3.5 APT1 and DHHC20 localized at the plasma membrane to domains rich in palmitoylated proteins. Confocal images of ABE immunofluorescence in non-dividing MDA-MB-231 cells showing all palmitoylated proteins (green), APT1 (A) or DHHC20 (B) (red), and nuclei (blue) by ABE immunofluorescence. White dotted boxes indicated magnified areas shown directly below (zoom). Samples without HAM (−HAM) were negative controls for the ABE reaction. Scale bars (including zoom), 15 μm.

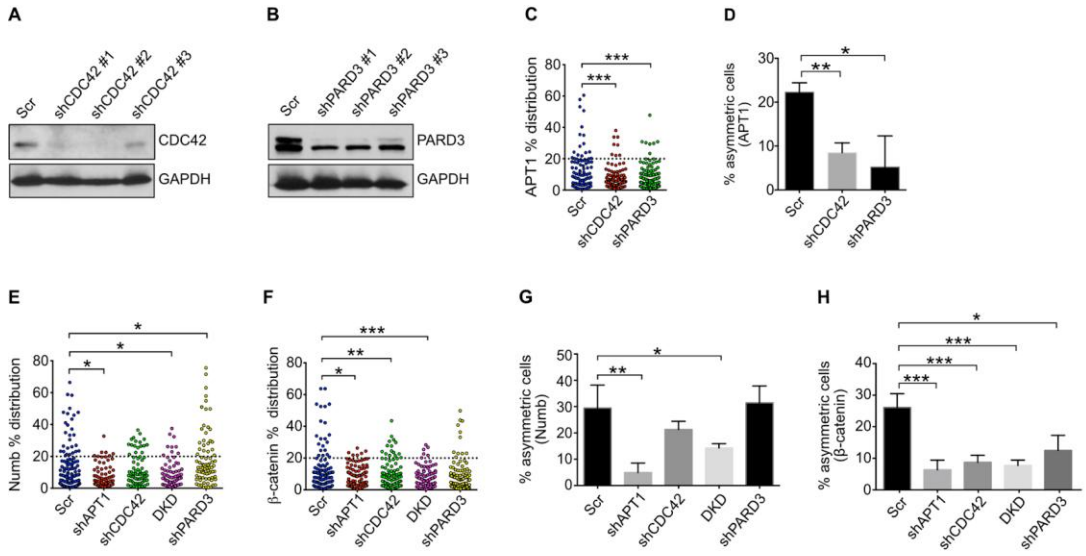

Figure 3.6 Effect of CDC42 and PARD3 knockdown on asymmetric APT1 Numb and β-catenin localization. (**A** and **B**) Immunoblot of MDA-MB-231 cell lysates when CDC42 (A) or PARD3 (B) was knocked down by shRNA. All subsequent experiments performed with shCDC42 #3 or shPARD3 #3 which showed strongest knockdown efficiency compared to GAPDH loading control. (**C, E, F**) Distribution dot plots showing the difference in mean fluorescence pixel intensity of APT1 (C), Numb (E), or β-catenin (F) across dividing MDA-MB-231 cells. The distribution of the percentage differences of all quantified cells was plotted, and cells with a difference of >20% (marked by black dotted line) were scored as asymmetric. n= 160-186 cells scored for each experimental group. Each dot represents a single cell. Asterisks indicate statistically significant differences between the indicated groups. (**D**, **G, H**) Quantifications of dividing MDA-MB-231 cells showing asymmetric APT1 (D), Numb (G) or β-catenin (H) with shAPT1, shCDC42, double knockdown using shAPT1 and shCDC42 (DKD), or shPARD3. Cells expressing a scrambled (Scr.) shRNA sequence were used as a negative control. **P* < 0.05; ***P* < 0.01, ****P* < 0.001 T-test (C and D) or ANOVA (E and F- compared to Scr.). Error bars indicate standard deviation (SD).

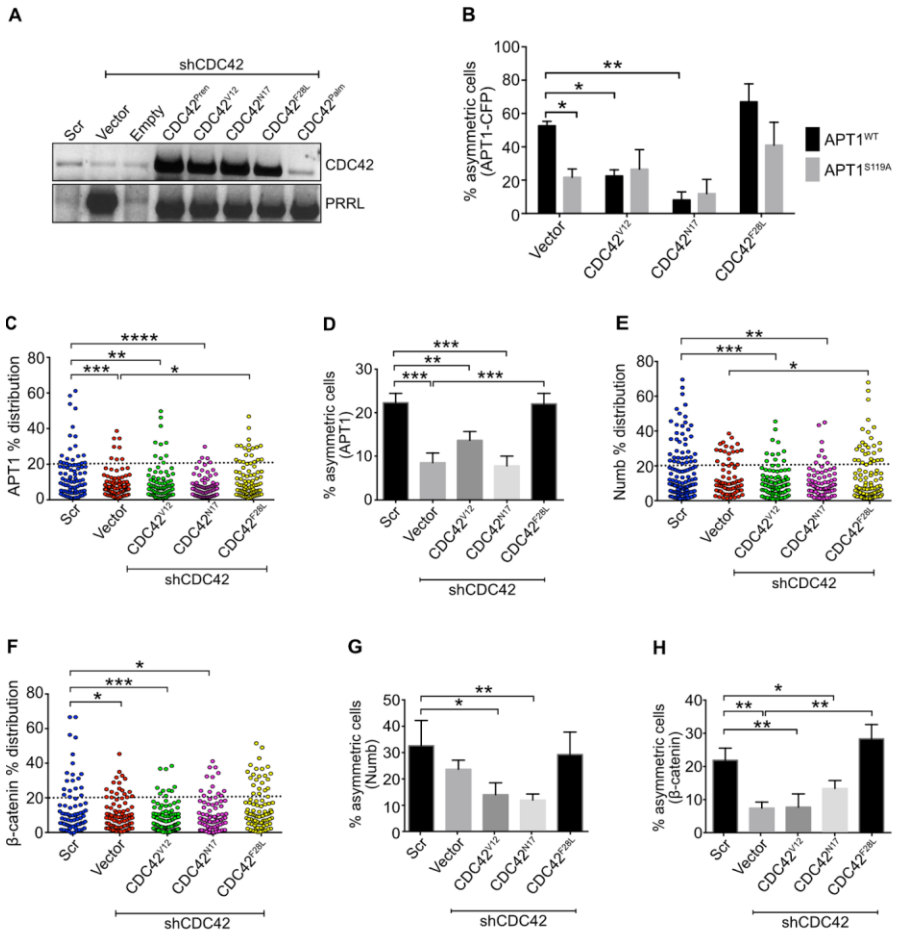

Figure 3.7 CDC42 activity promotes asymmetric APT1, Numb, and β-catenin localization. (**A**) PCR of FLAG-CDC42-PRRL plasmid expression of constitutively active $CDC42^{V12}$ or $CDC42^{F28L}$, dominant negative $CDC42^{N17}$, the prenylated CDC42 isoform ($CDC42^{Pren}$), and the CDC42 isoform that is both palmitoylated and prenylated ($CDC42^{Palm}$). Cells expressing a scrambled (Scr) shRNA sequence were used as a negative control for CDC42 knockdown, and cells expressing the empty vector were used as the negative control for the CDC42 rescue experiments. PRRL plasmid expression was confirmed using primers specific to the plasmid sequence. (**B**) Quantification of the number of dividing U2 OS cells showing asymmetric $APT1^{WT}$-CFP or $APT1^{S119A}$-CFP in cells expressing constitutively active ($CDC42^{V12}$ and $CDC42^{F28L}$) or dominant-negative ($CDC42^{N17}$) forms of CDC42. n = 152 to 288 cells scored for

each group from four independent experiments. (**C, E, F**) Distribution dot plots showing the mean fluorescence pixel intensity of APT1 (C), Numb (E), or β-catenin (F) across dividing cells. The distribution of the percentage differences of all quantified cells was plotted, and cells with a difference of >20% (dotted line) were scored as asymmetric. n= 430-465 cells scored for each experimental group. Each dot represents a single cell. Asterisks indicate statistically significant differences between the indicated groups. (**D, G, H**) Quantification of the number of dividing cells showing asymmetric localization of APT1 (D), Numb (G), or β-catenin (H) when constitutively active $CDC42^{V12}$ or $CDC42^{F28L}$, or dominant negative $CDC42^{N17}$ was co-expressed with shCDC42. Cells expressing a scrambled (Scr) shRNA sequence were used as a negative control for CDC42 knockdown, and cells expressing the empty vector were used as the negative control for the CDC42 rescue experiments. $*P < 0.05$, $**P < 0.01$, $***P < 0.001$, and $****P < 0.0001$, t test (B) and ANOVA (C-H). Error bars indicate SD.

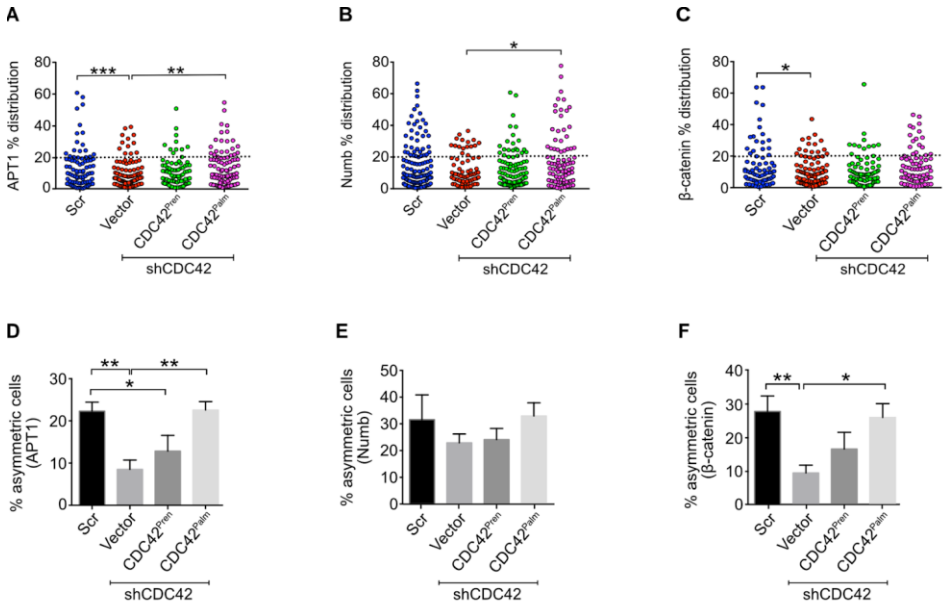

Figure 3.8 Palmitoylated CDC42 promotes asymmetric APT1 and β-catenin localization. (**A** to **C**) Distribution dot plots showing the mean fluorescence pixel intensity of APT1 (A), Numb (B), or β-catenin (C) across dividing cells. The distribution of the percentage differences of all quantified cells was plotted, and cells with a difference of >20% (dotted line) were scored as asymmetric. n= 241-390 cells scored for each experimental group. Each dot represents a single cell. Asterisks indicate statistically significant differences between the indicated groups. (**D** to **F**) Quantification of the number of dividing cells showing asymmetric localization of APT1 (D), Numb (E), or β-catenin (F) when $CDC42^{Pren}$ or $CDC42^{Palm}$ was co-expressed with shCDC42. Cells expressing a scrambled (Scr) shRNA sequence were used as a negative control for CDC42 knockdown, and cells expressing the empty vector were used as the negative control for the CDC42 rescue experiments. *$P < 0.05$, **$P < 0.01$, ***$P < 0.001$ ANOVA. Error bars indicate SD.

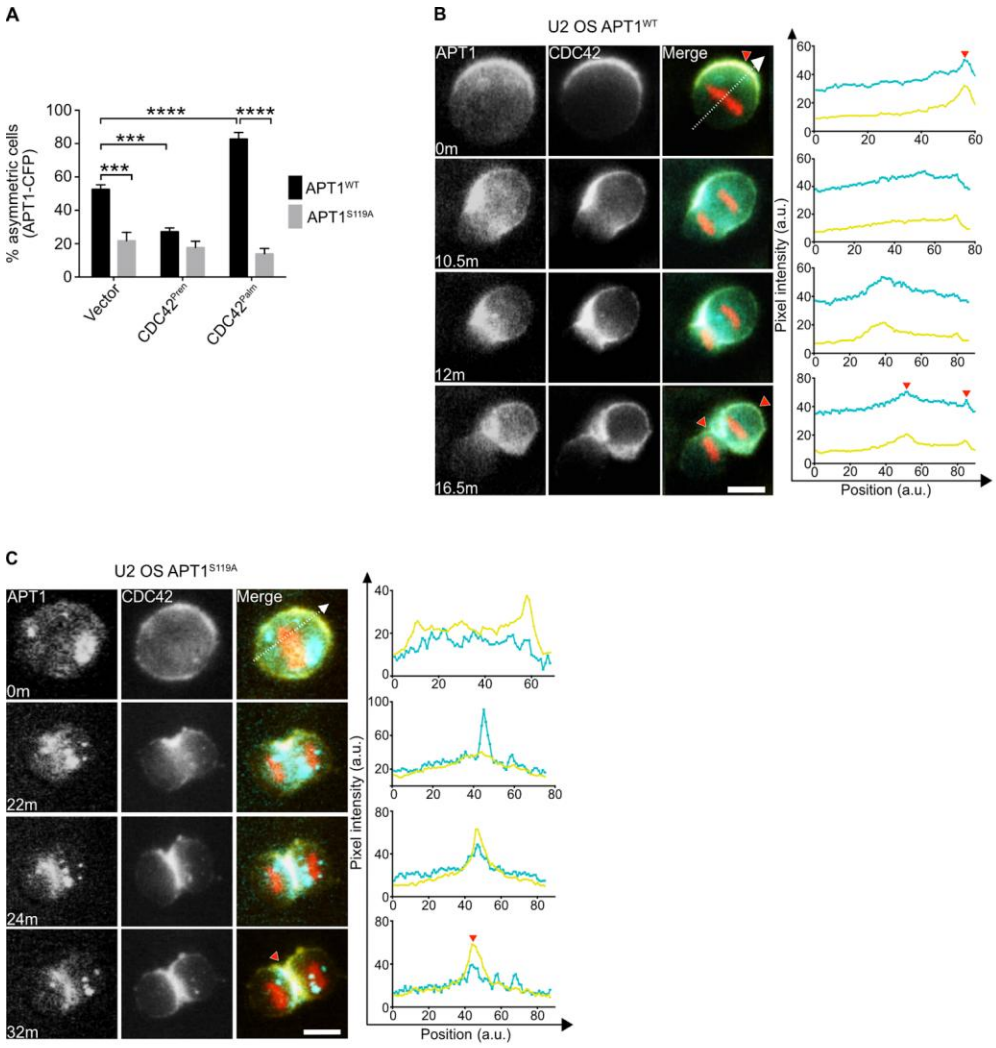

Figure 3.9 Spatio-temporal localization of CDC42^{Palm} requires APT1^{WT} activity. (**A**) Quantification of the number of dividing U2 OS cells showing asymmetric APT1^{WT}-CFP or APT1^{S119A}-CFP in cells expressing CDC42^{Pren} or CDC42^{Palm} (D). (**B and C**) Time-lapse images of dividing U2 OS cells coexpressing CDC42^{Palm}-YFP (yellow) and either APT1^{WT}-CFP (B) or APT1^{S119A}-CFP (C) (blue) and mCherry–Histone H2B (red). Overlapping CFP and YFP signal in the merge appears green. Fluorescence pixel intensity was measured along the division axis (dashed line), and the corresponding pixel values of CDC42 (yellow line) and APT1 (blue line) along the division axis were plotted. Red arrowheads on images and corresponding graphs mark

the peak asymmetric CDC42 and APT1 accumulation at the membrane or cytokinetic midbody. Time is shown in minutes (min). Scale bars, 15 μm. n = 152 to 288 cells scored for each group from four independent experiments. ***$P < 0.001$ and ****$P < 0.0001$, t test (A to D) and ANOVA (C and D). Error bars indicate SD.

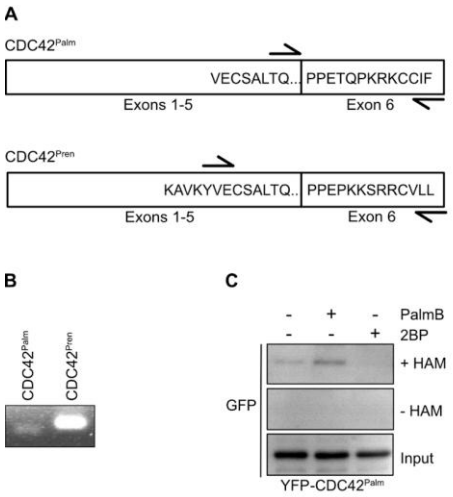

Figure 3.10 Expression of palmitoylated CDC42 in MDA-MB-231 and U2 OS cells. (**A**) Schematic of the amino acid sequence of prenylated or palmitoylated CDC42 portraying the alternatively spliced exon 6. Exon-spanning primers marked by arrows were designed to amplify the alternatively spliced exon to verify expression of the isoforms in MDA-MB-231 cells. (**B**) Expression of endogenous $CDC42^{Pren}$ or $CDC42^{Palm}$ in MDA-MB-231 cells by PCR using the primers in (H). (**C**) Immunoblot showing biotin-labeled $CDC42^{Palm}$-YFP pulled down on streptavidin beads (PD) following ABE assay of lysates from MDA-MB-231 cell that were treated with PalmB, 2BP, or DMSO control. Input lanes show lysate prior to pulldown. Samples without hydroxylamine (-HAM) samples were negative controls for the ABE reactions.

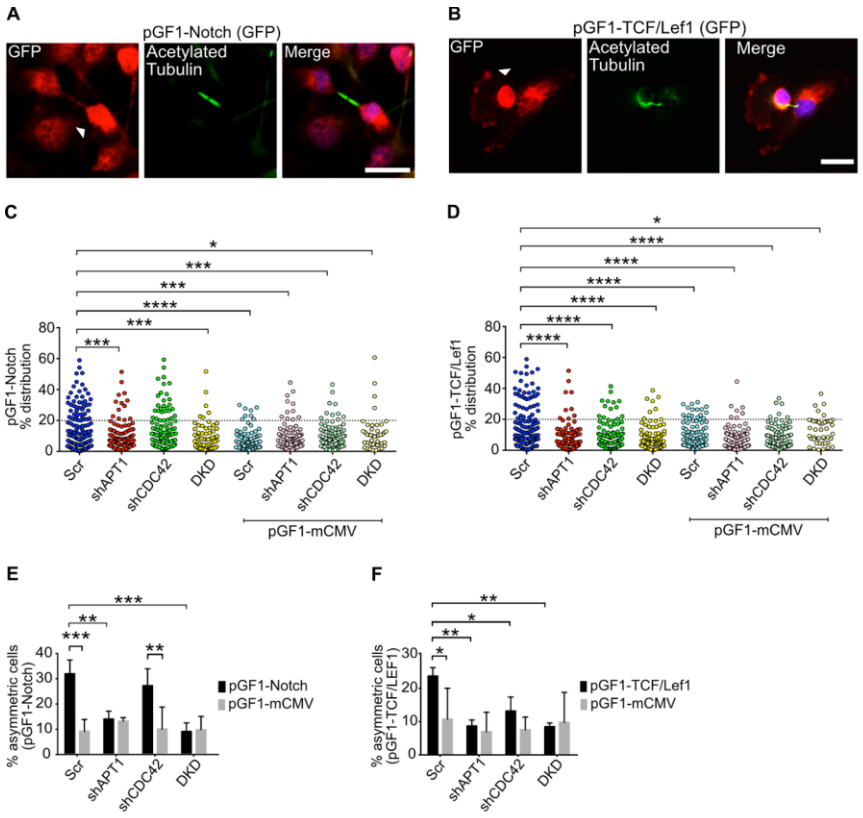

Figure 3.11 APT1 restricts Wnt and Notch transcriptional activity to one daughter cell. (**A and B**) Images of cytokinetic MDA-MB-231 cells stained to show the expression of the pGF1-Notch GFP reporter (A) or pGF-1 TCF/Lef1 GFP reporter (B) (red), acetylated tubulin (green), and nuclei (blue). Arrowheads indicate asymmetric localization. Scale bars, 15 µm. (**C and D**) Distribution dot plots showing the difference in mean fluorescence pixel intensity of pGF1-Notch reporter (C) or pGF1-TCF/Lef1 reporter (D) across dividing cells. Cells expressing an empty pGF1-mCMV GFP reporter were used as a negative control for the reporters. The distribution of the percentage differences of all quantified cells was plotted, and cells with a difference of >20% (dotted line) were scored as asymmetric. n = 784 to 822 cells scored for each experimental group. Each dot represents a single cell. Asterisks indicate statistically significant differences between the indicated groups. (**E and F**) Quantification of the number of dividing MDA-MB-231 cells showing asymmetric localization of the pGF1-Notch GFP reporter (G) or pGF1-TCF/Lef1 GFP

reporter (H) (black bars) when coexpressed with shAPT1, shCDC42, and shAPT1 and shCDC42 (DKD). Cells expressing an empty pGF1-mCMV GFP reporter (gray bars) were used as a negative control for reporter expression, and cells expressing a scrambled (Scr) shRNA sequence were used as a negative control for knockdown. *$P < 0.05$, **$P < 0.01$, ***$P < 0.001$, and ****$P < 0.001$, t-test (between reporters and pGF1-mCMV in E, F) or ANOVA (C to F). Error bars indicate SD.

CHAPTER 4: ROLE FOR PALMITOYLATION ON TUMOR DEVELOPMENT

From Stypulkowski, *et. al*. The depalmitoylase APT1 directs the asymmetric partitioning of Notch and Wnt signaling during cell division. *Sci. Signal.* **11,** (2018). Reprinted with permission from AAAS.

4.1 Summary:

The function of asymmetric cell division, if any, on tumor development remains contested and poorly understood. In this chapter, I present asymmetric cell division as a potential mechanism of maintaining cellular heterogeneity in tumors, and how this heterogeneity may be maintained by APT1 and CDC42. RNAseq analysis of MDA-MB-231 cell lines reveals APT1 expression may play a key role in regulating transcriptional programs involved in cell fate and cancer development. I identify a role for APT1 and CDC42 on the clonogenic growth, self-renewal potential, and population distribution of MDA-MB-231 cells. Together, these findings suggest that palmitoylation maintains diverse cell populations, including a pool of self-renewing tumorigenic cells, in a multi-cellular context relevant for tumor development.

4.2 Introduction

Similar to developing embryos and tissues, tumors also are comprised of phenotypically and functionally distinct cell populations (*287*, *288*). Within a tumor, cells can vary in the degree of genomic instability, epigenetic modification, invasiveness, proliferative potential, and self-renewal potential (*201*, *211*). As the different cell populations vary greatly in therapeutic

response, tumor heterogeneity presents a major challenge for cancer treatment and is closely associated with aggressive disease (*5*, *184*, *287*)(Fig. 4.1 A).

The ability to form tumors is attributed to tumor-initiating cells, which exhibit properties essential for tumor progression such as tumor formation upon single cell transplantation and generation of diverse cell populations (*227*, *287*, *289–291*) (Fig. 4.1 B). Early studies from patient samples revealed leukemia was predominantly comprised of post-mitotic cells, a smaller group of highly proliferative cells, and a rare population of quiescent cells (*287*, *292*). Subsequent studies aimed at isolating and characterizing tumor-initiating cells from murine models and patient derived samples by cell surface marker analysis, and report tumor-initiating cells exhibit stem-cell like properties such as high proliferative potential, self-renewal, quiescence, and therapeutic resistance *in vitro* and *in vivo* (*213*, *226*, *227*, *293–297*). Importantly, cellular heterogeneity is observed in tumors grown from a single tumor-initiating cell by surface marker and functional analysis (*226*, *289*, *291*, *293*, *298*). Furthermore, tumor-initiating cells may exhibit epigenetic alteration, genetic instability, and/or activation of metabolic pathways which promote cell survival and heterogeneity after treatment (*210*, *213*, *214*, *288*, *296*). While mechanisms have been proposed, the factors generating and maintaining tumor-initiating cells and tumor cell heterogeneity still remain unclear and present a challenge for successful, targeted treatment strategies.

Whether asymmetric cell division promotes tumor cell heterogeneity, as it does during development, remains to be determined. Loss of cell polarity is a classic hallmark of oncogenic transformation and tumor growth, and polarity regulators have been reported to function as tumor suppressors as discussed in Chapter III (*184*, *251*, *286*). Consequently, asymmetric cell division is also thought of as a tumor suppressor to prevent aberrant cell population expansion, which thought to be driven by symmetric cell division within tumors (*299–301*). However, transformed

cells undergo directed cell migration and directed vesicular transport, processes which required directional protein localization, suggesting that polarity is not completely disrupted (*70*, *93*). Although asymmetrically dividing cells have been observed in cancer cells (*218*, *219*, *294*, *299*, *302*), whether these divisions contribute to tumor cell heterogeneity and disease progression is still poorly understood.

As reviewed in chapter I, palmitoyltransferases display tumor suppressor or tumor promoting function. In contrast, the function of depalmitoylating enzymes within tumors is largely unknown. In this chapter, I find APT1 loss-of-function affects the transcriptional profile, anchorage independent growth, and self-renewal potential of MDA-MB-231 cells, which are derived from an aggressive breast cancer subtype known to exhibit a high degree of cellular heterogeneity (*298*). Moreover, I observe APT1 is required for the expression of Wnt, Notch, and Sox2 transcriptional reporters in clonogenically-derived colonies, which may correlate with cellular heterogeneity and tumorigenicity. Furthermore, flow cytometry analysis reveals the tumor-initiating cell population is decreased upon APT1 knockdown, implicating a function for APT1 in the maintenance of tumorigenicity through self-renewal. With these findings, I identify a potential role for APT1-mediated asymmetric cell division on tumor cell heterogeneity.

4.3 APT1 induces Wnt, Notch, and mammary stem cell transcriptional signatures in MDA-MB-231 triple receptor–negative breast cancer cells

To date, APT1 has not been shown to drive transcriptional changes in a developmental or disease context. To further investigate the observed influence of APT1 on asymmetric Notch and Wnt reporter activity, I employed RNA-seq analysis of wild-type control, APT1 knockdown, or $APT1^{WT}$-expressing MDA-MB-231 cells to ask whether APT1 influences a Notch or Wnt gene

signature (table S1). Gene set enrichment analysis (GSEA) was performed using a pre-ranked list of differentially expressed genes and compared $APT1^{WT}$-expressing cells vs. control cells, APT1 knockdown cells vs. control cells, and $APT1^{WT}$-expressing cells vs. APT1 knockdown cells to further examine whether previously defined gene signatures were altered. In APT1 knockdown cells compared to control cells, a high scoring signature [NES (normalized enrichment score) of 1.46 and a false discovery rate (FDR) q-value of 0.073] was identified that positively correlated with genes reported to increase with overexpression of active β-catenin (BCAT_UP.V1_UP), suggesting APT1 is inhibitory to β-catenin signaling (Fig. 4.2 A, D). When comparing $APT1^{WT}$-expressing cells to control cells, a negative correlation (NES 1.25 and FDR q-value 0.302) was identified for a signature of genes reported to decrease upon pharmacologic inhibition of Notch (NOTCH_DN.V1_DN). A similar pattern was observed with APT1 knockdown suggesting APT1 overexpression may function in a dominant negative manner to suppress Notch signaling (Fig. 4.2 B, D). Additionally, comparing $APT1^{WT}$-expressing cells to APT1 knockdown cells revealed a high scoring signature (NES 2.34, FDR q-value=0.0001) for genes reported to increase in mammary stem cells (PECE_MAMMARY_STEM_CELL_UP) (Fig. 4.2 C). Visualization of the leading-edge genes from the mammary stem cell signature also indicated a strong decrease in expression with APT1 knockdown when normalized to control wild-type cells, (Fig. 4.2 E), suggestive of an altered cell fate.

Two additional high scoring signatures found in $APT1^{WT}$-overexpressing cells compared to APT1 knockdown cells were signatures for Myc and Cyclin D1 overexpression, both of which are maintained by Wnt and Notch signaling (*303–305*) (NES 2.08, FDR q-value 0.0001; NES 1.69, FDR q-value 0.014) (Fig. 4.2 F, G). Target genes with high log_2FC (fold change) values were validated by qRT-PCR. Notable APT1-driven genes included *DKK1*, *BMP4*, *GATA6*, and *KLF5* (*306–308*) (Fig. 4.2 H, I; table S1).

Based on the high-scoring gene expression signature for mammary stem cells observed in APT^{WT}-overexpressing cells, it is possible APT1 asymmetrically restricts signaling pathways that are activated in stem cells. The transcription factor Sox2 has been implicated in mammary stem cell function (*309*), and expression of a Sox2-responsive reporter (pGF1-SRR2) revealed that its asymmetric signal was reduced with APT1 knockdown or PalmB treatment (Fig. 4.3 AD). DHHC20, CDC42, or APT1 and CDC42 double knockdown reduced the asymmetric SRR2 signal (Fig. 4.3 B, C, E). Asymmetric APT1 localization was also observed in dividing mouse embryonic stem cells expressing an $APT1^{WT}$ plasmid (Fig. 4. 4). These results imply a role for palmitoylation in promoting cell fate–related transcriptional signatures and maintaining asymmetric cell division in progenitor cells.

4.4 APT1 and CDC42 maintain unique cell populations in MDA-MB-231 colonies

Triple receptor–negative breast tumors, like that from which MDA-MB-231 cells were derived, contain subpopulations of cells that vary in proliferative, self-renewing, and tumor-initiating potential (*218*, *226*, *228*). However, whether asymmetric cell division contributes to the generation of functionally heterogeneous cells in tumors is unclear. The colony formation assay was utilized, which measures the growth and survival of transformed cells in anchorage-independent conditions. Because only a subset of transformed cells can form colonies, this assay may also indicate the degree of heterogeneity within a cell population and may correlate with tumor-initiating potential (*218*, *310*). Knocking down APT1 reduced the colony-forming potential of MDA-MB-231 cells by 2.3-fold (average colonies counted: shAPT1, 39 vs. Scr, 90), whereas expressing $APT1^{WT}$ increased colony numbers by 1.7-fold (average colonies counted: $APT1^{WT}$,

152 vs. Scr, 90), suggesting that APT1 is required for the anchorage-independent growth and tumorigenic potential of transformed cells (Fig. 4.5 A).

Self-renewing cells within the colony are expected to form new colonies upon serial dissociation and replating, indefinitely. To test whether APT1-mediated asymmetry maintains a self-renewing population within colonies, the self-renewal potential of APT1 knockdown or CDC42 knockdown MDA-MB-231 cells in colonies was examined over 3 rounds of dissociation and replating. APT1 knockdown significantly reduced the number of colonies on the second and third plating, suggesting depletion of colony-initiating cells (Fig. 4.5 B). Unexpectedly, CDC42 knockdown increased the number of colonies formed with each replating compared to control cells, suggesting an expansion of a colony-initiating cell population (Fig. 4.5 C). Colonies from APT1 and CDC42 double knockdown cells showed reduced replating ability (Fig. 4.5 D), again demonstrating that the expansion of this colony-forming population is dependent on APT1. Because a significant impairment of proliferation was not observed, this result would suggest that the reduced colony-forming potential is not due decreased proliferation under adherent growth conditions (Fig. 4.5 E-G).

Because the increase in colony-forming potential of CDC42 knockdown cells was unexpected, I hypothesized this could be caused by increased symmetric divisions of colony-initiating cells. A subset of highly tumorigenic cells in basal breast cancers have been shown to reactivate developmental signaling pathways such as those dependent on Notch, Wnt, or Sox2 (*226*, *298*, *311*, *312*). Pharmacologic inhibition of Wnt (with the Porcupine inhibitor IWP2) or Notch (with the γ-secretase inhibitor compound E) reduced the self-renewal potential of colonies similar to APT1 knockdown or double knockdown (Fig. 4.6 A). Furthermore, APT1 knockdown increased Wnt reporter signal and decreased Notch and Sox2 reporter signals in colonies (Fig. 4.6 B). This is consistent with GSEA analysis in Fig. 4.2 that indicated APT1 knockdown suppressed

Notch signaling and promoted β-catenin signaling and pathways active in mammary stem cells. Knocking down CDC42 reduced the Notch reporter signal, but increased the Sox2 reporter signal in most of the cells within the colony (Fig. 4.6 B). The Sox2 reporter has been previously shown to correlate with increased tumorigenicity (*298*)**;** these results therefore suggest that the increase in colony formation caused by CDC42 knockdown is due to an increase in Sox2 transcriptionally-active cells.

To address the possibility that APT1 maintains a specific subpopulation of tumorigenic cells, colonies were dissociated and analyzed by flow cytometry to test for the cell surface marker profile associated with highly tumorigenic cells in breast cancers: CD44 high, CD24 low, and Aldehyde dehydrogenase high ($CD44^+$/ $CD24^{lo}$/ $ALDH^+$) (*226*). The size of the $ALDH^+$ population was higher in APT1 knockdown cells (16.7%) as compared to control (7.3%) or CDC42 knockdown (7.8%) cells on the first replating (Fig. 4.7). A difference in the cell population distribution was observed in between colony replatings and also, cells grown in adherent culture conditions (Fig. 4.8 A). Further gating the $ALDH^+$ population for $CD44^+/CD24^{lo}$ cells revealed that knocking down APT1 reduced $CD44^+/CD24^{lo}$ cells (2.6%), whereas knocking down CDC42 increased this population (14.4%), as compared to control cells (5.3%) (Fig. 4.8 B). The trend of the number of $CD44^+/CD24^{lo}/ALDH^+$ cells being reduced in the APT1 knockdown condition and increased in the CDC42 knockdown condition was sustained on second and third replatings (Fig. 4.8 B). A similar pattern was observed to a lesser extent in adherent cells (Fig. 4.8 B). Consistent with the observed colony phenotypes, these results may explain why CDC42 knockdown cells form many colonies whereas APT1 knockdown cells are unable to do so. Taken together, these findings demonstrate that in an anchorage-independent setting, an APT1-CDC42 axis maintains the expansion of a self-renewing, tumorigenic cell population and activation of transcriptional profiles required to maintain this population.

4.5 Discussion

By manipulating APT1 expression, I have shown that the asymmetric activation of Notch, Wnt, and Sox2 transcriptional reporters can be altered without directly affecting the expression of transcription factors or upstream signaling factors. The fact that β-catenin and Notch gene signatures were not as high-scoring as compared to those of mammary stem cells, Myc, and Cyclin D1 signatures may indicate that APT1 directs combinatorial signaling to determine cell identity. Myc and Cyclin D1 are canonical downstream transcriptional targets of both Wnt and Notch and are also involved in determining mammary stem cell identity (*303–305*). Within the mammary stem cell signature was a notable abundance of ribosomal proteins. A similar abundance in ribosomal proteins was also present in the Myc signature, consistent with its role in driving ribosomal biogenesis and protein translation in the mammary gland, among other tissues, and in cancer (*313, 314*). Because Myc is a critical factor for mammary stem cell identity and function (*303*), these results would suggest APT1 has a role in translation in mammary stem cells. What remains unclear is whether altering APT1 protein amounts induces the expansion of a population of cells expressing a mammary stem cell transcriptional signature or induces a de novo transcriptional signature in most cells. Presented here is also evidence of asymmetric APT1 localization in dividing mouse embryonic stem cells expressing $APT1^{WT}$, suggesting that this mechanism may also have a broader and conserved role in development. Future experiments including single-cell RNAseq may address these questions.

Consistent with the concept of changing cell populations, these results suggest that APT1 is required to maintain a tumorigenic population of breast cancer cells whereas CDC42 appears to restrict the size of this population. These findings indicate that APT1 may contribute to the activation of transcriptional programs promoting colony-forming potential, whereas CDC42 could restrict APT1 activity to one daughter during asymmetric division. This would be

consistent with the increase in the $CD44^{+}$/ $CD24^{lo}$/$ALDH^{+}$ population in CDC42 knockdown colonies. The implications of this study may be relevant to human disease because APT1 is amplified in various cancers, and this amplification is correlated with poor patient prognosis, suggesting APT1 could function in the development and progression of human cancers (*315*, *316*). Although the importance of self-renewing, tumor-initiating, or stem-like cells in cancer is still unclear, the question of how tumors maintain and generate cells with diverse properties such as metastatic potential, dormancy, and drug resistance is still a critical one. Further exploration of the mechanisms that establish and direct asymmetric cell division and promote cellular heterogeneity may help us understand tumor development and progression.

Asymmetric cell division is thought to function as a tumor suppressor by restricting the size of cell populations, e.g. stem vs. differentiated cells. Symmetric cell divisions function to rapidly expand cell populations, allowing tissues and organisms to develop from a single cell. Applying these principles to tumor growth suggests symmetric cell divisions are tumor promoting (*201*, *299*, *300*). As discussed in the introduction, it is possible that asymmetric and symmetric cell division both occur in a tumor. Asymmetric cell divisions may thus be one mechanism of generating and maintaining diverse cell populations, while symmetric cell divisions may drive the expansion of these various populations.

Several studies have hypothesized that asymmetric cell divisions may also function to segregate damaged or old organelles, proteins, and damaged DNA template to prevent propagation of damage that would result in cell cycle arrest or death (*5*, *31*, *205*, *247*, *286*, *317*, *318*). Within a tumor, this could maintain a pool of therapy-resistant cells by ensuring that cells with sub-optimal fitness (likely to undergo treatment-induced apoptosis) are eliminated. Currently, imaging asymmetric cell division *in situ* remains a major challenge, but the development of new imaging assays and identification of asymmetric biomarkers may open up

possibilities for imaging explanted patient samples to better understand asymmetric cell division in disease progression (*287*, *294*, *319*, *320*). Understanding all possible factors that generate cellular heterogeneity may uncover new insights into the mechanisms of disease recurrence and therapeutic resistance.

MATERIALS AND METHODS

Cell Culture

MDA-MB-231 cells were cultured in DMEM + glutamax (Thermo Fisher; Cat. No. 10566-016) and 10% fetal bovine serum. For drug treatment, cells were treated with DMSO (Sigma; Cat. No. D2650), 10μM Palmostatin B (EMD Millipore; Cat. No. 178501) prepared in DMSO for 16 hours before staining or harvesting for cell lysates. Cells were treated with 0.5ug/mL puromycin for selection. E14 ESCs were cultured in DMEM Knockout (ThermoFisher. Cat. 10829-018), 15% fetal bovine serum, 1% L-glutamine, 1% Pen Strep, 1% Non-essential amino acids, 0.1 mM 2 mercaptoethanol, 1000 units/mL Leukemia inhibitory Factor (Sigma, Cat. L5158), 1 μM MEK I/II Inhibitor (Millipore, Cat. 444966), 3μM GSK3 Inhibitor XVI (Millipore, Cat. 361559) on gelatin coated tissue culture plates.

Stable cell lines

HEK cells were transfected with 0.69 μg/μL of a GAG, Rev, and Vsvg mix and 1.42 μg/μL of the following plasmids: Scramble control, pGF-SRR2-mCMV-GFP-puro (System Biosciences; Cat. No. SR20071-PA-P) or pGF-mCMV-GFP (System Biosciences; Cat. No. TR011PA-1), for 24 hours with LT-1 transfection reagent (Mirus Bio. Cat. MIR2300). Virus was collected 72 hours after infection with 0.5-1mL virus used for stable cell line generation. E14 ESCs were infected with $APT1^{WT}$ -CFP-FLAG lentivirus for 24 hours, then recovered in complete DMEM-knockout for 48 hours prior to cell culture. MDA-MB-231 were infected with the pGF-SRR2-mCMV-GFP-puro or pGF-mCMV-GFP lentivirus for 24 hours and recovered in complete DMEM for 48 hours prior to cell culture.

Short hairpin design

shRNA for CDC42

F: 5'-
CCGGAGATTACGACCGCTGAGTTATCTCGAGATAACTCAGCGGTCGTAATCTTTTTTG
-3'
R:
5'AATTCAAAAAAGATTACGACCGCTGAGTTATCTCGAGATAACTCAGCGGTCGTAAT
CT-3'

shRNA for APT1
F 5'-
CCGGTAGGCCTGTTACATTAAATATCTCGAGATATTTAATGTAACAGGCCTATTTTTG
-3'
R 5'-
AATTCAAAAATAGGCCTGTTACATTAAATATCTCGAGATATTTAATGTAACAGGCCT
A-3'

Immunofluorescence

MDA-MB-231 cells were plated on glass coverslips and treated as described. Cells were fixed in 10% formalin, blocked in 5% BSA in TBS containing 0.1% Triton-X (Roche), incubated in primary antibody (GFP (ab290), Abcam; 1:500) (Acetylated tubulin, Santa Cruz; Cat. No. sc23950; 1:1000), for 1-2 hours at room temperature, then incubated in secondary antibody (Alexafluor 488 goat anti-mouse (A11001)/ Alexafluor 594 goat anti-rabbit (A11012), Life Technologies; 1:1000) for 1 hour at room temperature, and mounted in DAPI-mount (Southern Biotech; Cat. No. 0100-20). ESCs were cultured without LIF, MEK or GSK inhibitors for 24 hours before staining with 1:1000 anti-GFP (ab290) as described. Cells were imaged using the Leica DMI6000B inverted microscope on 40X magnification and colonies were imaged on 20X magnification.

Quantification and line scan analysis

Cells were quantified by drawing around the mitotic spindle poles, or around each daughter cell in cytokinesis using the Leica LAS AF software as shown in Fig. S1A. Percent difference was calculated from the Mean Gray Values generated in Leica LAS AF and calculated as described in

Fig. S1A. The distribution of acquired percentage differences for each experimental condition were plotted as dot plots. Cells with a percentage difference of 20 or greater were counted as asymmetric and plotted in a bar graph. All graphs were generated with Prism software. Linescan analysis of pixel intensity was performed on still frames from live-cell movies using ImageJ software.

Colony Assays

MDA-MB-231 cells were plated on 6-well, low adhesion plates (Corning; Cat. No. 3471) in 2mL of WIT-P plus serum-free supplement growth media (Cellaria; Cat. No. 00-0045-500) containing 20ng/mL FGF (Life Technologies; Cat. No. PHG0024), 20ng/mL EGF (Life Technologies; Cat. No. PHG0311), and 10 μg /mL heparin (StemCell Technologies; Cat. No. 07980). Each well contained 4,000 cells. Cells were treated with 1 μM GSI (Compound E; Millipore; Cat. No. 565790), 5 μM IWP2 (StemCell Technologies; Cat. No. 72124), or DMSO (Sigma; Cat. No. D2650) and grown for 7 days before counting. For replating, cells were grown into colonies as described. On Day 7, colonies were spun down at 1000rpm x 5min, resuspended in 0.05% Trypsin-EDTA, reconstituted in growth media, and plated as described above. This process was repeated for three replatings in duplicate.

Proliferation Assays

15,000 MDA-MB-231 cells were plated on a 12-well dish (ThermoFisher; Cat. No. 087723A). At 24, 48, and 72 hours, cells were washed with 1X PBS, trypsinized, and spun at 1000rpm X 5 minutes. Pellets were resuspended in DMEM and counted by a hemocytometer.

RNA Isolation and Quantitative Real-Time PCR

Total RNA was isolated from cells using RNeasy Mini Kit (Qiagen; Cat. No. 74104) and cDNA

was synthesized from 2,000ng total RNA using SuperScript III First-Strand Synthesis SuperMix (Life Technologies; Cat. No. 18080400). qRT-PCRs were performed in triplicate using standard SYBR green reagents and protocols on a StepOnePlus Real-Time PCR system (Applied Biosystems). Target genes with high log_2FC values were chosen for validation. The target mRNA expression was quantified using $^{\Delta\Delta}$Ct method and normalized to GAPDH expression. The following primers were used for validation:

hDKK1
F: 5'- CAGGCGTGCAAATCTGTCT – 3'
R: 5'- AATGATTTTGATCAGAAGACACACATA – 3'

hFGF5
F: 5'- CCCAGAATCAGCCCTACAAG – 3'
R: 5'- GAGGAGGAAGGACAAGCTCA – 3'

hGATA6
F: 5'- GCAAAAATACTTCCCCCACA – 3'
R: 5'- TCTCCCGCACCAGTCATC – 3'

hKLF5
F: 5'- CTGCCTCCAGAGGACCTG – 3'
R: 5'- TCGTCTATACTTTTTATGCTCTGGAAT – 3'

hITGB4
F: 5'- TCAGCCTCTCTGGGACCTT – 3'
R: 5'- TCCTTATCCACACGGACACA – 3'

hBMP4
F: 5'- TCCACAGCACTGGTCTTGAG – 3'
R: 5'- TGGGATGTTCTCCAGATGTTCT – 3'

hPTK7
F: 5'- CAGAGGACTCACGGTTCGAG – 3'
R: 5'- TACCAGGGTCTCTGCCACTC – 3'

hGAPDH
F: 5'- ACA CCA TGG GGA AGG TGA AG-3'
R: 5'-AAG GGG TCA TTG ATG GCA AC -3'

hCDC42 palm
F: 5'-TGGAGTGTTCTGCACTTACA-3;
R: 5'-GAATATACAGCACTTCCTTTTGGG-3'

hCDC42 prenyl
F: 5'-AGGCTGTCAAGTATGTGG-3'
R: 5'-TAGCAGCACACACCTGCG-3'

RNA Isolation and analysis for RNA-seq

Total RNA was harvested from MDA-MB-231 control, $APT1^{WT}$-overexpressing or shAPT1 cells using the RNeasy RNA isolation kit (Qiagen; Cat. No. 74104). 100ng of RNA was used to generate cDNA libraries with the Illumina TruSeq mRNA Library Prep Kit for NeoPrep library preparation system (Illumina; Cat. No. NP-202-1001) and reaction was performed on a NextSeq500 sequencer. Analysis was prepared by the DNA Sequencing Facility at the Perelman School of Medicine, University of Pennsylvania as follows: estimated transcript levels were ranked with Salmon, TX Import was used to condense transcript levels to gene intensity, and Deseq2 was used to calculate statistical levels for each condition. The scaled values (determined by DeSeq2) were input to Gene Set Enrichment Analysis software (Broad Institute) and analyzed against the C2 Chemical and Genetic perturbations, C6 Oncogenic, and Hallmark signatures gene matrix applying classic enrichment statistic. Heat maps were generated by taking the $\log_2$ values with an offset of 1 for all conditions and targets were chosen by taking the leading-edge targets from GSEA BCAT, NOTCH, and mammary stem cell sets. The average of the 3 control wild-type values were subtracted from each individual value. Values were clustered for samples and genes using Euclidean similarity measure with average linkage.

Flow cytometry

Adherent non-confluent MDA-MB-231 cells or colony-dissociated cells were treated to detect ALDH activity using the ALDEFLUOR assay (Stem Cell Technologies; Cat. No. 01702) according to manufacturer's protocol. Diethylaminobenzaldehyde (DEAB) was used as a negative control to set ALDH + gates. Cells were stained for surface markers with CD44-APC

(BD Biosciences; Cat. No. 560890), CD24-PE (BD Biosciences; Cat. No. 560991), and Live/Dead Violet (Thermo Fisher; Cat. No. L34963) for viability. Compensation was performed using Ultra Comp beads (Thermo Fisher; Cat. No. 01-2222-41). Experiments were run on the Attune NxT flow cytometer system (Life Technologies) and analyzed with FlowJo software. ALDH+ cells (Fig. S7) were gated for $CD44^{+}/CD24^{lo}$ (Fig. 7C) for comparison.

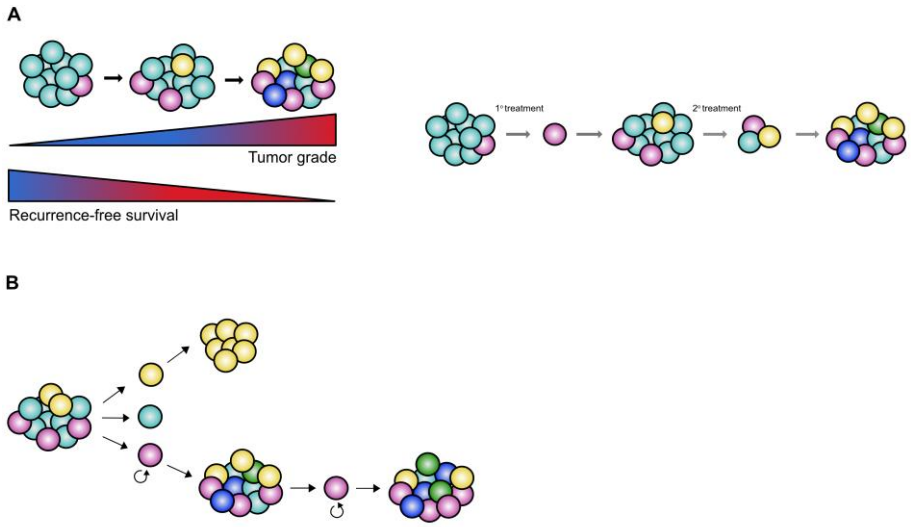

Figure 4.1 Schematic representation of tumor cell heterogeneity on tumor development and therapeutic resistance. (A) Increasing cellular heterogeneity is associated with aggressive, drug-resistant disease. Cells may exhibit various properties such as therapeutic resistance, genomic instability, epigenetic modification, metabolic alteration, self-renewal, and quiescence, which promote cell survival during therapy. (**B**) Tumor-initiating cells are believed to exhibit stem-like properties such as self-renewal, quiescent, and generation of diverse cell types from a single cell, which contributes to tumor cell heterogeneity and facilitates therapeutic resistance. Tumor-initiating cells may arise stochastically from any cell within the tumor, suggesting plasticity in cell behavior. Alternatively, tumor-initiating cells may represent a distinct population within a cellular hierarchy. Although the mechanisms that generate and maintain tumor-initiating cells remain unknown, this cell population represents a major challenge to overcoming drug resistance. Adapted from Meacham *et. al.* and Michor *et. al.* (*211*, *287*).

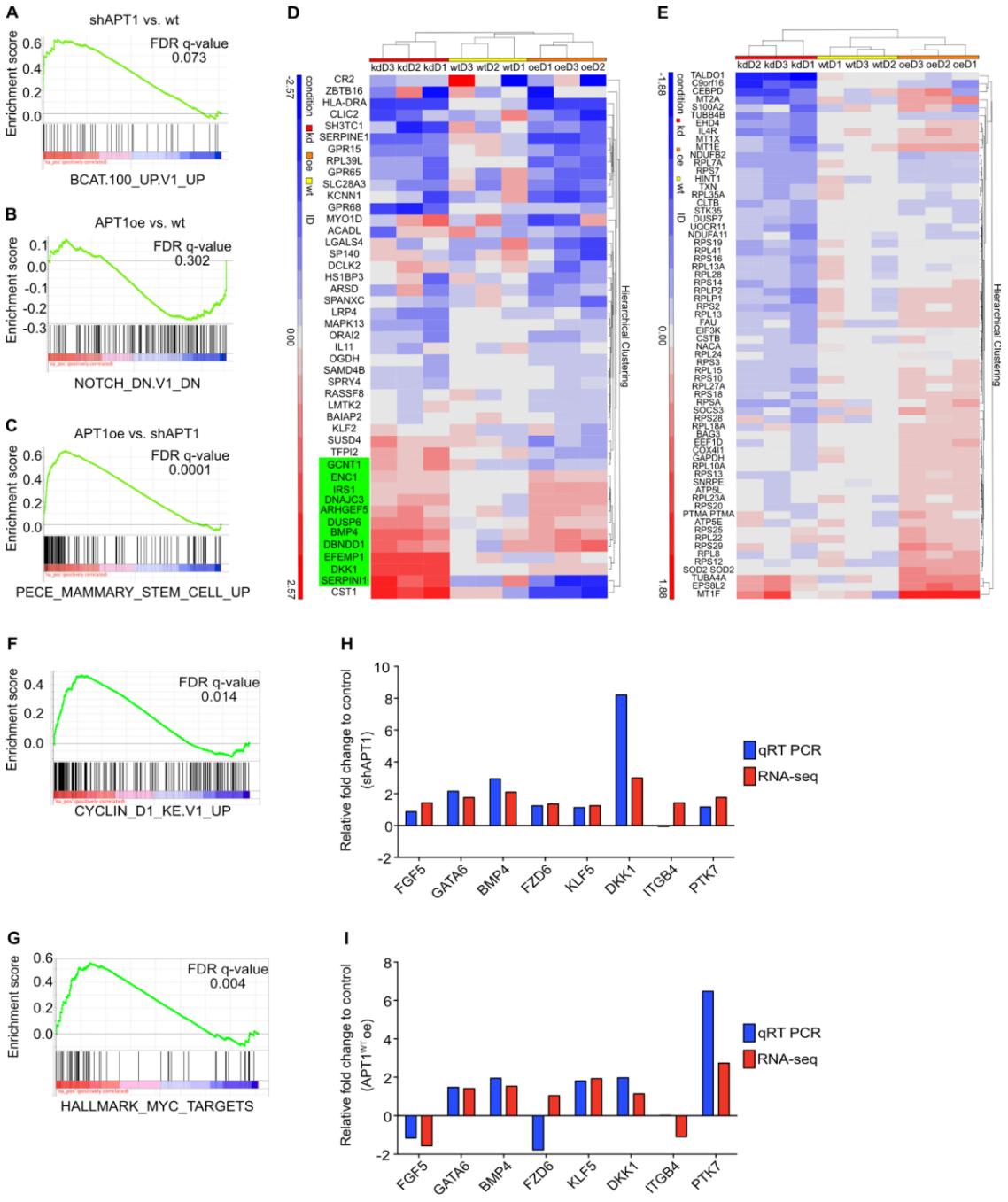

Figure 4.2 Altering APT1 expression changes β-catenin and Notch gene signatures in MDA-MB-231 cells. (**A** to **C**) Gene set enrichment analysis (GSEA) of a top-scoring β-catenin overexpression transcriptional signature in MDA-MB-231 cells when APT1 was knocked down and compared against control cells [false discovery rate (FDR) q value, 0.073] (A), a Notch

inhibition signature when APT1^{WT} was overexpressed and compared against control cells (FDR q value, 0.302) (B), and a mammary stem cell signature when APT1^{WT} was overexpressed and compared against shAPT1 cells (FDR q value, 0.0001) (C). (**D**) Heat map of leading edge genes identified in the β-catenin and Notch gene signatures shown in Fig. (A) and (B). Data are grouped by APT1 knockdown (kd) cells, APT1^{WT} overexpressing (oe) cells, and control (wt) cells. Genes identified in the β-catenin signature are highlighted in green. (**E**) Heat map of leading-edge genes obtained from the mammary stem cell signature shown in (C). Data are grouped by APT1 knockdown (kd) cells, APT1^{WT}-overexpressing (oe) cells, and control (wt) cells. (**F** and **G**) Gene set enrichment analysis (GSEA) of additional top-scoring Cyclin D1 (FDR q-value= 0.014) (B) or Myc (FDR q-value= 0.004) (C) transcriptional signatures in MDA-MB-231 cells when APT1^{WT} was overexpressed and compared against shAPT1 cells. (**H** and **I**) Quantitative RT-PCR (qRT-PCR) validation of target genes identified from the RNA-seq in shAPT1 (D) cells or APT1^{WT}-overexpressing (E) cells**.** Average fold change in expression shown by qRT-PCR (blue bars) and RNA-seq (red bars). Graphs show average of three independent experiments.

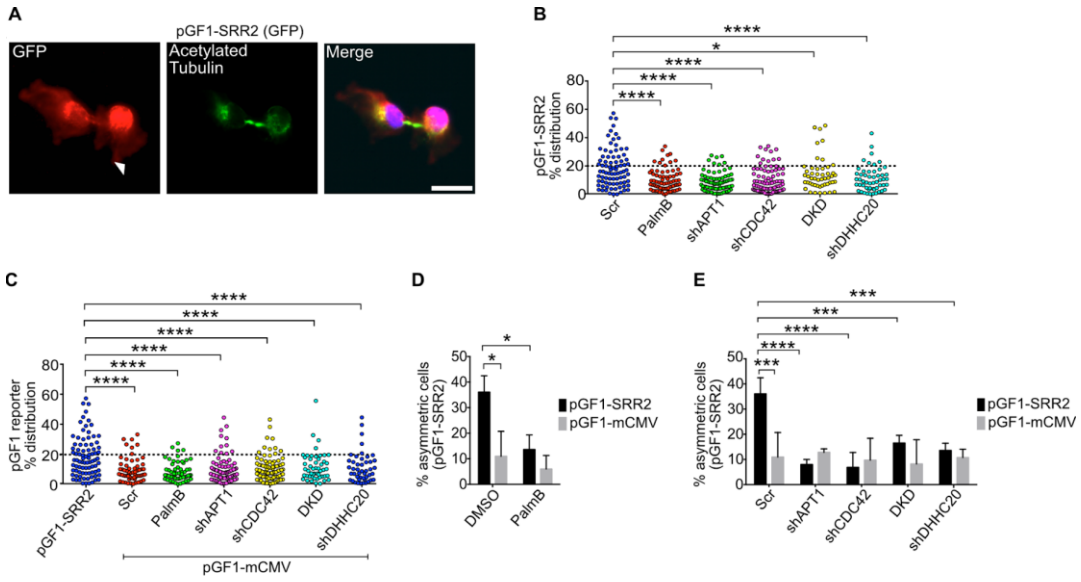

Figure 4.3 Asymmetric expression of a Sox2-responsive transcriptional reporter requires palmitoylation and CDC42. (**A**) Images of cytokinetic MDA-MB-231 cells stained to show the pGF1-SRR2 GFP reporter (red), acetylated tubulin (green), and nuclei (blue). Arrowheads indicate asymmetric localization of pGF1-SRR2. Scale bar, 15 µm. (**B** to **C**) Distribution dot plots showing the difference in mean fluorescence pixel intensity of the pGF1-SRR2 reporter (B) across dividing MDA-MB-231 cells. Cells expressing an empty pGF1-mCMV GFP reporter (C) were used as a negative control for the reporters. The distribution of the percentage differences of all quantified cells was plotted, and cells with a difference of >20% (dotted line) were scored as asymmetric. n = 959 cells scored for the experimental group. Each dot represents a single cell. Asterisks indicate statistically significant differences between the indicated groups. (**D**) Quantification of dividing MDA-MB-231 cells showing asymmetric localization of the pGF1-SRR2 GFP reporter after treatment with PalmB or DMSO control (black bars). Cells expressing an empty pGF1-mCMV reporter (gray bars) were used as a negative control for reporter expression. (**E**) Quantification of the number of dividing MDA-MB-231 cells showing asymmetric localization of pGF1-SRR2 GFP reporter (black bars) when coexpressed with

shAPT1, shCDC42, shAPT1 and shCDC42 [double knockdown (DKD)], or shDHHC20. Cells expressing an empty pGF1-mCMV GFP reporter (gray bars) were used as a negative control for reporter expression, and cells expressing a scrambled (Scr) shRNA sequence were used as a negative control for knockdown conditions. $^{**}P < 0.01$ and $^{****}P < 0.0001$, t test (between reporters and pGF1-mCMV, D, E) or ANOVA (H). Error bars indicate SD.

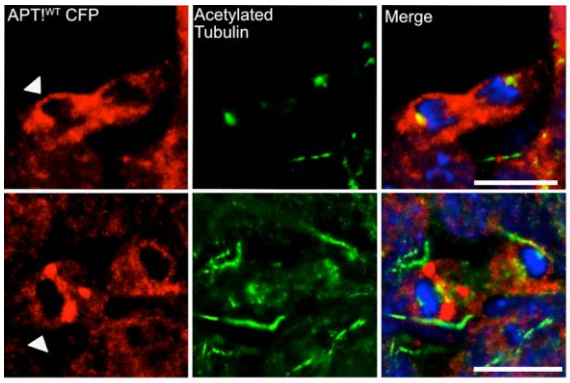

Figure 4.4 APT1^{WT} is asymmetrically expressed of in dividing mouse embryonic stem cells. Representative immunofluorescence of E14 mouse embryonic stem cells overexpressing APT1^{WT}-CFP-FLAG stained to show APT1 localization with a GFP antibody that cross-reacts with CFP (red), acetylated tubulin (green), and nuclei (blue). Scale bars, 15 μm.

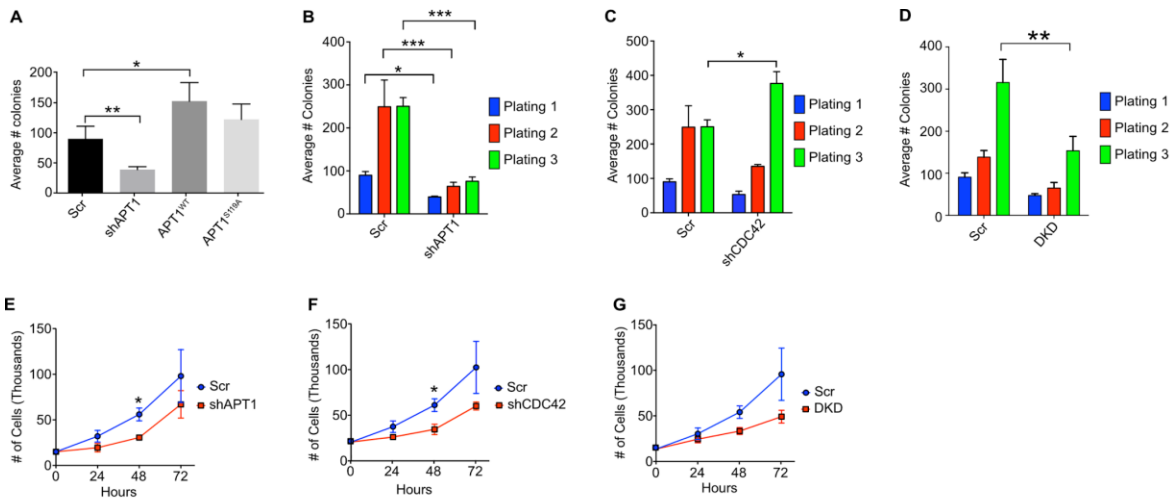

Figure 4.5 APT1 is required for *in vitro* colony formation and self-renewal but is dispensable for 2D proliferation. (**A**) Quantification of the average number of shAPT1-, $APT1^{WT}$- or $APT1^{S119A}$-expressing colonies grown from MDA-MB-231 cells in soft agar. Cells expressing a scrambled (Scr) shRNA sequence were used as a negative control. (**B to D**) Quantification of the average number of colonies formed from MDA-MB-231 shAPT1 cells (B), shCDC42 cells (C), both shAPT1 and shCDC42 (double knockdown, DKD) (D) over three serial replatings. Cells expressing a scrambled (Scr) shRNA sequence were used as a negative control for knockdown. (**E** to **G**) Proliferation curve of adherent MDA-MB-231 cells grown over 72 hours with knockdown of shAPT1 (E), shCDC42 (F), or both shAPT1 and shCDC42 (double knockdown, DKD) (G). Cells expressing a scrambled (Scr) shRNA sequence were used as a negative control for knockdown conditions. Each graph shows means taken from three independent experiments. *$P < 0.05$, **$P < 0.01$, and ***$P < 0.001$, as measured by t test. Error bars indicate SEM.

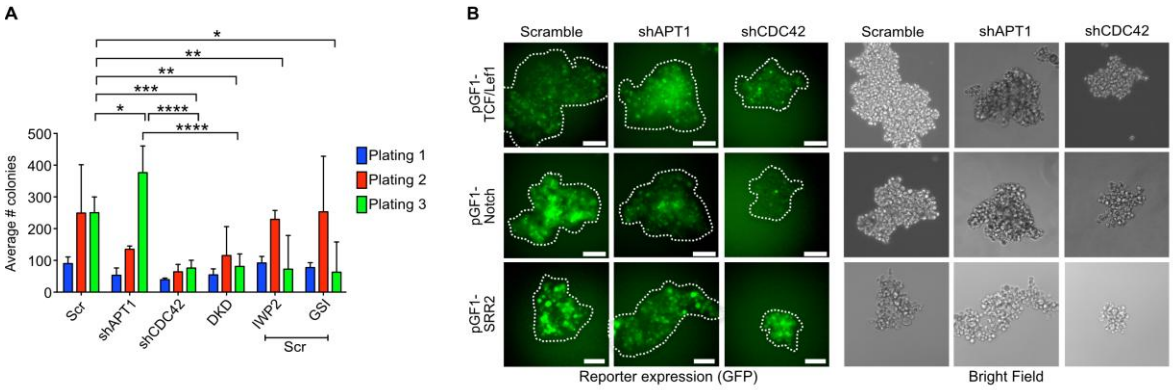

Figure 4.6 APT1 and CDC42 regulate the heterogeneous expression of Notch, Wnt, and SRR2 transcriptional reporters in colonies. (**A**) Quantification of the average number of colonies formed from MDA-MB-231 cells expressing shAPT1, shCDC42, both shAPT1 and shCDC42, or control cells treated with Wnt inhibitor (IWP2), or Notch inhibitor (GSI) over 3 serial replatings. Cells expressing a scrambled (Scr) shRNA sequence were used as a negative control for knockdown conditions. (**B**) Representative fluorescence and bright field images of colonies expressing pGF1-Notch, pGF1-TCF/LEF1, or pGF1-SRR2 GFP reporters in MDA-MB-231 colonies derived from control (Scramble), shAPT1-, or shCDC42-expressing cells. Graphs show average of three independent experiments. Scale bars, 100μm. *$P < 0.05$; **$P < 0.01$; ***$P < 0.001$; ****$P < 0.0001$ ANOVA (A) or T-test (Scr Plating 3 vs. shAPT1 Plating 3). Error bars indicate standard deviation SD.

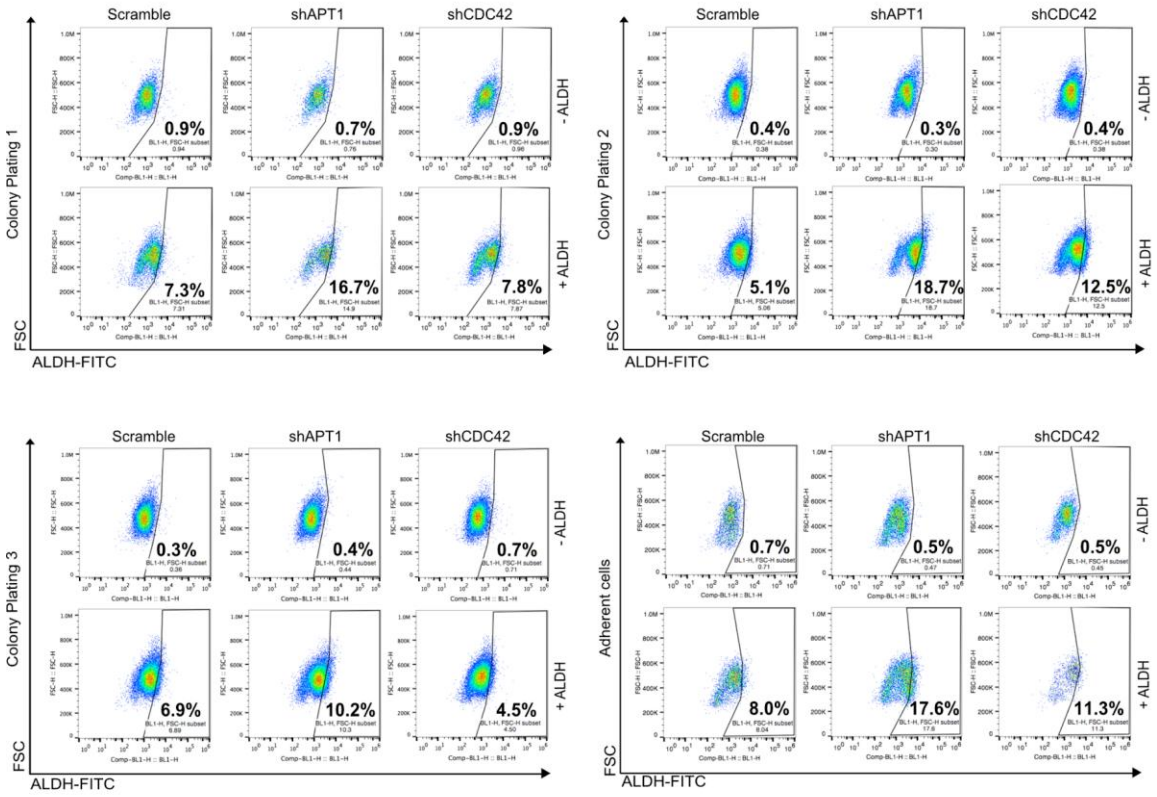

Figure 4.7 Gating scheme for ALDH+ cells on dissociated colonies or adherent cells. Gating strategy for flow cytometry analysis to detect Aldehyde dehydrogenase expressing cells (+ ALDH) within dissociated colonies or adherent cells from Fig. 7. DEAB-treated cells served as negative control (- ALDH) and were used to determine gating for ALDH+ cells. Size of population denoted with percentages. Flow cytometry lots are representative of six independent experiments.

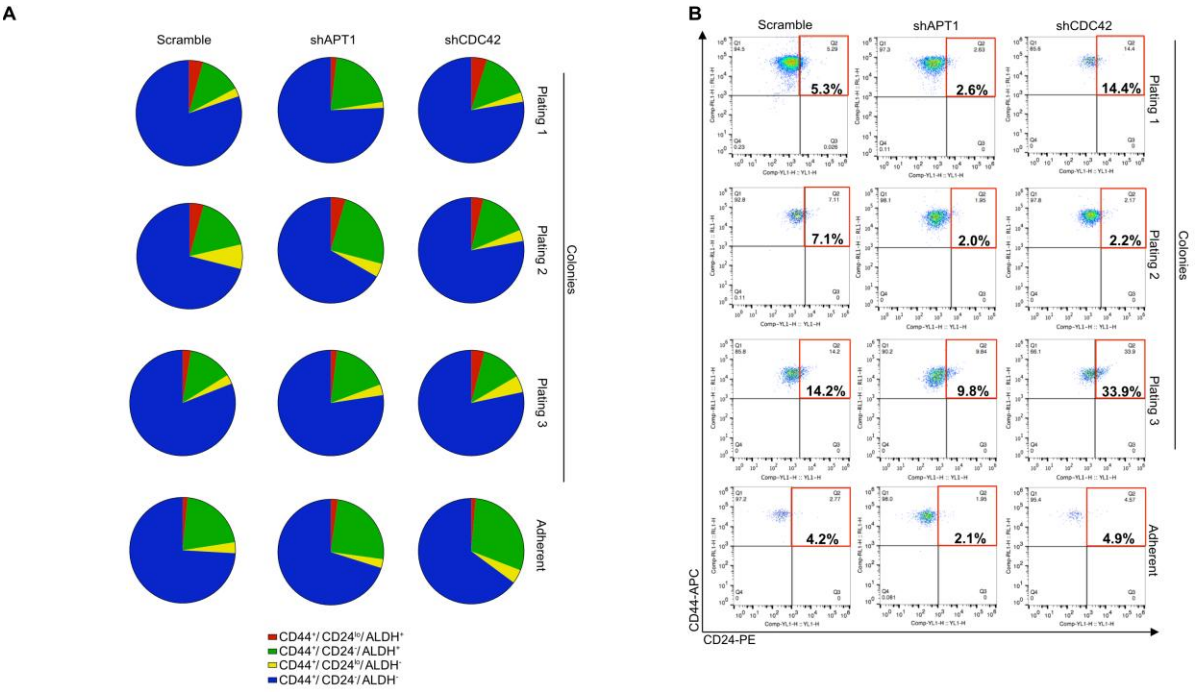

	Plating 1			Plating 2			Plating 3			Adherent		
	Scr	shAPT1	shCDC42	Scr	shAPT1	shCDC42	Scr	shAPT1	shCDC42	Scr	shAPT1	shCDC42
CD44+/ CD24lo/ ALDH+	4.0	1.8	4.8	3.8	4.5	3.8	2.5	1.9	3.7	1.4	2.1	1.3
CD44+/ CD24-/ ALDH+	14.3	20.5	14.6	14.0	24.5	15.0	13.6	17.3	11.2	19.6	24.3	27.1
CD44+/ CD24lo/ ALDH-	2.3	1.8	2.8	6.2	4.1	3.5	2.8	3.3	4.6	3.1	2.6	3.9
CD44+/ CD24-/ ALDH-	79.6	75.1	77.0	74.1	66.5	78.2	81.0	76.8	70.6	68.9	68.0	59.4

Figure 4.8 APT1 and CDC42 regulate the distribution of cell populations within colonies. (**A**) Pie chart analysis of $CD44^{+}/CD24^{lo}/ALDH^{+}$, $CD44^{+}/CD24^{-}/ALDH^{+}$, $CD44^{+}/CD24^{lo}/ALDH^{-}$, $CD44^{+}/CD24^{-}/ALDH^{-}$ populations from cells grown in colonies or adherent. Values listed in table as percentage. n = 8 independent experiments. Representative flow cytometry analysis showing gating strategy of $CD44^{+}/ CD24^{lo}$ cells (red box) in cells dissociated from colonies or adherent. The population was gated off of $ALDH^{+}$ cells, as shown in fig. S7. The percentages inside the red box indicate the relative proportion of the $CD44^{+}/CD24^{lo}$ cell population. Cells were stained with phycoerythrin (PE)–conjugated anti-CD24 (CD24-PE) (x axis) and allophycocyanin (APC)–conjugated CD44-APC (y axis). Flow cytometry plots are representative of results from six independent experiments.

CHAPTER 5: CONCLUSIONS AND FUTURE DIRECTIONS

5.1 Summary

Numerous recent studies have unearthed novel roles for palmitoylation on various cellular processes, especially during development and within tumors. However, the biological function of the depalmitoylating enzyme APT1 still remains poorly characterized. I have identified a mechanism for palmitoylation that regulates the asymmetric localization of the cell-fate determinants in dividing cancer cells through interaction with a canonical polarity regulator in a potential feedforward manner. In addition to protein localization, I have also demonstrated that palmitoylation promotes the asymmetric expression Wnt, Notch, and Sox2 transcriptional reporters between daughter cells. Suggestive of cell fate regulation, gene set enrichment analysis (GSEA) revealed gene signatures correlating with cell identity and Wnt and Notch signaling activity when APT1 was silenced or overexpressed. Finally, I have shown a requirement for APT1 on the anchorage independent growth, clonal expansion, self-renewal, and cellular heterogeneity of triple receptor negative breast cancer cells. In this dissertation, I have presented palmitoylation as a major mechanism of asymmetric cell division that maintains Notch- and Wnt-associated protein dynamics, gene expression, and cellular functions.

In Chapter 2, I utilized an RNAi approach, pharmacologic inhibition, and palmitoylation-deficient mutants to establish a requirement for palmitoylation on asymmetric Numb and β-catenin localization. For the first time, I demonstrated that human MDA-MB-231 breast cancer cells underwent asymmetric division *in vitro* under normal growth conditions. By expressing Wnt and Notch transcriptional GFP reporters, I demonstrated asymmetric reporter activity was established by APT1 and DHHC20. These data together establish a precedent for palmitoylation on asymmetric protein localization and downstream Notch and Wnt signaling activity.

In Chapter 3, I employed a cell-imaging based approach to interrogate how palmitoylation-mediated protein polarity was established. With fixed immunofluorescence, live-cell imaging, and modification of the ABE assay, I observed APT1 and bulk palmitoylated proteins were asymmetrically localized in dividing cells, and this localization required APT1 catalytic activity. Furthermore, I observed APT1 and zDHHC20 were spatially segregated to membrane regions enriched for lipid rafts and palmitoylated proteins. Together, these data suggest protein asymmetry may be reinforced by local palmitoylation cycles at the plasma membrane. Utilizing point mutants of constitutively active CDC42, catalytically inactive APT1, and CDC42 and APT1 double knockdown, I found APT1 asymmetric localization was reinforced by CDC42 activity. Palmitoylated CDC42 was observed to also promote asymmetric APT1 localization, suggesting it is a substrate of APT1. Similar observations were found for asymmetric β-catenin (and, to a lesser extent, Numb) localization. The data presented in Chapter 3 demonstrate an interdependence of APT1 and CDC42 activity for their own asymmetric localization, which may regulate cell polarity in a feedforward manner

In Chapter 4, I applied GSEA on RNAseq data generated from APT1 knockdown or expression to determine whether palmitoylation affected gene expression in MDA-MB-231 on a global scale. I observed gene signatures associated with Wnt and Notch signaling and cell fate determination, in addition to a requirement for palmitoylation on asymmetric Sox2 reporter expression, a pathway implicated in stem-cell fate. Together, these results suggest a larger role for APT1 expression on cell identity. Utilizing the colony formation and replating assays, I discovered APT1 was required for the clonogenic growth and self-renewal of MDA-MB-231 cells. Applying flow cytometry and transcriptional reporter expression, I found the cellular heterogeneity of colonies required APT1 (and CDC42). Together, these findings imply a role for APT1 specifically, and palmitoylation in general, on the regulation of cell identity and function.

This dissertation provides novel insights into the role of APT1 and palmitoylation on cellular processes necessary for cancer and stem cell biology. In this chapter, I will outline two key areas for further exploration to explore the role of APT1 on the cell fate determination of progenitor cells, and during tumor development.

5.2 Understanding regulation of signaling activity by palmitoylation

Many outstanding questions remain, including the identification of palmitoylated substrates and how the palmitoyl group affects substrate activity and localization. The experiments proposed in this subsection seek to shed light on how palmitoylation affects cell identity through signaling activity.

β-catenin cortical localization is mediated through association with cadherins at tight junctions (*237*, *238*). Having shown palmitoylation of β-catenin and enhanced downstream Wnt activity in APT1 knockdown cells, I will examine whether β-catenin palmitoylation maintains its stability and nuclear translocation, its cortical association, or both. A screen identified Cys^{466}, within armadillo repeat domains, may be palmitoylated (*245*). I have also identified 3 additional cytosolic facing and potentially conserved sites (Cys^{429}, Cys^{439}, and Cys^{619}) with CSS-Palm (Fig. 5.1 A). I hypothesize these four residues promote β-catenin stability to propagate downstream Wnt, or promotes cadherin and cytoskeletal interaction. Cys^{429} and Cys^{466} are also located near a TCF/Lef binding cleft indicating these two residues may regulate β-catenin nuclear activity (Fig. 5.1 B). Having generated single and combination point mutants of Cys^{429}, Cys^{439}, Cys^{466}, and Cys^{619}, I will assess whether mutation of these sites affects palmitoylated β-catenin protein levels, and if these sites sterically hinder interaction with the GSK3β-Axin2-APC destruction complex or

cadherins. I could also test whether β-catenin palmitoylation is modulated by exogenous Wnt stimulation to determine how palmitoylation affects downstream signaling responses.

Live-cell analysis of U2OS cells shows β-catenin^{WT} is partitioned to the plasma membrane of the daughter cell that emerged from the same side of the mother cell where β-catenin^{WT} was initially concentrated. APT1^{WT} co-segregated with β-catenin^{WT}, and was retained in the daughter cell with high β-catenin signal as indicated by line-scan analysis of YFP and CFP pixel intensity along the division axis (Fig. 5.1 C). Interestingly, β-catenin^{WT} appears to be restricted to the plasma membrane while APT1^{WT} was predominantly cytosolic, suggesting asymmetric β-catenin localization could be maintained in a negative feedback manner (Fig. 5.1 C). Finally, knocking down APT1 decreased the percentage of cells with asymmetric β-catenin (Fig. 5.1 D). Using the palmitoylation-deficient mutants, I would interrogate whether these palmitoylation deficient mutants are unable to: 1) asymmetrically localize during cell division, and 2) localize to the plasma membrane. Further examination of GSEA signatures reveals a negative correlation with protein-membrane trafficking in APT1 knockdown cells, supporting conclusions that loss of protein asymmetry was due to disrupted protein transport to the plasma membrane (Fig. 5.2 A). High resolution TIRF microscopy could also be employed to investigate how palmitoylation affects the membrane turnover of APT1, β-catenin, and also Numb.

How palmitoylation regulates transcription is also poorly understood. To determine whether Cys^{429}, Cys^{439}, Cys^{466}, and Cys^{619} disrupt Wnt-induced transcriptional activity, I could express these point mutants in pGF1-TCF/Lef1 GFP reporter cells to examine if asymmetric reporter activity is disrupted and/or suppressed. This strategy will also be employed to examine whether the Numb^{AAA} palmitoylation-deficient mutant affects Notch signaling and reporter activity.

CDC42 did not significantly affect Numb asymmetric localization or Notch reporter expression in daughter cells. As mentioned in Chapter 3, Numb localization may instead require the Scribble and Crumbs polarity complexes. As components of these two complexes are known to be palmitoylated, I could examine if Scribble and Crumbs palmitoylation-deficient mutants disrupt Numb asymmetric localization and if Numb palmitoylation facilitates interactions with these two complexes. This may uncover potential palmitoylation-driven crosstalk between the CDC42, Scribble, and Crumbs complexes during the establishment of cell polarity.

A recent RNAi and misexpression screen identified wing development defects in *D. melanogaster* when DHHCs were overexpressed (*321*), providing insights into a role for palmitoylation on tissue morphogenesis. Positive correlations with late stem-cell differentiation in APT1 knockdown cells and downregulation of a mammary luminal signature in APT1 overexpressing cells (Fig. 5.2 B) also support a role for APT1 on cell identity. Knocking down APT1 was associated with suppressed 3'UTR regulation and ribosome biogenesis, while $APT1^{WT}$ overexpression was correlated with chromosome segregation as compared to control cells (Fig. 5.3 A). Furthermore, APT1 overexpression or knockdown was strongly correlated with progenitor cell identity pathways and epigenetic regulation (Fig. 5.3 B). These preliminary findings imply APT1 may have a role on the regulation of gene expression and signaling pathways involved in stem cell fate determination and embryonic patterning, which are also frequently disrupted in tumors (*322–326*). Expression of Numb and β-catenin palmitoylation-deficient mutants in progenitor cells or in embryos would also clarify if palmitoylation is vital for embryonic and stem cell development.

The experiments presented in this section will provide key insights into the spatio-temporal regulation of palmitoylation on protein-protein interactions and developmental

processes. This will greatly contribute to our understanding of how developmental signaling pathways and processes activity may be disrupted in disease progression.

5.3 Determining role of palmitoylation on drug resistance and therapeutic potential for APT1 inhibitors

Increasing cellular heterogeneity is a key contributor to tumor recurrence, and may arise from an accumulation of mutations as a consequence of therapeutic resistance. How distinct tumor subpopulations inherit mutations is unclear, but may involve asymmetric cell division. In Chapter I, various studies were described demonstrating zDHHC function on tumor progression; in contrast, the biological function of APT1 is largely unknown. According to TCGA, APT1 is predominantly amplified in human tumors, including invasive breast carcinomas, and may correlate with shortened survival. Here, I will outline a strategy to examine the regulation of survival, cellular heterogeneity, and drug resistance of tumor cells by APT1.

Cisplatin is a common first-line therapy for breast cancer, but cisplatin-resistance is common to triple receptor negative breast cancer and contributes to poor patient prognosis (*327*, *328*). I hypothesize loss or inhibition of APT1 may increase the sensitivity of MDA-MB-231 cells to cisplatin. Preliminary data indicates cisplatin treatment decreases the size and number of APT1 knockdown colonies as compared to control (Fig. 5.4 A). The findings in Chapter 4 imply APT1 maintains self-renewing, tumorigenic $CD44^{+}$/ $CD24^{lo}$/ $ALDH^{+}$ cells, which are known to be therapy resistant and able to generate cell diversity. Further analysis of cisplatin-treated colonies reveals an expected expansion of $CD44^{+}$/ $CD24^{lo}$/ $ALDH^{+}$ cells, representative of drug resistant cell, and altered population distribution. Interestingly, an approximately 1.2-fold reduction of the $CD44^{+}$/ $CD24^{lo}$/ $ALDH^{+}$ population was observed in treated APT1 knockdown cells as compared

to treated control conditions (12.0% vs. 13.9%) (Fig. 5.4 B). Cell death was also increased in APT1 knockdown cells treated with cisplatin for 72 hours as compared to control (Fig. 5.4 C). While these observations must be validated, these preliminary findings suggest loss of APT1 increases the sensitivity of MDA-MB-231 cells to cisplatin. Importantly, repeating these experiments in control cells treated with PalmB or ML-348 would determine if pharmacologic APT1 inhibition: 1) phenocopies APT1 silencing, and 2) sensitizes resistant cells to cisplatin. Sorting and replating cisplatin-treated cells would further test if the self-renewal of $CD44^{+}$/ $CD24^{lo}$/ $ALDH^{+}$ and population distribution is exhausted by loss of APT1. I could also examine APT1 knockdown or pharmacologic inhibition in combination with other common breast cancer therapies (e.g. cytoskeletal disruptors, receptor tyrosine kinase inhibitors, radiotherapy, etc. (*329, 330*)) to assess alterations in cell survival, heterogeneity, and drug sensitivity. Repeating these experiments with patient-derived cells in combination with organoid formation and xenograft transplantation would give greater insights into the clinical impact of APT1 inhibition.

GSEA indicates APT1 knockdown cells are negatively correlated with DNA repair and G2M checkpoint signatures as compared to control cells, and APT1 overexpression correlates with chromosome segregation (Fig. 5.2 A, 5.5 A). These signatures suggest perturbations to APT1 disrupt genome stability and cell cycle progression. Segregating DNA and damaged organelles to one daughter cell has been proposed as a potential mechanism of ensuring stem cell fitness and survival (*205, 317, 331–333*). It is entirely possible this partitioning may be employed by tumor cells to promote the unequal inheritance of mutations, while eliminating cells fated for apoptosis in order to promote tumor growth and metastasis. A preliminary observation of control MDA-MB-231 cells shows asymmetric expression of the DNA repair enzymes 53BP1 and BRCA1 in daughter nuclei (Fig. 5.5 B). This result implies that the DNA repair machinery is recruited to the cell with greater damage, or DNA repair is suppressed in one daughter cell upon

recruitment. I could examine the expression of 53BP1, BRCA1, Chk1, and γ-H2AX to determine if APT1 knockdown or pharmacologic inhibition increases DNA damage. To address the mechanism of asymmetric DNA repair, I could initiate DNA damage (drug- or radio-induced) and examine γ-H2AX focus formation over time to: 1) ascertain unequal foci distribution between daughter cells, 2) at what point in the DNA damage response is asymmetry first observed, and 3) if APT1 knockdown or pharmacologic inhibition increases symmetric accumulation of damage.

Cell death is a fate decision and may be asymmetrically induced in one daughter cell (*334*). Glioma initiating cells have been reported to undergo asymmetric division and apoptosis as well (*335*). I find APT1 knockdown cells positively correlate with an apoptotic execution gene signature, which may promote the observed increase in cisplatin-induced cell death (Fig. 5.5 C). As mentioned in Chapter I, several apoptotic regulators are palmitoylated, and thus, may be asymmetrically partitioned or induced. Preliminary quantification of cleaved caspase-3 fluorescence intensity in non-mitotic MDA-MB-231 cells indicates increased expression in APT1 knockdown cells (Fig. 5.5 D, E). Cleaved caspase-3 is moderately increased in DHHC20 knockdown cells, implying greater specificity for apoptotic regulators not seen with APT1. I would assess asymmetric expression of cleaved caspase-3, BAX, and Fas death receptor between daughter cells, and determine whether cisplatin, APT1 inhibition, and combination treatment modulates asymmetric apoptosis. Additionally, staining isolated CD^{44}/ $CD24^{lo}$/ $ALDH^{+}$ would also clarify whether APT1 knockdown or pharmacologic inhibition increases cell death, which would contribute to a decreased tumorigenic population. These experiments would assess if accumulating DNA damage promote cell death induced by silencing APT1.

Asymmetric organelle segregation may also be a way to induce unequal protein translation. As shown in Fig. 5.2 A, APT1 knockdown negatively correlates with ribosome

biogenesis and 3'UTR translational regulation. Asymmetric induction of histone modifications have been observed in germline stem cells (*336*), and it is possible this process may occur in tumor cells to differentially regulate gene expression between daughter cells. GSEA shown in Fig. 5.2 B suggests epigenetic regulation may be altered by APT1 overexpression or knockdown. I could assess cells for asymmetric expression of HDACs, HATs, and HMTs in control cells, and determine if asymmetry is disrupted with APT1 inhibition. The experiments to this point would provide insights into whether favorable mutations are unequally inherited, with implications for the development of disease recurrence.

Ultimately, I could examine how protein palmitoylation affects signaling pathways necessary for tumor initiation and growth. Expression of Numb and β-catenin palmitoylation deficient mutants would determine if loss of palmitoylation inhibits or exacerbates colony formation and self-renewal. I could also examine transcriptional Wnt and Notch reporter expression to better understand if signaling activity is altered and if expression is symmetric within colonies with these mutants. These experiments could be extended to other palmitoylated substrates such as EGFR and Ras. Single RNAseq of dissociated colonies expressing Numb and β-catenin palmitoylation deficient mutants could potentially identify novel biomarkers that could be targeted therapeutically.

The experiment in this section can be applied to various cancer including blood, ovarian, glioblastoma, and lung to better understand the requirement for APT1 on tumor progression. Together, the proposed experiments would contribute to our understanding of how tumor heterogeneity is established through asymmetric cell division, and may uncover a role for palmitoylation inhibitors in the clinic.

5.4 Conclusions

This work presents a conceptual framework for palmitoylation-mediated asymmetric cell division, with implications for tumor cell heterogeneity and stem cell homeostasis. The future experiments proposed in this chapter will build on this work to provide greater understanding into the spatio-temporal regulation of proteins at the plasma membrane, and into the regulation of signaling activity and gene expression during development and disease.

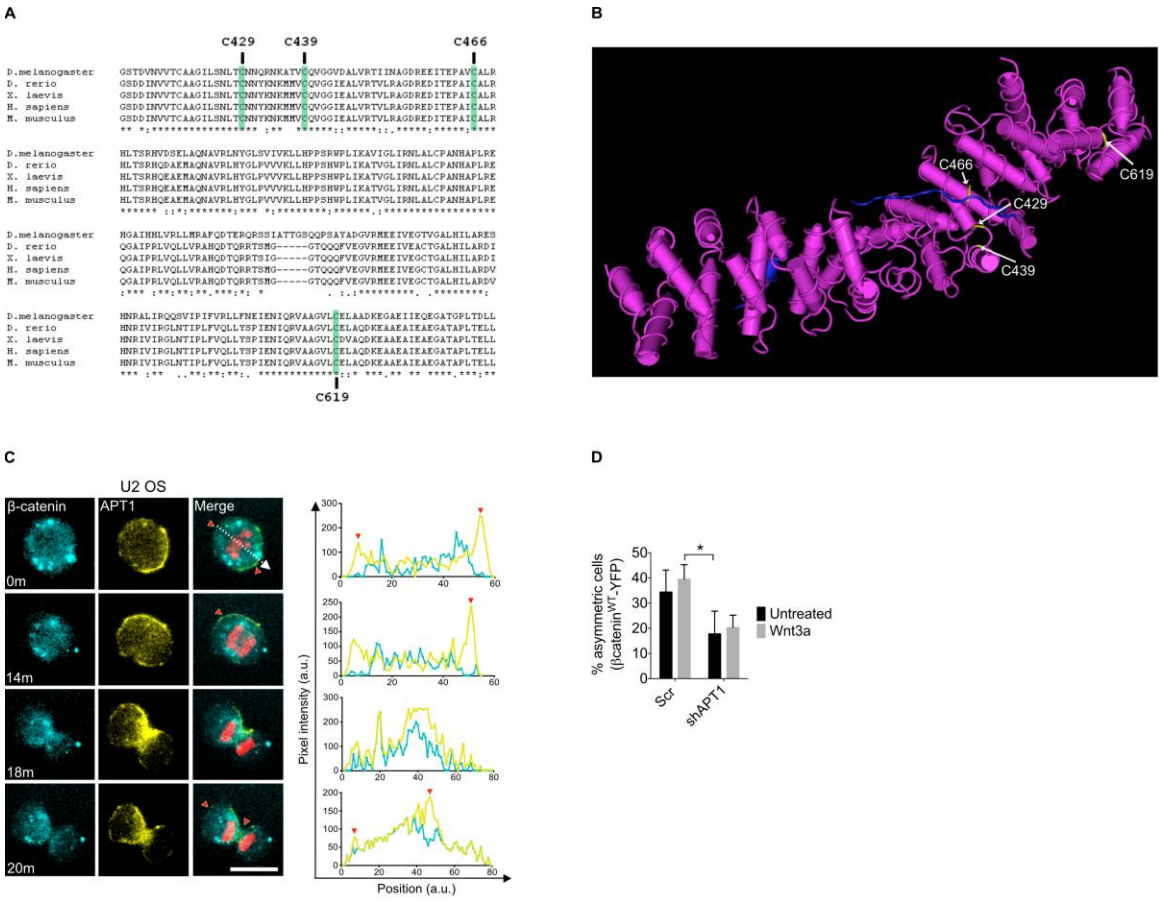

Figure 5.1 Role of palmitoylation on asymmetric β-catenin localization. (**A**) Sequence comparison of β-catenin armadillo repeats from fruit fly (*Drosophila melanogaster*), zebrafish (*Danio rerio*), mouse (*Mus musculus*), and human (*Homo sapiens*). Putative palmitoylated cysteines are highlighted in green. (**B**) Crystal structure of the *D. melanogaster* β-catenin armadillo repeats indicating putative palmitoylated residues C429, C439, C466 and C619 in yellow. (**C**) Time-lapse images of dividing U2 OS cells coexpressing β-catenin^{WT}-YFP (yellow), APT1^{WT}-CFP (blue), and mCherry–Histone H2B (red). Fluorescence pixel intensity was measured along the division axis (dashed line), and the corresponding pixel values of β-catenin (yellow line) and APT1 (blue line) along the division axis were plotted on graphs. Red arrowheads on images and graphs indicate the peak β-catenin and APT1 pixel intensity at the membrane or cytokinetic midbody. Time is shown in minutes (min). a.u., arbitrary units. Scale

bar, 15 μm. (**E**) Quantification of the number of dividing U2 OS cells showing asymmetric localization of β-catenin^{WT}-YFP in control or shAPT1 cells treated with CHAPS (black bar) or Wnt3a (gray bar). Cells expressing a scrambled (Scr) shRNA sequence were used as a negative control for APT1 knockdown. $*P < 0.05$, t test and ANOVA. Error bars indicate SD.

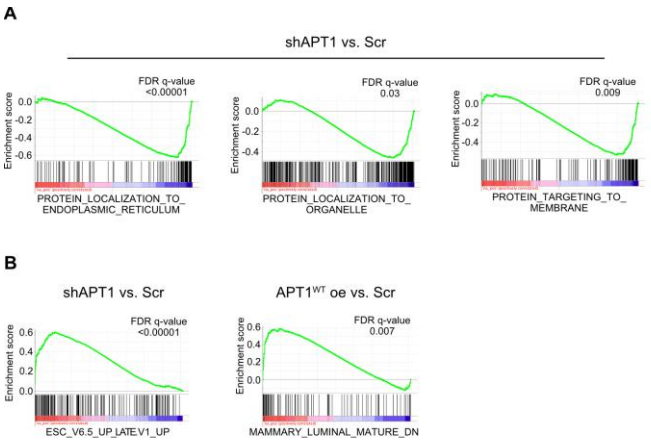

Figure 5.2 GSEA signatures correlating with protein trafficking and cell identity in APT1 knockdown or APT1^{WT} overexpressing cells. (**A** and **B**) Gene set enrichment analysis (GSEA) of a top-scoring protein localization to the endoplasmic reticulum, [false discovery rate (FDR) q value, <0.0001], localization to organelles [FDR q-value= 0.03], and targeting to membrane when APT1 was knocked down and compared against control cells [FDR q-value= 0.009] (A). Gene set enrichment analysis (GSEA) of additional top-scoring late embryonic cell differentiation (FDR q-value <0.0001) or genes downregulated in mature mammary luminal cells (FDR q-value= 0.007) (B).

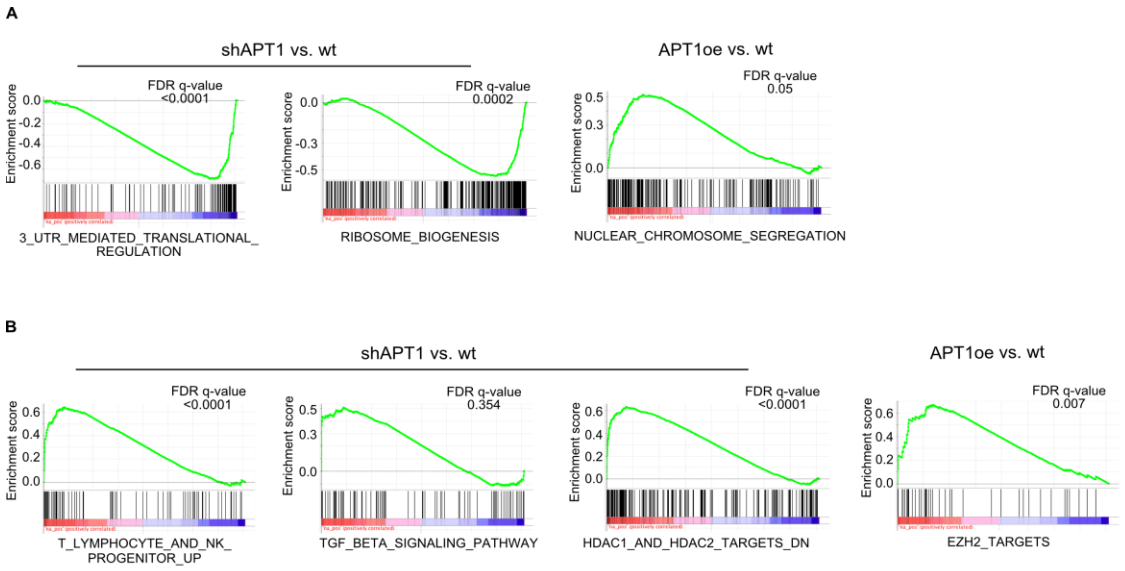

Figure 5.3 GSEA signatures correlating with protein translation, cell identity, and epigenetic modification protein trafficking and cell identity in APT1 knockdown or APT1^{WT} overexpressing cells. (**A** and **B**) Gene set enrichment analysis (GSEA) of a top-scoring 3'UTR mediated translation [false discovery rate (FDR) q value, <0.0001] and ribosome biogenesis [FDR q-value= 0.0002] signatures when APT1 was knocked down and compared against control cells. Top-scoring chromosome segregation [FDR q-value= 0.05] signature when APT^{WT} was overexpressed and compared against control cells (A). Gene set enrichment analysis (GSEA) of top-scoring T lymphocyte progenitor (FDR q-value <0.0001), TGF- β signaling [FDR q-value= 0.354], and downregulation of target genes upon HDAC1 or HDAC1 pharmacologic inhibition [FDR q-value <0.0001] when APT1 was knocked down and compared against control cells. Top-scoring EZH2 target gene expression [FDR q-value= 0.007] signature when APT^{WT} was overexpressed and compared against control cells (B).

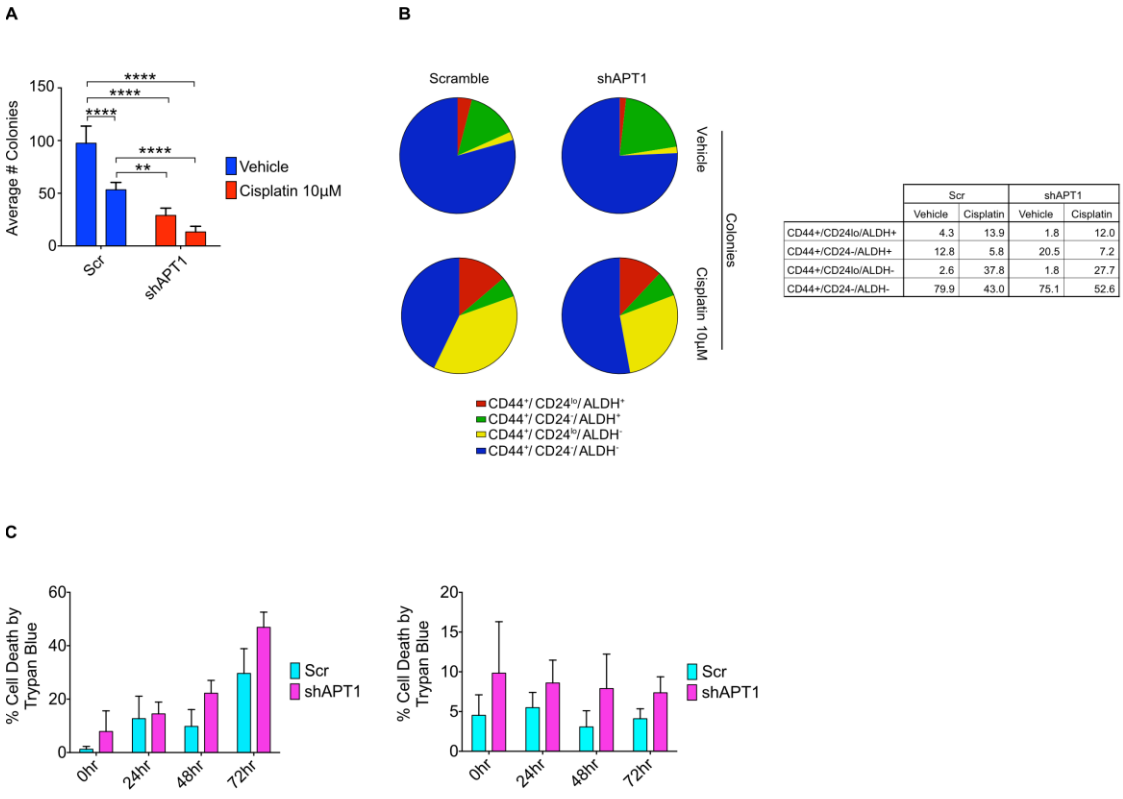

	Scr		shAPT1	
	Vehicle	Cisplatin	Vehicle	Cisplatin
CD44+/CD24lo/ALDH+	4.3	13.9	1.8	12.0
CD44+/CD24-/ALDH+	12.8	5.8	20.5	7.2
CD44+/CD24lo/ALDH-	2.6	37.8	1.8	27.7
CD44+/CD24-/ALDH-	79.9	43.0	75.1	52.6

Figure 5.4 APT1 knockdown may increase sensitivity of cisplatin-resistant MDA-MB-231 cells to drug treatment. A) Preliminary quantification of the average number of colonies grown in 10μm cisplatin or vehicle from MDA-MB-231 shAPT1 cells. Cells expressing a scrambled (Scr) shRNA sequence were used as a negative control. n = 3 independent experiments. (**B**) Pie chart analysis of $CD44^{+}/CD24^{lo}/ALDH^{+}$, $CD44^{+}/CD24^{-}/ALDH^{+}$, $CD44^{+}/CD24^{lo}/ALDH^{-}$, $CD44^{+}/CD24^{-}/ALDH^{-}$ populations from colonies isolated in (A). Values listed in table as percentage. n = 3 independent experiments. (**C**) Proliferation curve of adherent shAPT1 MDA-MB-231 cells grown over 72 hours and treated with 10μm cisplatin or vehicle. Cells expressing a scrambled (Scr) shRNA sequence were used as a negative control for knockdown conditions. Each graph shows means taken from three independent experiments. $^{**}P < 0.01$, $^{***}P < 0.001$, and $^{****}P < 0.0001$, as measured by t test (vehicle vs cisplatin) or ANOVA. Error bars indicate SEM.

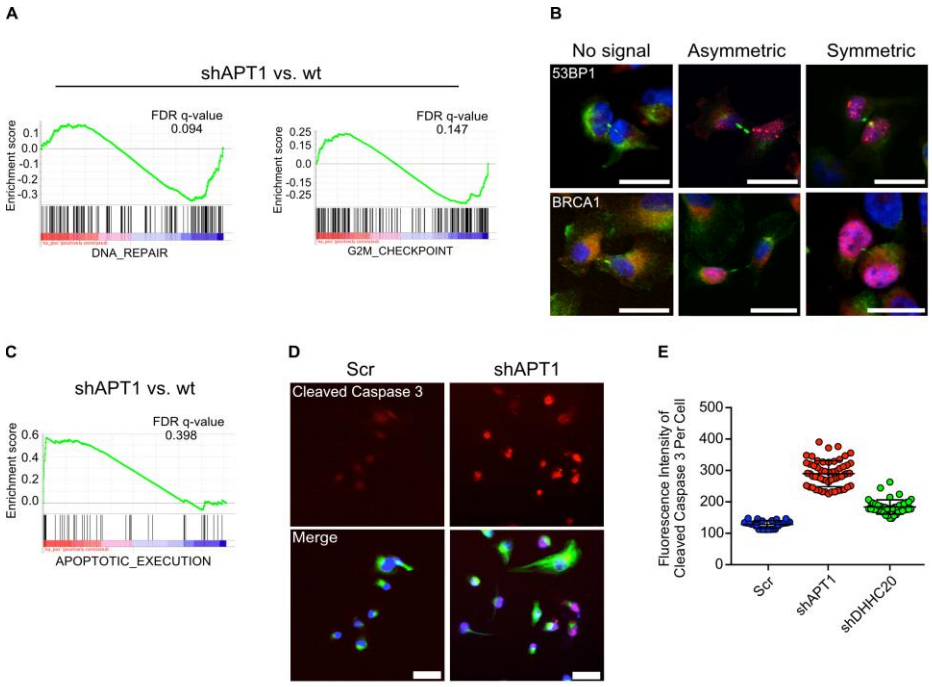

Figure 5.5 DNA damage repair and apoptosis may be dependent on APT1. (**A**) Gene set enrichment analysis (GSEA) of a top-scoring DNA repair [false discovery rate (FDR) q value, 0.094] and G2M checkpoint [FDR q-value= 0.147] signatures when APT1 was knocked down and compared against control cells. (**B**) Representative immunofluorescence of cytokinetic MDA-MB-231 control cells stained to show asymmetric or symmetric 53BP1 or BRCA1 (red), acetylated tubulin (green), and nuclei (blue). Scale bars, 15 μm. (**C**) Gene set enrichment analysis (GSEA) of a top-scoring apoptotic [FDR q-value= 0.398] signature when APT1 was knocked down and compared against control cells. (**D**) Representative immunofluorescence of non-dividing MDA-MB-231 shAPT1 or scrambled (Scr) control cells stained for cleaved caspase 3 (red), acetylated tubulin (green), and nuclei (blue). Scale bars, 30 μm. (**E**) Distribution dot plots showing mean fluorescence pixel intensity of cleaved caspase 3 signal of MDA-MB-231 shAPT1 (D) and shDHHC20 cells. Cells expressing a scrambled (Scr) shRNA sequence were used as a negative control for knockdown conditions. n = 127 cells scored for the experimental group from 1 experiment. Each dot represents a single cell

BIBLIOGRAPHY

1. I. G. Macara, Parsing the polarity code. *Nat. Rev. Mol. Cell Biol.* **5**, 220–231 (2004).

2. J. a Knoblich, Asymmetric cell division during animal development. *Nat. Rev. Mol. Cell Biol.* **2**, 11–20 (2001).

3. M.-C. Hung, W. Link, Protein localization in disease and therapy. *J. Cell Sci.* **124**, 3381–92 (2011).

4. J. Greaves, L. H. Chamberlain, Palmitoylation-dependent protein sorting. *J. Cell Biol.* **176**, 249–254 (2007).

5. R. A. Neumüller, J. A. Knoblich, Dividing cellular asymmetry: Asymmetric cell division and its implications for stem cells and cancer. *Genes Dev.* **23**, 2675–2699 (2009).

6. F. B. Young, S. L. Butland, S. S. Sanders, L. M. Sutton, M. R. Hayden, Putting proteins in their place: Palmitoylation in Huntington disease and other neuropsychiatric diseases. *Prog. Neurobiol.* **97**, 220–238 (2012).

7. A. Gupta, STOCHASTIC MODEL FOR CELL POLARITY. *Ann. Appl. Probab.* **22**, 827–859 (2012).

8. S. J. Altschuler, S. B. Angenent, Y. Wang, L. F. Wu, On the spontaneous emergence of cell polarity. *Nature*. **454**, 886–889 (2008).

9. E. Conibear, N. G. Davis, Palmitoylation and depalmitoylation dynamics at a glance. *J. Cell Sci.* **123**, 4007–4010 (2010).

10. M. D. Resh, Covalent lipid modifications of proteins. *Curr. Biol.* **23**, R431–R435 (2013).

11. Y. Fukata, M. Fukata, Protein palmitoylation in neuronal development and synaptic plasticity. *Nat Rev Neurosci*. **11**, 161–175 (2010).

12. E. Tortosa, C. C. Hoogenraad, Polarized trafficking: the palmitoylation cycle distributes cytoplasmic proteins to distinct neuronal compartments. *Curr. Opin. Cell Biol.* **50**, 64–71 (2018).

13. J. E. Smotrys, M. E. Linder, Palmitoylation of intracellular signaling proteins: regulation and function. *Annu. Rev. Biochem.* **73**, 559–87 (2004).

14. M. E. Linder, R. J. Deschenes, Palmitoylation: policing protein stability and traffic. *Nat. Rev. Mol. Cell Biol.* **8**, 74–84 (2007).

15. Y. Fukata, T. Murakami, N. Yokoi, M. Fukata, in *Current topics in membranes* (2016; http://www.ncbi.nlm.nih.gov/pubmed/26781831), vol. 77, pp. 97–141.

16. Y. Li, B. Qi, Progress toward Understanding Protein S-acylation: Prospective in Plants. *Front. Plant Sci.* **8**, 1–20 (2017).

17. S. Blaskovic, M. Blanc, F. G. van der Goot, What does S-palmitoylation do to membrane

proteins? *FEBS J.* **280**, 2766–2774 (2013).

18. M. M. Zhang, H. C. Hang, Protein S-palmitoylation in cellular differentiation. *Biochem. Soc. Trans.* **45**, 275–285 (2017).

19. M. Veit, M. F. Schmidt, Enzymatic depalmitoylation of viral glycoproteins with acyl-protein thioesterase 1 in vitro. *Virology*. **288**, 89–95 (2001).

20. M. F. Schmidt, M. Bracha, M. J. Schlesinger, Evidence for covalent attachment of fatty acids to Sindbis virus glycoproteins. *Proc. Natl. Acad. Sci. U. S. A.* **76**, 1687–91 (1979).

21. R. E. Bishop, S.-H. Kim, A. El Zoeiby, Role of lipid A palmitoylation in bacterial pathogenesis. *J. Endotoxin Res.* **11**, 174–180 (2005).

22. M. P. Running, The role of lipid post-translational modification in plant developmental processes. *Front. Plant Sci.* **5**, 50 (2014).

23. M. Yeste-Velasco, M. E. Linder, Y. J. Lu, Protein S-palmitoylation and cancer. *Biochim. Biophys. Acta - Rev. Cancer*. **1856**, 107–120 (2015).

24. T. Honda *et al.*, Protective role for lipid modifications of Src-family kinases against chromosome missegregation. *Sci. Rep.* **6**, 38751 (2016).

25. P. Mill *et al.*, Palmitoylation Regulates Epidermal Homeostasis and Hair Follicle Differentiation. *PLoS Genet.* **5**, e1000748 (2009).

26. K. B. Runkle *et al.*, Inhibition of DHHC20-Mediated EGFR Palmitoylation Creates a Dependence on EGFR Signaling. *Mol. Cell*. **62**, 385–396 (2016).

27. L. R. Bollu *et al.*, Intracellular activation of EGFR by fatty acid synthase dependent palmitoylation. *Oncotarget*. **6**, 34992–5003 (2015).

28. P. Babu, R. J. Deschenes, L. C. Robinson, Akr1p-dependent palmitoylation of Yck2p yeast casein kinase 1 is necessary and sufficient for plasma membrane targeting. *J. Biol. Chem.* **279**, 27138–47 (2004).

29. A. M. Akimzhanov, D. Boehning, Rapid and transient palmitoylation of the tyrosine kinase Lck mediates Fas signaling. *Proc. Natl. Acad. Sci.* **112**, 11876–11880 (2015).

30. R. Liu *et al.*, Palmitoylation Regulates Intracellular Trafficking of β2 Adrenergic Receptor/Arrestin/Phosphodiesterase 4D Complexes in Cardiomyocytes. *PLoS One*. **7**, e42658 (2012).

31. T. Koyano *et al.*, Casein kinase 1γ ensures monopolar growth polarity under incomplete DNA replication downstream of Cds1 and calcineurin in fission yeast. *Mol. Cell. Biol.* **35**, 1533–42 (2015).

32. S. Oku, N. Takahashi, Y. Fukata, M. Fukata, *In Silico* Screening for Palmitoyl Substrates Reveals a Role for DHHC1/3/10 (zDHHC1/3/11)-mediated Neurochondrin Palmitoylation in Its Targeting to Rab5-positive Endosomes. *J. Biol. Chem.* **288**, 19816–19829 (2013).

33. B. Li, F. Cong, C. P. Tan, S. X. Wang, S. P. Goff, Aph2, a Protein with a *zf* -DHHC Motif,

Interacts with c-Abl and Has Pro-apoptotic Activity. *J. Biol. Chem.* **277**, 28870–28876 (2002).

34. U. Heindel, M. F. G. Schmidt, M. Veit, Palmitoylation sites and processing of synaptotagmin I, the putative calcium sensor for neurosecretion. *FEBS Lett.* **544**, 57–62 (2003).

35. L. Tian, H. McClafferty, O. Jeffries, M. J. Shipston, Multiple Palmitoyltransferases Are Required for Palmitoylation-dependent Regulation of Large Conductance Calcium- and Voltage-activated Potassium Channels. *J. Biol. Chem.* **285**, 23954–23962 (2010).

36. A. S. Kazim, P. Storm, E. Zhang, E. Renström, Palmitoylation of Ca 2+ channel subunit Ca V β 2a induces pancreatic beta-cell toxicity via Ca 2+ overload. *Biochem. Biophys. Res. Commun.* **491**, 740–746 (2017).

37. L. Tian *et al.*, Palmitoylation gates phosphorylation-dependent regulation of BK potassium channels. *Proc. Natl. Acad. Sci.* **105**, 21006–21011 (2008).

38. F. Bosmans, M. Milescu, K. J. Swartz, Palmitoylation influences the function and pharmacology of sodium channels. *Proc. Natl. Acad. Sci.* **108**, 20213–20218 (2011).

39. L. B. Tulloch *et al.*, The Inhibitory Effect of Phospholemman on the Sodium Pump Requires Its Palmitoylation. *J. Biol. Chem.* **286**, 36020–36031 (2011).

40. L. Reilly *et al.*, Palmitoylation of the Na/Ca exchanger cytoplasmic loop controls its inactivation and internalization during stress signaling. *FASEB J.* **29**, 4532–4543 (2015).

41. D. Purves *et al.*, Voltage-Gated Ion Channels (2001) (available at https://www.ncbi.nlm.nih.gov/books/NBK10883/).

42. M. Fröhlich, B. Dejanovic, H. Kashkar, G. Schwarz, S. Nussberger, S-palmitoylation represents a novel mechanism regulating the mitochondrial targeting of BAX and initiation of apoptosis. *Cell Death Dis.* **5**, e1057–e1057 (2014).

43. E. M. Lynes *et al.*, Palmitoylation is the switch that assigns calnexin to quality control or ER Ca2+ signaling. *J. Cell Sci.* **126**, 3893–3903 (2013).

44. C. K. Underwood, K. Reid, L. M. May, P. F. Bartlett, E. J. Coulson, Palmitoylation of the C-terminal fragment of p75NTR regulates death signaling and is required for subsequent cleavage by γ-secretase. *Mol. Cell. Neurosci.* **37**, 346–358 (2008).

45. Y. Liu *et al.*, Involvement of the HCK and FGR src-Family Kinases in FCRL4-Mediated Immune Regulation. *J. Immunol.* **194**, 5851–5860 (2015).

46. N. Ladygina, B. R. Martin, A. Altman, *Dynamic Palmitoylation and the Role of DHHC Proteins in T Cell Activation and Anergy* (Elsevier inc., ed. 1, 2011; http://dx.doi.org/10.1016/B978-0-12-387664-5.00001-7), vol. 109.

47. M. Hundt *et al.*, Impaired Activation and Localization of LAT in Anergic T Cells as a Consequence of a Selective Palmitoylation Defect. *Immunity*. **24**, 513–522 (2006).

48. M. Hundt *et al.*, Palmitoylation-Dependent Plasma Membrane Transport but Lipid Raft-

Independent Signaling by Linker for Activation of T Cells. *J. Immunol.* **183**, 1685–1694 (2009).

49. S. Komaniwa *et al.*, Lipid-mediated presentation of MHC class II molecules guides thymocytes to the CD4 lineage. *Eur. J. Immunol.* **39**, 96–112 (2009).

50. F. Balamuth, J. L. Brogdon, K. Bottomly, Synapse Site Molecular Clustering at the Immunological CD4 Raft Association and Signaling Regulate CD4 Raft Association and Signaling Regulate Molecular Clustering at the Immunological Synapse Site 1. *J Immunol Ref. J. Immunol.* **172**, 5887–5892 (2004).

51. P. Aramsangtienchai, N. A. Spiegelman, J. Cao, H. Lin, *S* -Palmitoylation of Junctional Adhesion Molecule C Regulates Its Tight Junction Localization and Cell Migration. *J. Biol. Chem.* **292**, 5325–5334 (2017).

52. B. J. Roberts *et al.*, Palmitoylation of plakophilin is required for desmosome assembly. *J. Cell Sci.* **127**, 3782–3793 (2014).

53. B. Chen *et al.*, ZDHHC7-mediated S-palmitoylation of Scribble regulates cell polarity. *Nat. Chem. Biol.* **12**, 686–93 (2016).

54. S. J. Zoltewicz *et al.*, The Palmitoylation State of PMP22 Modulates Epithelial Cell Morphology and Migration. *ASN Neuro*. **4**, AN20120045 (2012).

55. G. S. Brigidi *et al.*, Palmitoylation of δ-catenin by DHHC5 mediates activity-induced synapse plasticity. *Nat. Neurosci.* **17**, 522–532 (2014).

56. C. Sharma *et al.*, Protein Acyltransferase DHHC3 Regulates Breast Tumor Growth, Oxidative Stress, and Senescence. *Cancer Res.* **77**, 6880–6890 (2017).

57. S. Chen *et al.*, Palmitoylation-dependent activation of MC1R prevents melanomagenesis. *Nature*. **549**, 399–403 (2017).

58. J. Lai *et al.*, Two homologous protein *S* -acyltransferases, PAT13 and PAT14, cooperatively regulate leaf senescence in *Arabidopsis*. *J. Exp. Bot.* **66**, 6345–6353 (2015).

59. N. Cao *et al.*, A potential role for protein palmitoylation and zDHHC16 in DNA damage response. *BMC Mol. Biol.* **17**, 12 (2016).

60. X. Chen *et al.*, EZH2 Palmitoylation Mediated by ZDHHC5 in p53-Mutant Glioma Drives Malignant Development and Progression. *Cancer Res.* **77**, 4998–5010 (2017).

61. S. Park *et al.*, Palmitoylation controls the dynamics of budding-yeast heterochromatin via the telomere-binding protein Rif1. *Proc. Natl. Acad. Sci.* **108**, 14572–14577 (2011).

62. H. Sudo *et al.*, ZDHHC8 knockdown enhances radiosensitivity and suppresses tumor growth in a mesothelioma mouse model. *Cancer Sci.* **103**, 203–209 (2012).

63. W. Shi *et al.*, ZDHHC16 modulates FGF/ERK dependent proliferation of neural stem/progenitor cells in the zebrafish telencephalon. *Dev. Neurobiol.* **76**, 1014–1028 (2016).

64. X. Chen *et al.*, Protein Palmitoylation Regulates Neural Stem Cell Differentiation by Modulation of EID1 Activity. *Mol. Neurobiol.* **53**, 5722–5736 (2016).

65. X. Chen *et al.*, Zinc Finger DHHC-Type Containing 13 Regulates Fate Specification of Ectoderm and Mesoderm Cell Lineages by Modulating Smad6 Activity. *Stem Cells Dev.* **23**, 1899–1909 (2014).

66. J. M. Gagne, L. A. Gish, S. E. Clark, The role of the acyl modification, palmitoylation, in Arabidopsis stem cell regulation. *Plant Signal. Behav.* **5**, 1048–1051 (2010).

67. J. Xu *et al.*, Inhibiting the palmitoylation/depalmitoylation cycle selectively reduces the growth of hematopoietic cells expressing oncogenic Nras. *Blood*. **119**, 1032–1035 (2012).

68. L. Abrami, B. Kunz, I. Iacovache, F. G. van der Goot, Palmitoylation and ubiquitination regulate exit of the Wnt signaling protein LRP6 from the endoplasmic reticulum. *Proc. Natl. Acad. Sci.* **105**, 5384–5389 (2008).

69. K. Willert *et al.*, Wnt proteins are lipid-modified and can act as stem cell growth factors. *Nature*. **423**, 448–452 (2003).

70. W. Wang, K. B. Runkle, S. M. Terkowski, R. I. Ekaireb, E. S. Witze, Protein depalmitoylation is induced by Wnt5a and promotes polarized cell behavior. *J. Biol. Chem.* **290**, 15707–15716 (2015).

71. E. Stypulkowski, I. A. Asangani, E. S. Witze, The depalmitoylase APT1 directs the asymmetric partitioning of Notch and Wnt signaling during cell division. *Sci. Signal.* **11** (2018), doi:10.1126/scisignal.aam8705.

72. J. A. Duncan, A. G. Gilman, A cytoplasmic acyl-protein thioesterase that removes palmitate from G protein ?? subunits and p21(RAS). *J. Biol. Chem.* **273**, 15830–15837 (1998).

73. G. Siegel *et al.*, A functional screen implicates microRNA-138-dependent regulation of the depalmitoylation enzyme APT1 in dendritic spine morphogenesis. *Nat. Cell Biol.* **11**, 705–16 (2009).

74. J. Steinhauer, H. H. Liu, E. Miller, J. E. Treisman, Trafficking of the EGFR ligand Spitz regulates its signaling activity in polarized tissues. *J. Cell Sci.* **126**, 4469–4478 (2013).

75. M. Rusch *et al.*, Identification of acyl protein thioesterases 1 and 2 as the cellular targets of the ras-signaling modulators palmostatin B and M. *Angew. Chemie - Int. Ed.* **50**, 9838–9842 (2011).

76. O. Rocks *et al.*, An Acylation Cycle Regulates Localization and Activity of Palmitoylated Ras Isoforms. *Science (80-.).* **307**, 1746–1752 (2005).

77. D. B. Rush, R. T. Leon, M. H. McCollum, R. W. Treu, J. Wei, Palmitoylation and trafficking of GAD65 are impaired in a cellular model of Huntington's disease. *Biochem. J.* **442**, 39–48 (2012).

78. L. M. Sutton *et al.*, Hip14l-deficient mice develop neuropathological and behavioural features of Huntington disease. *Hum. Mol. Genet.* **22**, 452–465 (2013).

79. F. B. Young *et al.*, Low Levels of Human HIP14 Are Sufficient to Rescue Neuropathological, Behavioural, and Enzymatic Defects Due to Loss of Murine HIP14 in Hip14−/− Mice. *PLoS One*. **7**, e36315 (2012).

80. A. Yanai *et al.*, Palmitoylation of huntingtin by HIP14is essential for its trafficking and function. *Nat. Neurosci.* **9**, 824–831 (2006).

81. T. Suzuki, C. Mizumaru, Regulation of APP α-secretase activity involved in protein palmitoylation by DHHC-12. *Alzheimer's Dement.* **6**, S260 (2010).

82. R. Bhattacharyya, C. Barren, D. M. Kovacs, Palmitoylation of amyloid precursor protein regulates amyloidogenic processing in lipid rafts. *J. Neurosci.* **33**, 11169–83 (2013).

83. J. Wang *et al.*, SCG10 promotes non-amyloidogenic processing of amyloid precursor protein by facilitating its trafficking to the cell surface. *Hum. Mol. Genet.* **22**, 4888–4900 (2013).

84. E. Napoli *et al.*, Zdhhc13-dependent Drp1 S-palmitoylation impacts brain bioenergetics, anxiety, coordination and motor skills. *Sci. Rep.* **7**, 12796 (2017).

85. J. Mukai *et al.*, Evidence that the gene encoding ZDHHC8 contributes to the risk of schizophrenia. *Nat. Genet.* **36**, 725–731 (2004).

86. Y. Li, B. R. Martin, B. F. Cravatt, S. L. Hofmann, DHHC5 protein palmitoylates flotillin-2 and is rapidly degraded on induction of neuronal differentiation in cultured cells. *J. Biol. Chem.* **287**, 523–530 (2012).

87. Z. Qin *et al.*, Chronic Stress Induces Anxiety via an Amygdalar Intracellular Cascade that Impairs Endocannabinoid Signaling. *Neuron*. **85**, 1319–1331 (2015).

88. S. Heiler, W. Mu, M. Zöller, F. Thuma, The importance of claudin-7 palmitoylation on membrane subdomain localization and metastasis-promoting activities. *Cell Commun. Signal.* **13**, 29 (2015).

89. H. Z. Oo *et al.*, Overexpression of ZDHHC14 promotes migration and invasion of scirrhous type gastric cancer. *Oncol. Rep.* **32**, 403–410 (2014).

90. T. Oyama *et al.*, Isolation of a novel gene on 8p21.3-22 whose expression is reduced significantly in human colorectal cancers with liver metastasis. *Genes. Chromosomes Cancer*. **29**, 9–15 (2000).

91. Y. Yamamoto *et al.*, Gain of 5p15.33 Is Associated with Progression of Bladder Cancer. *Oncology*. **72**, 132–138 (2007).

92. D. T. Coleman, A. L. Gray, S. J. Kridel, J. A. Cardelli, Palmitoylation regulates the intracellular trafficking and stability of c-Met. *Oncotarget*. **7**, 32664–77 (2016).

93. I. S. Babina, E. A. McSherry, S. Donatello, A. D. Hill, A. M. Hopkins, A novel mechanism of regulating breast cancer cell migration via palmitoylation-dependent alterations in the lipid raft affiliation of CD44. *Breast Cancer Res.* **16**, R19 (2014).

94. J. M. Draper, C. D. Smith, DHHC20: a human palmitoyl acyltransferase that causes

cellular transformation. *Mol. Membr. Biol.* **27**, 123–136 (2010).

95. K. Du, S. Murakami, Y. Sun, C. L. Kilpatrick, B. Luscher, DHHC7 Palmitoylates Glucose Transporter 4 (Glut4) and Regulates Glut4 Membrane Translocation. *J. Biol. Chem.* **292**, 2979–2991 (2017).

96. W. Ren, Y. Sun, K. Du, DHHC17 palmitoylates ClipR-59 and modulates ClipR-59 association with the plasma membrane. **33** (2013), doi:10.1128/MCB.00527-13.

97. Z. Xu, L. Zhong, New insights into the posttranslational regulation of human cytosolic thioredoxin by S-palmitoylation. *Biochem. Biophys. Res. Commun.* **460**, 949–956 (2015).

98. J. Howie, L. B. Tulloch, M. J. Shattock, W. Fuller, Regulation of the cardiac Na^+ pump by palmitoylation of its catalytic and regulatory subunits. *Biochem. Soc. Trans.* **41**, 95–100 (2013).

99. B. J. Roberts *et al.*, Palmitoylation of Desmoglein 2 Is a Regulator of Assembly Dynamics and Protein Turnover. *J. Biol. Chem.* **291**, 24857–24865 (2016).

100. R. Chaube *et al.*, Regulation of the Skeletal Muscle Ryanodine Receptor/Ca^{2+} -release Channel RyR1 by *S* -Palmitoylation. *J. Biol. Chem.* **289**, 8612–8619 (2014).

101. P. Chan *et al.*, Autopalmitoylation of TEAD proteins regulates transcriptional output of the Hippo pathway. *Nat. Chem. Biol.* **12**, 282–289 (2016).

102. X. Gao, R. N. Hannoush, A Decade of Click Chemistry in Protein Palmitoylation: Impact on Discovery and New Biology. *Cell Chem. Biol.* (2018), doi:10.1016/j.chembiol.2017.12.002.

103. F. J. Dekker *et al.*, Small-molecule inhibition of APT1 affects Ras localization and signaling. *Nat. Chem. Biol.* **6**, 449–456 (2010).

104. S. Kakugawa *et al.*, Notum deacylates Wnt proteins to suppress signalling activity. *Nature* (2015), doi:10.1038/nature14259.

105. S. Lobo, W. K. Greentree, M. E. Linder, R. J. Deschenes, Identification of a Ras Palmitoyltransferase in *Saccharomyces cerevisiae*. *J. Biol. Chem.* **277**, 41268–41273 (2002).

106. A. F. Roth, Y. Feng, L. Chen, N. G. Davis, The yeast DHHC cysteine-rich domain protein Akr1p is a palmitoyl transferase. *J. Cell Biol.* **159**, 23–8 (2002).

107. M. Fukata, Y. Fukata, H. Adesnik, R. A. Nicoll, D. S. Bredt, Identification of PSD-95 palmitoylating enzymes. *Neuron.* **44**, 987–96 (2004).

108. K. Lemonidis, M. C. Sanchez-Perez, L. H. Chamberlain, Identification of a Novel Sequence Motif Recognized by the Ankyrin Repeat Domain of zDHHC17/13 *S* -Acyltransferases. *J. Biol. Chem.* **290**, 21939–21950 (2015).

109. S. S. Sanders, K. K. N. Mui, L. M. Sutton, M. R. Hayden, Identification of Binding Sites in Huntingtin for the Huntingtin Interacting Proteins HIP14 and HIP14L. *PLoS One*. **9**, e90669 (2014).

110. J. Greaves, L. H. Chamberlain, DHHC palmitoyl transferases: Substrate interactions and (patho)physiology. *Trends Biochem. Sci.* **36** (2011), pp. 245–253.

111. B. C. Jennings, M. E. Linder, DHHC protein S-acyltransferases use similar ping-pong kinetic mechanisms but display different Acyl-CoA specificities. *J. Biol. Chem.* **287**, 7236–7245 (2012).

112. D. A. Mitchell, A. Vasudevan, M. E. Linder, R. J. Deschenes, Protein palmitoylation by a family of DHHC protein S-acyltransferases. *J Lipid Res.* **47**, 1118–1127 (2006).

113. Y. Fukata *et al.*, Local palmitoylation cycles define activity-regulated postsynaptic subdomains. *J. Cell Biol.* **202**, 145–161 (2013).

114. J. Greaves, J. A. Carmichael, L. H. Chamberlain, The palmitoyl transferase DHHC2 targets a dynamic membrane cycling pathway: regulation by a C-terminal domain. *Mol. Biol. Cell*. **22**, 1887–1895 (2011).

115. R. N. Hannoush, N. Arenas-Ramirez, Imaging the Lipidome: ω-Alkynyl Fatty Acids for Detection and Cellular Visualization of Lipid-Modified Proteins. *ACS Chem. Biol.* **4**, 581–587 (2009).

116. M. M. Zhang, P. Y. J. Wu, F. D. Kelly, P. Nurse, H. C. Hang, Quantitative Control of Protein S-Palmitoylation Regulates Meiotic Entry in Fission Yeast. *PLoS Biol.* **11** (2013), doi:10.1371/journal.pbio.1001597.

117. Y. Devedjiev, Z. Dauter, S. R. Kuznetsov, T. L. Z. Jones, Z. S. Derewenda, Crystal structure of the human acyl protein thioesterase I from a single X-ray data set to 1.5 ?? *Structure*. **8**, 1137–1146 (2000).

118. A. M. Anderson, M. A. Ragan, Palmitoylation: a protein S-acylation with implications for breast cancer. *npj Breast Cancer*. **2**, 16028 (2016).

119. D. T. S. Lin, E. Conibear, ABHD17 proteins are novel protein depalmitoylases that regulate N-Ras palmitate turnover and subcellular localization. *Elife*. **4**, e11306 (2015).

120. S. Chai, X. A. Cambronne, S. W. Eichhorn, R. H. Goodman, MicroRNA-134 activity in somatostatin interneurons regulates H-Ras localization by repressing the palmitoylation enzyme, DHHC9. *Proc. Natl. Acad. Sci.* **110**, 17898–17903 (2013).

121. J. L. Hernandez *et al.*, Correlated S-palmitoylation profiling of Snail-induced epithelial to mesenchymal transition. *Mol. Biosyst.* **12**, 1799–808 (2016).

122. D. Choquet, A. Triller, The dynamic synapse. *Neuron*. **80**, 691–703 (2013).

123. L. J. Hanley, J. M. Henley, Differential roles of GRIP1a and GRIP1b in AMPA receptor trafficking. *Neurosci. Lett.* **485**, 167–172 (2010).

124. G. M. Thomas, T. Hayashi, S.-L. Chiu, C.-M. Chen, R. L. Huganir, Palmitoylation by DHHC5/8 Targets GRIP1 to Dendritic Endosomes to Regulate AMPA-R Trafficking. *Neuron*. **73**, 482–496 (2012).

125. I. Kaur *et al.*, Activity-Dependent Palmitoylation Controls SynDIG1 Stability,

Localization, and Function. *J. Neurosci.* **36**, 7562–7568 (2016).

126. T. Hayashi, G. Rumbaugh, R. L. Huganir, Differential Regulation of AMPA Receptor Subunit Trafficking by Palmitoylation of Two Distinct Sites. *Neuron.* **47**, 709–723 (2005).

127. C. A. Keller *et al.*, The 2 Subunit of GABAA Receptors Is a Substrate for Palmitoylation by GODZ. *J. Neurosci.* **24**, 5881–5891 (2004).

128. Y. Webb, L. Hermida-Matsumoto, M. D. Resh, Inhibition of protein palmitoylation, raft localization, and T cell signaling by 2-bromopalmitate and polyunsaturated fatty acids. *J. Biol. Chem.* **275**, 261–70 (2000).

129. A. Arcaro *et al.*, Essential role of CD8 palmitoylation in CD8 coreceptor function. *J. Immunol.* **165**, 2068–76 (2000).

130. B. Crise, J. K. Rose, Identification of palmitoylation sites on CD4, the human immunodeficiency virus receptor. *J. Biol. Chem.* **267**, 13593–7 (1992).

131. S. A. Walker, P. J. Lockyer, Visualizing Ras signalling in real-time. *J. Cell Sci.* **117**, 2879–86 (2004).

132. E. Kong *et al.*, Dynamic palmitoylation links cytosol-membrane shuttling of acyl-protein thioesterase-1 and acyl-protein thioesterase-2 with that of proto-oncogene H-Ras product and growth-associated protein-43. *J. Biol. Chem.* **288**, 9112–9125 (2013).

133. C. Aicart-Ramos, R. A. Valero, I. Rodriguez-Crespo, Protein palmitoylation and subcellular trafficking. *Biochim. Biophys. Acta - Biomembr.* **1808** (2011), pp. 2981–2994.

134. A. K. Lakkaraju *et al.*, Palmitoylated calnexin is a key component of the ribosome-translocon complex. *EMBO J.* **31**, 1823–1835 (2012).

135. P. J. McCormick *et al.*, Palmitoylation Controls Recycling in Lysosomal Sorting and Trafficking. *Traffic*. **9**, 1984–1997 (2008).

136. E. Gottlieb-Abraham, O. Gutman, G. M. Pai, I. Rubio, Y. I. Henis, The residue at position 5 of the N-terminal region of Src and Fyn modulates their myristoylation, palmitoylation, and membrane interactions. *Mol. Biol. Cell*. **27**, 3926–3936 (2016).

137. H. Kwon, J. Lee, K. Jeong, D. Jang, Y. Pak, Fatty acylated caveolin-2 is a substrate of insulin receptor tyrosine kinase for insulin receptor substrate-1-directed signaling activation. *Biochim. Biophys. Acta - Mol. Cell Res.* **1853**, 1022–1034 (2015).

138. H. Matakatsu, S. S. Blair, R. G. Fehon, The palmitoyltransferase Approximated promotes growth via the Hippo pathway by palmitoylation of Fat. *J. Cell Biol.* **216**, 265–277 (2017).

139. Y. Zhang, X. Wang, H. Matakatsu, R. Fehon, S. S. Blair, The novel SH3 domain protein Dlish/CG10933 mediates fat signaling in Drosophila by binding and regulating Dachs. *Elife*. **5**, e16624 (2016).

140. W. Li *et al.*, Membrane targeting of inhibitory Smads through palmitoylation controls TGF-β/BMP signaling. *Proc. Natl. Acad. Sci.* **114**, 13206–13211 (2017).

141. J. Valdez-Taubas, H. Pelham, Swf1-dependent palmitoylation of the SNARE Tlg1 prevents its ubiquitination and degradation. *EMBO J.* **24**, 2524–2532 (2005).

142. C. L. Noland *et al.*, Palmitoylation of TEAD Transcription Factors Is Required for Their Stability and Function in Hippo Pathway Signaling. *Structure*. **24**, 179–86 (2016).

143. L. Abrami, S. H. Leppla, F. G. van der Goot, Receptor palmitoylation and ubiquitination regulate anthrax toxin endocytosis. *J. Cell Biol.* **172**, 309–320 (2006).

144. X. Yuan *et al.*, Putative DHHC-Cysteine-Rich Domain S-Acyltransferase in Plants. *PLoS One*. **8**, e75985 (2013).

145. J. Chaudhary, M. K. Skinner, Identification of a Novel Gene Product, Sertoli Cell Gene with a Zinc Finger Domain, That Is Important for FSH Activation of Testicular Sertoli Cells. *Endocrinology*. **143**, 426–435 (2002).

146. C. J. Perez *et al.*, Increased Susceptibility to Skin Carcinogenesis Associated with a Spontaneous Mouse Mutation in the Palmitoyl Transferase Zdhhc13 Gene. *J. Invest. Dermatol.* **135**, 3133–3143 (2015).

147. I.-W. Song *et al.*, Palmitoyl Acyltransferase, Zdhhc13, Facilitates Bone Mass Acquisition by Regulating Postnatal Epiphyseal Development and Endochondral Ossification: A Mouse Model. *PLoS One*. **9**, e92194 (2014).

148. A. N. Saleem *et al.*, Mice with Alopecia, Osteoporosis, and Systemic Amyloidosis Due to Mutation in Zdhhc13, a Gene Coding for Palmitoyl Acyltransferase. *PLoS Genet.* **6**, e1000985 (2010).

149. W. Ren, U. S. Jhala, K. Du, Proteomic analysis of protein palmitoylation in adipocytes. *Adipocyte*. **2**, 17–27 (2013).

150. J. J. F. P. Luiken, D. Chanda, M. Nabben, D. Neumann, J. F. C. Glatz, Post-translational modifications of CD36 (SR-B2): Implications for regulation of myocellular fatty acid uptake. *Biochim. Biophys. Acta - Mol. Basis Dis.* **1862**, 2253–2258 (2016).

151. L.-F. Shen *et al.*, Role of S-Palmitoylation by ZDHHC13 in Mitochondrial function and Metabolism in Liver. *Sci. Rep.* **7**, 2182 (2017).

152. M. Blanc *et al.*, SwissPalm: Protein Palmitoylation database. *F1000Research*. **4** (2015), doi:10.12688/f1000research.6464.1.

153. J. L. Hernandez *et al.*, APT2 Inhibition Restores Scribble Localization and S-Palmitoylation in Snail-Transformed Cells. *Cell Chem. Biol.* **24**, 87–97 (2017).

154. J. M. Berg, J. L. Tymoczko, L. Stryer, Membrane Channels and Pumps (2002) (available at https://www.ncbi.nlm.nih.gov/books/NBK21140/).

155. M.-J. Lin *et al.*, Massive palmitoylation-dependent endocytosis during reoxygenation of anoxic cardiac muscle. *Elife*. **2**, e01295 (2013).

156. Y. Li, R. Scott, J. Doughty, M. Grant, B. Qi, Protein *S* -Acyltransferase 14: A Specific Role for Palmitoylation in Leaf Senescence in Arabidopsis. *Plant Physiol.* **170**, 415–428

(2016).

157. A. Honda *et al.*, Extracellular Signals Induce Glycoprotein M6a Clustering of Lipid Rafts and Associated Signaling Molecules. *J. Neurosci.* **37**, 4046–4064 (2017).

158. S. L. Butland *et al.*, The palmitoyl acyltransferase HIP14 shares a high proportion of interactors with huntingtin: implications for a role in the pathogenesis of Huntington's disease. *Hum. Mol. Genet.* **23**, 4142–4160 (2014).

159. R. R. Singaraja *et al.*, Altered palmitoylation and neuropathological deficits in mice lacking HIP14. *Hum. Mol. Genet.* **20**, 3899–3909 (2011).

160. C. Mizumaru *et al.*, Suppression of APP-containing vesicle trafficking and production of β-amyloid by AID/DHHC-12 protein. *J. Neurochem.* **111**, 1213–1224 (2009).

161. K. Huang *et al.*, Neuronal palmitoyl acyl transferases exhibit distinct substrate specificity. *FASEB J.* **23**, 2605–15 (2009).

162. J. T. Dearborn *et al.*, Histochemical localization of palmitoyl protein thioesterase-1 activity. *Mol. Genet. Metab.* **117**, 210–216 (2016).

163. S.-M. Yan *et al.*, Reduced expression of ZDHHC2 is associated with lymph node metastasis and poor prognosis in gastric adenocarcinoma. *PLoS One*. **8**, e56366 (2013).

164. C. Sharma, I. Rabinovitz, M. E. Hemler, Palmitoylation by DHHC3 is critical for the function, expression, and stability of integrin α6β4. *Cell. Mol. Life Sci.* **69**, 2233–2244 (2012).

165. Y.-W. Choi *et al.*, Gene expression profiles in squamous cell cervical carcinoma using array-based comparative genomic hybridization analysis. *Int. J. Gynecol. Cancer*. **17**, 687–96 (2007).

166. H. Tian *et al.*, Systematic siRNA Screen Unmasks NSCLC Growth Dependence by Palmitoyltransferase DHHC5. *Mol. Cancer Res.* **13**, 784–94 (2015).

167. A. Pedram, M. Razandi, R. J. Deschenes, E. R. Levin, DHHC-7 and -21 are palmitoylacyltransferases for sex steroid receptors. *Mol. Biol. Cell*. **23**, 188–199 (2012).

168. C. Sharma, X. H. Yang, M. E. Hemler, DHHC2 Affects Palmitoylation, Stability, and Functions of Tetraspanins CD9 and CD151. *Mol. Biol. Cell*. **19**, 3415–3425 (2008).

169. R. S. Sadeghi *et al.*, Wnt5a signaling induced phosphorylation increases APT1 activity and promotes melanoma metastatic behavior. *Elife*. **7** (2018), doi:10.7554/eLife.34362.

170. A. Kharbanda, K. Runkle, W. Wang, E. S. Witze, Induced sensitivity to EGFR inhibitors is mediated by palmitoylated cysteine 1025 of EGFR and requires oncogenic Kras. *Biochem. Biophys. Res. Commun.* **493**, 213–219 (2017).

171. I. Vujic *et al.*, Acyl protein thioesterase 1 and 2 (APT-1, APT-2) inhibitors palmostatin B, ML348 and ML349 have different effects on NRAS mutant melanoma cells. *Oncotarget*. **7**, 7297–306 (2016).

172. I. M. Ahearn *et al.*, FKBP12 Binds to Acylated H-Ras and Promotes Depalmitoylation. *Mol. Cell*. **41**, 173–185 (2011).

173. Y.-L. Zhang *et al.*, Protein palmitoylation is critical for the polar growth of root hairs in Arabidopsis. *BMC Plant Biol.* **15**, 50 (2015).

174. A. Dudak, J. Kim, B. Cheong, H. J. Federoff, S. T. Lim, Membrane palmitoylated proteins regulate trafficking and processing of nectins☆. *Eur. J. Cell Biol.* **90**, 365–375 (2011).

175. C. Zihni, C. Mills, K. Matter, M. S. Balda, Tight junctions: from simple barriers to multifunctional molecular gates. *Nat. Rev. Mol. Cell Biol.* **17**, 564–580 (2016).

176. a M. Zambito, J. Wolff, Palmitoylation of tubulin. *Biochem. Biophys. Res. Commun.* **239**, 650–654 (1997).

177. X. Gao, R. N. Hannoush, Method for Cellular Imaging of Palmitoylated Proteins with Clickable Probes and Proximity Ligation Applied to Hedgehog, Tubulin, and Ras. *J. Am. Chem. Soc.* **136**, 4544–4550 (2014).

178. J. M. Caron, L. R. Vega, J. Fleming, R. Bishop, F. Solomon, Single site alpha-tubulin mutation affects astral microtubules and nuclear positioning during anaphase in Saccharomyces cerevisiae: possible role for palmitoylation of alpha-tubulin. *Mol. Biol. Cell*. **12**, 2672–87 (2001).

179. I. Navarro-Lérida *et al.*, A palmitoylation switch mechanism regulates Rac1 function and membrane organization. *EMBO J.* **31**, 534–551 (2012).

180. D. A. Wang, S. M. Sebti, Palmitoylated cysteine 192 is required for RhoB tumor-suppressive and apoptotic activities. *J. Biol. Chem.* **280**, 19243–19249 (2005).

181. A. Wirth *et al.*, Dual lipidation of the brain-specific Cdc42 isoform regulates its functional properties. *Biochem. J.* **456**, 311–22 (2013).

182. A. Nishimura, M. E. Linder, Identification of a novel prenyl and palmitoyl modification at the CaaX motif of Cdc42 that regulates RhoGDI binding. *Mol. Cell. Biol.* **33**, 1417–1429 (2013).

183. R. Kang *et al.*, Neural palmitoyl-proteomics reveals dynamic synaptic palmitoylation. *Nature*. **456**, 904–9 (2008).

184. M. Lee, V. Vasioukhin, Cell polarity and cancer--cell and tissue polarity as a non-canonical tumor suppressor. *J. Cell Sci.* **121**, 1141–50 (2008).

185. M. F. G. Schmidt, M. J. Schlesinger, Fatty acid binding to vesicular stomatitis virus glycoprotein: a new type of post-translational modification of the viral glycoprotein. *Cell*. **17**, 813–819 (1979).

186. G. Goldstein *et al.*, Isolation of a polypeptide that has lymphocyte-differentiating properties and is probably represented universally in living cells. *Proc. Natl. Acad. Sci. U. S. A.* **72**, 11–5 (1975).

187. W. Eckhart, M. A. Hutchinson, T. Hunter, An activity phosphorylating tyrosine in

polyoma T antigen immunoprecipitates. *Cell*. **18**, 925–33 (1979).

188. B. Zhou, M. An, M. R. Freeman, W. Yang, Technologies and Challenges in Proteomic Analysis of Protein S-acylation. *J. Proteomics Bioinform.* **07** (2014), doi:10.4172/jpb.1000327.

189. B. A. Bannan *et al.*, The drosophila protein palmitoylome characterizing palmitoyl-thioesterases and DHHC palmitoyl-transferases. *Fly (Austin).* **2**, 198–214 (2008).

190. J. P. Wilson, A. S. Raghavan, Y.-Y. Yang, G. Charron, H. C. Hang, *Mol. Cell. Proteomics*, in press, doi:10.1074/mcp.M110.001198.

191. L. Dowal, W. Yang, M. R. Freeman, H. Steen, R. Flaumenhaft, Proteomic analysis of palmitoylated platelet proteins. *Blood*. **118**, e62-73 (2011).

192. G. S. Brigidi, S. X. Bamji, Detection of Protein Palmitoylation in Cultured Hippocampal Neurons by Immunoprecipitation and Acyl-Biotin Exchange (ABE). *J. Vis. Exp.* (2013), doi:10.3791/50031.

193. R. N. P. Rodenburg *et al.*, Stochastic palmitoylation of accessible cysteines in membrane proteins revealed by native mass spectrometry. *Nat. Commun.* **8**, 1280 (2017).

194. J. Wan, A. F. Roth, A. O. Bailey, N. G. Davis, Palmitoylated proteins: purification and identification. *Nat. Protoc.* **2**, 1573–84 (2007).

195. M. T. Forrester *et al.*, Site-specific analysis of protein *S* -acylation by resin-assisted capture. *J. Lipid Res.* **52**, 393–398 (2011).

196. A. Percher *et al.*, Mass-tag labeling reveals site-specific and endogenous levels of protein S-fatty acylation. *Proc. Natl. Acad. Sci. U. S. A.* **113**, 4302–7 (2016).

197. M. Burger *et al.*, Crystal structure of the predicted phospholipase LYPLAL1 reveals unexpected functional plasticity despite close relationship to acyl protein thioesterases. *J. Lipid Res.* **53**, 43–50 (2012).

198. R. Verardi, J.-S. Kim, R. Ghirlando, A. Banerjee, Structural Basis for Substrate Recognition by the Ankyrin Repeat Domain of Human DHHC17 Palmitoyltransferase. *Structure*. **25**, 1337–1347.e6 (2017).

199. M. S. Rana *et al.*, Fatty acyl recognition and transfer by an integral membrane *S* -acyltransferase. *Science (80-.).* **359**, eaao6326 (2018).

200. B. Sun, L. Chen, W. Cao, A. F. Roth, N. G. Davis, The yeast casein kinase Yck3p is palmitoylated, then sorted to the vacuolar membrane with AP-3-dependent recognition of a YXXPhi adaptin sorting signal. *Mol. Biol. Cell*. **15**, 1397–406 (2004).

201. J. a Knoblich, Asymmetric cell division: recent developments and their implications for tumour biology. *Nat. Rev. Mol. Cell Biol.* **11**, 849–860 (2010).

202. J. T. Chang *et al.*, Asymmetric T lymphocyte division in the initiation of adaptive immune responses. *Science*. **315**, 1687–1691 (2007).

203. J. T. Chang *et al.*, Asymmetric Proteasome Segregation as a Mechanism for Unequal Partitioning of the Transcription Factor T-bet during T Lymphocyte Division. *Immunity*. **34**, 492–504 (2011).

204. K. Mizumoto, H. Sawa, Cortical β-Catenin and APC Regulate Asymmetric Nuclear β-Catenin Localization during Asymmetric Cell Division in C. elegans. *Dev. Cell*. **12**, 287–299 (2007).

205. P. Katajisto *et al.*, Stem cells. Asymmetric apportioning of aged mitochondria between daughter cells is required for stemness. *Science*. **348**, 340–3 (2015).

206. M. S. Rhyu, L. Y. Jan, Y. N. Jan, Asymmetric distribution of numb protein during division of the sensory organ precursor cell confers distinct fates to daughter cells. *Cell*. **76**, 477–491 (1994).

207. W. Zhong *et al.*, Asymmetric localization of a mammalian numb homolog during mouse cortical neurogenesis. *Neuron*. **17**, 43–53 (1996).

208. P. Gönczy, Mechanisms of asymmetric cell division: flies and worms pave the way. *Nat. Rev. Mol. Cell Biol.* **9**, 355–66 (2008).

209. P. C. Nowell, The clonal evolution of tumor cell populations. *Science*. **194**, 23–8 (1976).

210. A. S. Cleary, T. L. Leonard, S. A. Gestl, E. J. Gunther, Tumour cell heterogeneity maintained by cooperating subclones in Wnt-driven mammary cancers. *Nature*. **508**, 113–117 (2014).

211. F. Michor, K. Polyak, The origins and implications of intratumor heterogeneity. *Cancer Prev. Res.* **3**, 1361–1364 (2010).

212. L. R. Yates, P. J. Campbell, Evolution of the cancer genome. *Nat. Rev. Genet.* **13**, 795–806 (2012).

213. M. R. Junttila, F. J. de Sauvage, Influence of tumour micro-environment heterogeneity on therapeutic response. *Nature*. **501**, 346–54 (2013).

214. H. Easwaran, H.-C. Tsai, S. B. Baylin, Cancer epigenetics: tumor heterogeneity, plasticity of stem-like states, and drug resistance. *Mol. Cell*. **54**, 716–27 (2014).

215. S. X. Atwood, K. E. Prehoda, aPKC Phosphorylates Miranda to Polarize Fate Determinants during Neuroblast Asymmetric Cell Division. *Curr. Biol.* **19**, 723–729 (2009).

216. F. Wirtz-Peitz, T. Nishimura, J. A. Knoblich, Linking Cell Cycle to Asymmetric Division: Aurora-A Phosphorylates the Par Complex to Regulate Numb Localization. *Cell*. **135**, 161–173 (2008).

217. Q. Shen, W. Zhong, Y. N. Jan, S. Temple, Asymmetric Numb distribution is critical for asymmetric cell division of mouse cerebral cortical stem cells and neuroblasts. *Development*. **129**, 4843–4853 (2002).

218. A. Cicalese *et al.*, The Tumor Suppressor p53 Regulates Polarity of Self-Renewing

Divisions in Mammary Stem Cells. *Cell* (2009), doi:10.1016/j.cell.2009.06.048.

219. B. Zimdahl *et al.*, Lis1 regulates asymmetric division in hematopoietic stem cells and in leukemia. *Nat. Genet.* **46**, 245–52 (2014).

220. S. J. Habib *et al.*, A localized Wnt signal orients asymmetric stem cell division in vitro. *Science (80-.).* **339**, 1445–1448 (2013).

221. K. Sugioka, K. Mizumoto, H. Sawa, Wnt regulates spindle asymmetry to generate asymmetric nuclear β-catenin in C. elegans. *Cell*. **146**, 942–54 (2011).

222. R. S. Demarco, Å. H. Eikenes, K. Haglund, D. L. Jones, Investigating spermatogenesis in Drosophila melanogaster. *Methods*. **68**, 218–27 (2014).

223. B. Goldstein, H. Takeshita, K. Mizumoto, H. Sawa, Wnt signals can function as positional cues in establishing cell polarity. *Dev. Cell*. **10**, 391–396 (2006).

224. J. Betschinger, K. Mechtler, J. A. Knoblich, The Par complex directs asymmetric cell division by phosphorylating the cytoskeletal protein Lgl. *Nature*. **422**, 326–330 (2003).

225. C. A. Smith *et al.*, aPKC-mediated phosphorylation regulates asymmetric membrane localization of the cell fate determinant Numb. *EMBO J.* **26**, 468–480 (2007).

226. D. J. Azzam *et al.*, Triple negative breast cancer initiating cell subsets differ in functional and molecular characteristics and in γ-secretase inhibitor drug responses. *EMBO Mol. Med.* **5**, 1502–1522 (2013).

227. N. Moore, J. Houghton, S. Lyle, Slow-cycling therapy-resistant cancer cells. *Stem Cells Dev.* **21**, 1822–30 (2012).

228. A. Prat *et al.*, Phenotypic and molecular characterization of the claudin-low intrinsic subtype of breast cancer. *Breast cancer Res.* **12**, R68 (2010).

229. A. B. Mohseny *et al.*, Functional characterization of osteosarcoma cell lines provides representative models to study the human disease. *Lab. Invest.* **91**, 1195–1205 (2011).

230. V. Tirino *et al.*, Detection and characterization of CD133+ cancer stem cells in human solid tumours. *PLoS One*. **3** (2008), doi:10.1371/journal.pone.0003469.

231. P. Adamson, C. J. Marshall, A. Hall, P. A. Tilbrook, Post-translational modifications of p21rho proteins. *J. Biol. Chem.* **267**, 20033–20038 (1992).

232. S. P. Thankamony, W. Knudson, Acylation of CD44 and its association with lipid rafts are required for receptor and hyaluronan endocytosis. *J. Biol. Chem.* **281**, 34601–34609 (2006).

233. G. Piperno, M. LeDizet, X. J. Chang, Microtubules containing acetylated alpha-tubulin in mammalian cells in culture. *J. Cell Biol.* **104**, 289–302 (1987).

234. M. Biel, P. Deck, A. Giannis, H. Waldmann, Synthesis and evaluation of acyl protein thioesterase 1 (APT1) inhibitors. *Chem. - A Eur. J.* **12**, 4121–4143 (2006).

235. N. Vartak *et al.*, The autodepalmitoylating activity of APT maintains the spatial organization of palmitoylated membrane proteins. *Biophys. J.* **106**, 93–105 (2014).

236. Y. Ohno, A. Kihara, T. Sano, Y. Igarashi, Intracellular localization and tissue-specific distribution of human and yeast DHHC cysteine-rich domain-containing proteins. *Biochim. Biophys. Acta - Mol. Cell Biol. Lipids*. **1761**, 474–483 (2006).

237. A. H. Huber, W. J. Nelson, W. I. Weis, Three-Dimensional Structure of the Armadillo Repeat Region of β-Catenin. *Cell*. **90**, 871–882 (1997).

238. R. L. Daugherty *et al.*, Phospho-regulation of Beta-catenin adhesion and signaling functions. *Physiology (Bethesda).* **22**, 303–9 (2007).

239. J. A. Knoblich, L. Y. Jan, Y. N. Jan, The N terminus of the Drosophila Numb protein directs membrane association and actin-dependent asymmetric localization. *Proc. Natl. Acad. Sci.* **94**, 13005–13010 (1997).

240. F. Zhou, Y. Xue, X. Yao, Y. Xu, CSS-Palm: Palmitoylation site prediction with a clustering and scoring strategy (CSS). *Bioinformatics*. **22**, 894–896 (2006).

241. C. Zwahlen, S. C. Li, L. E. Kay, T. Pawson, J. D. Forman-Kay, Multiple modes of peptide recognition by the PTB domain of the cell fate determinant Numb. *EMBO J.* **19**, 1505–1515 (2000).

242. L. Lasagni *et al.*, Notch activation differentially regulates renal progenitors proliferation and differentiation toward the podocyte lineage in glomerular disorders. *Stem Cells*. **28**, 1673–1685 (2010).

243. N. Brimer, C. Lyons, A. E. Wallberg, S. B. Vande Pol, Cutaneous papillomavirus E6 oncoproteins associate with MAML1 to repress transactivation and NOTCH signaling. *Oncogene*. **31**, 4639–46 (2012).

244. W. Benetka *et al.*, Experimental testing of predicted myristoylation targets involved in asymmetric cell division and calcium-dependent signalling. *Cell Cycle*. **7**, 3709–3719 (2008).

245. C. Fang *et al.*, Identification of Palmitoylated Transitional Endoplasmic Reticulum ATPase by Proteomic Technique and Pan Antipalmitoylation Antibody. *J. Proteome Res.* **15**, 956–962 (2016).

246. R. A. Serwa *et al.*, Systems Analysis of Protein Fatty Acylation in Herpes Simplex Virus-Infected Cells Using Chemical Proteomics. *Chem. Biol.* **22**, 1008–1017 (2015).

247. L. C. Fuentealba, E. Eivers, D. Geissert, V. Taelman, E. M. De Robertis, Asymmetric mitosis: Unequal segregation of proteins destined for degradation. *Proc. Natl. Acad. Sci. U. S. A.* **105**, 7732–7737 (2008).

248. R. a Neumüller *et al.*, Mei-P26 regulates microRNAs and cell growth in the Drosophila ovarian stem cell lineage. *Nature*. **454**, 241–5 (2008).

249. P. Fichelson *et al.*, Live-imaging of single stem cells within their niche reveals that a U3snoRNP component segregates asymmetrically and is required for self-renewal in

Drosophila. *Nat. Cell Biol.* **11**, 685–693 (2009).

250. K. L. Congdon, T. Reya, Divide and conquer: how asymmetric division shapes cell fate in the hematopoietic system. *Curr. Opin. Immunol.* **20**, 302–307 (2008).

251. M. T. Niessen, S. Iden, C. M. Niessen, The in vivo function of mammalian cell and tissue polarity regulators - how to shape and maintain the epidermal barrier. *J. Cell Sci.* **125**, 3501–3510 (2012).

252. A. Wodarz, Establishing cell polarity in development. *Nat. Cell Biol.* **4**, E39-44 (2002).

253. M. P. Stein, A. Wandinger-Ness, T. Roitbak, Altered trafficking and epithelial cell polarity in disease. *Trends Cell Biol.* **12**, 374–381 (2002).

254. B. J. Thompson, Cell polarity: models and mechanisms from yeast, worms and flies. *Development*. **140**, 13–21 (2013).

255. S. Etienne-Manneville, Cdc42--the centre of polarity. *J. Cell Sci.* **117**, 1291–1300 (2004).

256. A. F. Palazzo *et al.*, Cdc42, dynein, and dynactin regulate MTOC reorientation independent of Rho-regulated microtubule stabilization. *Curr. Biol.* **11**, 1536–1541 (2001).

257. J. Cau, A. Hall, Cdc42 controls the polarity of the actin and microtubule cytoskeletons through two distinct signal transduction pathways. *J. Cell Sci.* **118**, 2579–2587 (2005).

258. T. Freisinger *et al.*, Establishment of a robust single axis of cell polarity by coupling multiple positive feedback loops. *Nat. Commun.* **4**, 1807 (2013).

259. M. Stamnes, Regulating the actin cytoskeleton during vesicular transport. *Curr. Opin. Cell Biol.* **14**, 428–433 (2002).

260. S. X. Atwood, C. Chabu, R. R. Penkert, C. Q. Doe, K. E. Prehoda, Cdc42 acts downstream of Bazooka to regulate neuroblast polarity through Par-6 aPKC. *J. Cell Sci.* **120**, 3200–6 (2007).

261. A. J. Kay, C. P. Hunter, CDC-42 regulates PAR protein localization and function to control cellular and embryonic polarity in C. elegans. *Curr. Biol.* **11**, 474–81 (2001).

262. A. Wodarz, A. Ramrath, A. Grimm, E. Knust, Drosophila atypical protein kinase C associates with Bazooka and controls polarity of epithelia and neuroblasts. *J. Cell Biol.* **150**, 1361–74 (2000).

263. A. E. M. Adams, D. I. Johnson, R. M. Longnecker, B. F. Sloat, J. R. Pringle, CDC42 and CDC43, two additional genes involved in budding and the establishment of cell polarity in the yeast Saccharomyces cerevisiae. *J. Cell Biol.* **111**, 131–142 (1990).

264. A. S. Gladfelter, I. Bose, T. R. Zyla, E. S. G. Bardes, D. J. Lew, Septin ring assembly involves cycles of GTP loading and hydrolysis by Cdc42p. *J. Cell Biol.* **156**, 315–326 (2002).

265. H. Court, P. Sudbery, Regulation of Cdc42 GTPase Activity in the Formation of Hyphae

in Candida albicans. *Mol. Biol. Cell*. **18**, 265–281 (2006).

266. C. Vanni *et al.*, Constitutively active Cdc42 mutant confers growth disadvantage in cell transformation. *Cell Cycle*. **4**, 1675–1682 (2005).

267. F. D. Kelly, P. Nurse, Spatial control of Cdc42 activation determines cell width in fission yeast. *Mol. Biol. Cell*. **22**, 3801–11 (2011).

268. W. Yang, D. Di Vizio, M. Kirchner, H. Steen, M. R. Freeman, Proteome-scale characterization of human s-acylated proteins in lipid raft-enriched and non-raft membranes. *Mol. Cell. Proteomics*, 1–53 (2009).

269. E. Moutin *et al.*, Palmitoylation of cdc42 Promotes Spine Stabilization and Rescues Spine Density Deficit in a Mouse Model of 22q11.2 Deletion Syndrome. *Cereb. Cortex*. **27**, 3618–3629 (2016).

270. D. J. Dietzen, W. R. Hastings, D. M. Lublin, Caveolin is palmitoylated on multiple cysteine residues. Palmitoylation is not necessary for localization of caveolin to caveolae. *J. Biol. Chem.* **270**, 6838–6842 (1995).

271. J. M. Johnson, M. Jin, D. J. Lew, Symmetry breaking and the establishment of cell polarity in budding yeast. *Curr. Opin. Genet. Dev.* **21**, 740–746 (2011).

272. T. Nishimura, Role of Numb in Dendritic Spine Development with a Cdc42 GEF Intersectin and EphB2. *Mol. Biol. Cell*. **17**, 1273–1285 (2005).

273. J. Schulz, K. Franke, M. Frick, S. Schumacher, Different roles of the small GTPases Rac1, Cdc42, and RhoG in CALEB/NGC-induced dendritic tree complexity. *J. Neurochem.* **139**, 26–39 (2016).

274. T. Sudhaharan *et al.*, Rho GTPase Cdc42 is a direct interacting partner of adenomatous polyposis coli protein and can alter its cellular localization. *PLoS One*. **6** (2011), doi:10.1371/journal.pone.0016603.

275. T. Watanabe *et al.*, Interaction with IQGAP1 links APC to Rac1, Cdc42, and actin filaments during cell polarization and migration. *Dev. Cell*. **7**, 871–883 (2004).

276. M. Baron, V. O'Leary, D. a Evans, M. Hicks, K. Hudson, Multiple roles of the Dcdc42 GTPase during wing development in Drosophila melanogaster. *Mol. Gen. Genet.* **264**, 98–104 (2000).

277. M. Horwitz *et al.*, Role of neutrophil elastase in bone marrow failure syndromes: Molecular genetic revival of the chalone hypothesis. *Curr. Opin. Hematol.* **10**, 49–54 (2003).

278. L. Redmond, A. Ghosh, The role of Notch and Rho GTPases signaling in the control of dendritic development. *Curr. Opin. Neurobiol.* **11**, 111–117 (2001).

279. A. Karaczyn *et al.*, Two novel human NUMB isoforms provide a potential link between development and cancer. *Neural Dev.* **5**, 31 (2010).

280. L. Nemetschke, E. Knust, *Drosophila* Crumbs prevents ectopic Notch activation in

developing wings by inhibiting ligand-independent endocytosis. *Development*. **143**, 4543–4553 (2016).

281. H. Herranz, E. Stamataki, F. Feiguin, M. Milán, Self-refinement of Notch activity through the transmembrane protein Crumbs: modulation of γ-Secretase activity. *EMBO Rep.* **7**, 297–302 (2006).

282. N. Osmani, N. Vitale, J.-P. Borg, S. Etienne-Manneville, Scrib Controls Cdc42 Localization and Activity to Promote Cell Polarization during Astrocyte Migration. *Curr. Biol.* **16**, 2395–2405 (2006).

283. C. Royer, X. Lu, Epithelial cell polarity: A major gatekeeper against cancer. *Cell Death Differ*. **18** (2011), pp. 1470–1477.

284. O. M. Schlüter, W. Xu, R. C. Malenka, Alternative N-Terminal Domains of PSD-95 and SAP97 Govern Activity-Dependent Regulation of Synaptic AMPA Receptor Function. *Neuron*. **51**, 99–111 (2006).

285. S. A. van de Pavert *et al.*, Crumbs homologue 1 is required for maintenance of photoreceptor cell polarization and adhesion during light exposure. *J. Cell Sci.* **117**, 4169–77 (2004).

286. S. K. Muthuswamy, B. Xue, Cell Polarity as a Regulator of Cancer Cell Behavior Plasticity. *Annu. Rev. Cell Dev. Biol.* **28**, 599–625 (2012).

287. C. E. Meacham, S. J. Morrison, Tumour heterogeneity and cancer cell plasticity. *Nature*. **501**, 328–37 (2013).

288. J. Calbo *et al.*, A functional role for tumor cell heterogeneity in a mouse model of small cell lung cancer. *Cancer Cell*. **19**, 244–56 (2011).

289. E. Louie *et al.*, Identification of a stem-like cell population by exposing metastatic breast cancer cell lines to repetitive cycles of hypoxia and reoxygenation. *Breast Cancer Res.* **12**, R94 (2010).

290. S. Liu *et al.*, Hedgehog signaling and Bmi-1 regulate self-renewal of normal and malignant human mammary stem cells. *Cancer Res.* **66**, 6063–6071 (2006).

291. L. Cao *et al.*, Sphere-forming cell subpopulations with cancer stem cell properties in human hepatoma cell lines. *BMC Gastroenterol.* **11**, 71 (2011).

292. J. E. Dick, Stem cell concepts renew cancer research. *Blood*. **112**, 4793–4807 (2008).

293. C. M. Fillmore, C. Kuperwasser, Human breast cancer cell lines contain stem-like cells that self-renew, give rise to phenotypically diverse progeny and survive chemotherapy. *Breast Cancer Res.* **10**, R25 (2008).

294. J. D. Lathia *et al.*, Direct in vivo evidence for tumor propagation by glioblastoma cancer stem cells. *PLoS One*. **6**, e24807 (2011).

295. J. Tsoi *et al.*, Multi-stage Differentiation Defines Melanoma Subtypes with Differential Vulnerability to Drug-Induced Iron-Dependent Oxidative Stress. *Cancer Cell*. **33**, 890–

904.e5 (2018).

296. M. J. Hangauer *et al.*, Drug-tolerant persister cancer cells are vulnerable to GPX4 inhibition. *Nature*. **551**, 247 (2017).

297. V. S. Viswanathan *et al.*, Dependency of a therapy-resistant state of cancer cells on a lipid peroxidase pathway. *Nature*. **547**, 453–457 (2017).

298. K. Jung *et al.*, Triple negative breast cancers comprise a highly tumorigenic cell subpopulation detectable by its high responsiveness to a Sox2 regulatory region 2 (SRR2) reporter. *Oncotarget*. **6**, 10366–73 (2015).

299. S. Gomez-Lopez *et al.*, Asymmetric cell division of stem and progenitor cells during homeostasis and cancer. *Cmls*. **71**, 575–597 (2013).

300. L. Shahriyari, N. L. Komarova, Symmetric vs. asymmetric stem cell divisions: an adaptation against cancer? *PLoS One*. **8**, e76195 (2013).

301. W.-L. Hwang *et al.*, MicroRNA-146a directs the symmetric division of Snail-dominant colorectal cancer stem cells. *Nat. Cell Biol.* **16**, 268–80 (2014).

302. S. Mukherjee, J. Kong, D. J. Brat, Cancer stem cell division: when the rules of asymmetry are broken. *Stem Cells Dev.* **24**, 405–16 (2015).

303. M. Moumen *et al.*, Myc is required for β-catenin-mediated mammary stem cell amplification and tumorigenesis. *Mol. Cancer*. **12**, 132 (2013).

304. R. Jeselsohn *et al.*, Cyclin D1 Kinase Activity Is Required for the Self-Renewal of Mammary Stem and Progenitor Cells that Are Targets of MMTV-ErbB2 Tumorigenesis. *Cancer Cell*. **17**, 65–76 (2010).

305. T. Bouras *et al.*, Notch Signaling Regulates Mammary Stem Cell Function and Luminal Cell-Fate Commitment. *Cell Stem Cell*. **3**, 429–441 (2008).

306. E. E. Morrisey *et al.*, GATA6 regulates HNF4 and is required for differentiation of visceral endoderm in the mouse embryo. *Genes Dev.* **12**, 3579–3590 (1998).

307. J. Jiang *et al.*, A core Klf circuitry regulates self-renewal of embryonic stem cells. *Nat. Cell Biol.* **10**, 353–60 (2008).

308. X. B. Kong, C. Zhang, Dickkopf (Dkk) 1 promotes the differentiation of mouse embryonic stem cells toward neuroectoderm. *Vitr. Cell. Dev. Biol. - Anim.* **45**, 185–193 (2009).

309. Y. Wang *et al.*, Lgr4 regulates mammary gland development and stem cell activity through the pluripotency transcription factor Sox2. *Stem Cells.* **31**, 1921–1931 (2013).

310. N. a P. Franken, H. M. Rodermond, J. Stap, J. Haveman, C. van Bree, Clonogenic assay of cells in vitro. *Nat. Protoc.* **1**, 2315–9 (2006).

311. M. C. Rangel *et al.*, Developmental signaling pathways regulating mammary stem cells and contributing to the etiology of triple-negative breast cancer. *Breast Cancer Res. Treat.*

(2016), pp. 1–16.

312. J. Xu, J. R. Prosperi, N. Choudhury, O. I. Olopade, K. H. Goss, β-catenin is required for the tumorigenic behavior of triple-negative breast cancer cells. *PLoS One*. **10** (2015), doi:10.1371/journal.pone.0117097.

313. T. Stoelzle, P. Schwarb, A. Trumpp, N. E. Hynes, c-Myc affects mRNA translation, cell proliferation and progenitor cell function in the mammary gland. *BMC Biol.* **7**, 63 (2009).

314. E. V Schmidt, The role of c-myc in regulation of translation initiation. *Oncogene*. **23**, 3217–3221 (2004).

315. E. Cerami *et al.*, The cBio Cancer Genomics Portal: An Open Platform for Exploring Multidimensional Cancer Genomics Data. *Cancer Discov.* **2** (2012).

316. J. Gao *et al.*, Integrative analysis of complex cancer genomics and clinical profiles using the cBioPortal. *Sci. Signal.* **6**, pl1 (2013).

317. S. R. Pine, W. Liu, Asymmetric cell division and template DNA co-segregation in cancer stem cells. *Front. Oncol.* **4**, 226 (2014).

318. S. Vedel, H. Nunns, A. Ko, S. Semsey, A. Trusina, Asymmetric Damage Segregation Constitutes an Emergent Population-Level Stress Response. *Cell Syst.* **3**, 187–198 (2016).

319. P. Rompolas *et al.*, Live imaging of stem cell and progeny behaviour in physiological hair-follicle regeneration. *Nature*. **487**, 496–499 (2012).

320. M. Wu *et al.*, Imaging Hematopoietic Precursor Division in Real Time. *Cell Stem Cell*. **1**, 541–554 (2007).

321. C. Schertel *et al.*, A large-scale, in vivo transcription factor screen defines bivalent chromatin as a key property of regulatory factors mediating Drosophila wing development. *Genome Res.* **25**, 514–23 (2015).

322. J. Massagué, TGFβ in Cancer. *Cell*. **134**, 215–230 (2008).

323. A. Brombin, J.-S. Joly, F. Jamen, New tricks for an old dog: ribosome biogenesis contributes to stem cell homeostasis. *Curr. Opin. Genet. Dev.* **34**, 61–70 (2015).

324. B. Srinageshwar, P. Maiti, G. L. Dunbar, J. Rossignol, Role of Epigenetics in Stem Cell Proliferation and Differentiation: Implications for Treating Neurodegenerative Diseases. *Int. J. Mol. Sci.* **17** (2016), doi:10.3390/ijms17020199.

325. X. Cai *et al.*, Runx1 Deficiency Decreases Ribosome Biogenesis and Confers Stress Resistance to Hematopoietic Stem and Progenitor Cells. *Cell Stem Cell*. **17**, 165–77 (2015).

326. J. Pelletier, G. Thomas, S. Volarević, Ribosome biogenesis in cancer: new players and therapeutic avenues. *Nat. Rev. Cancer*. **18**, 51–63 (2017).

327. R. Dent *et al.*, Triple-negative breast cancer: Clinical features and patterns of recurrence. *Clin. Cancer Res.* **13**, 4429–4434 (2007).

328. F. Tomao *et al.*, Triple-negative breast cancer: New perspectives for targeted therapies. *Onco. Targets. Ther.* **8**, 177–193 (2015).

329. F. André, C. C. Zielinski, Optimal strategies for the treatment of metastatic triple-negative breast cancer with currently approved agents. *Ann. Oncol.* **23** (2012), doi:10.1093/annonc/mds195.

330. S. B. Zeichner, H. Terawaki, K. Gogineni, A Review of Systemic Treatment in Metastatic Triple-Negative Breast Cancer, 25–36 (2016).

331. L. Espada, M. A. Ermolaeva, DNA Damage as a Critical Factor of Stem Cell Aging and Organ Homeostasis. *Curr. Stem Cell Reports*. **2**, 290–298 (2016).

332. P. T. McHale, A. D. Lander, The Protective Role of Symmetric Stem Cell Division on the Accumulation of Heritable Damage. *PLoS Comput. Biol.* **10** (2014), doi:10.1371/journal.pcbi.1003802.

333. D. L. Moore, S. Jessberger, Creating Age Asymmetry: Consequences of Inheriting Damaged Goods in Mammalian Cells. *Trends Cell Biol.* **27** (2017), pp. 82–92.

334. J. Hatzold, B. Conradt, Control of apoptosis by asymmetric cell division. *PLoS Biol.* **6**, e84 (2008).

335. J. D. Lathia *et al.*, Distribution of CD133 reveals glioma stem cells self-renew through symmetric and asymmetric cell divisions. *Cell Death Dis.* **2**, e200–e200 (2011).

336. J. Xie *et al.*, Histone H3 Threonine Phosphorylation Regulates Asymmetric Histone Inheritance in the Drosophila Male Germline. *Cell*. **163**, 920–33 (2015).